

DEC 29 1981

Branch Library

WIND-TUNNEL STUDY OF THE
EAST HUNTINGTON BRIDGE
(Concrete Cable-Stayed Alternate)

by

J. E. Cermak,* B. Bienkiewicz,**
and
J. A. Peterka***

for

ARVID GRANT AND ASSOCIATES, INC.
1600 East Fourth Avenue
Olympia, Washington 98506

Fluid Dynamics and Diffusion Laboratory
College of Engineering
Colorado State University
Fort Collins, Colorado 80523

*Director, Fluid Dynamics and Diffusion Laboratory

**Research Associate, Fluid Mechanics and Wind Engineering
Program, Department of Civil Engineering

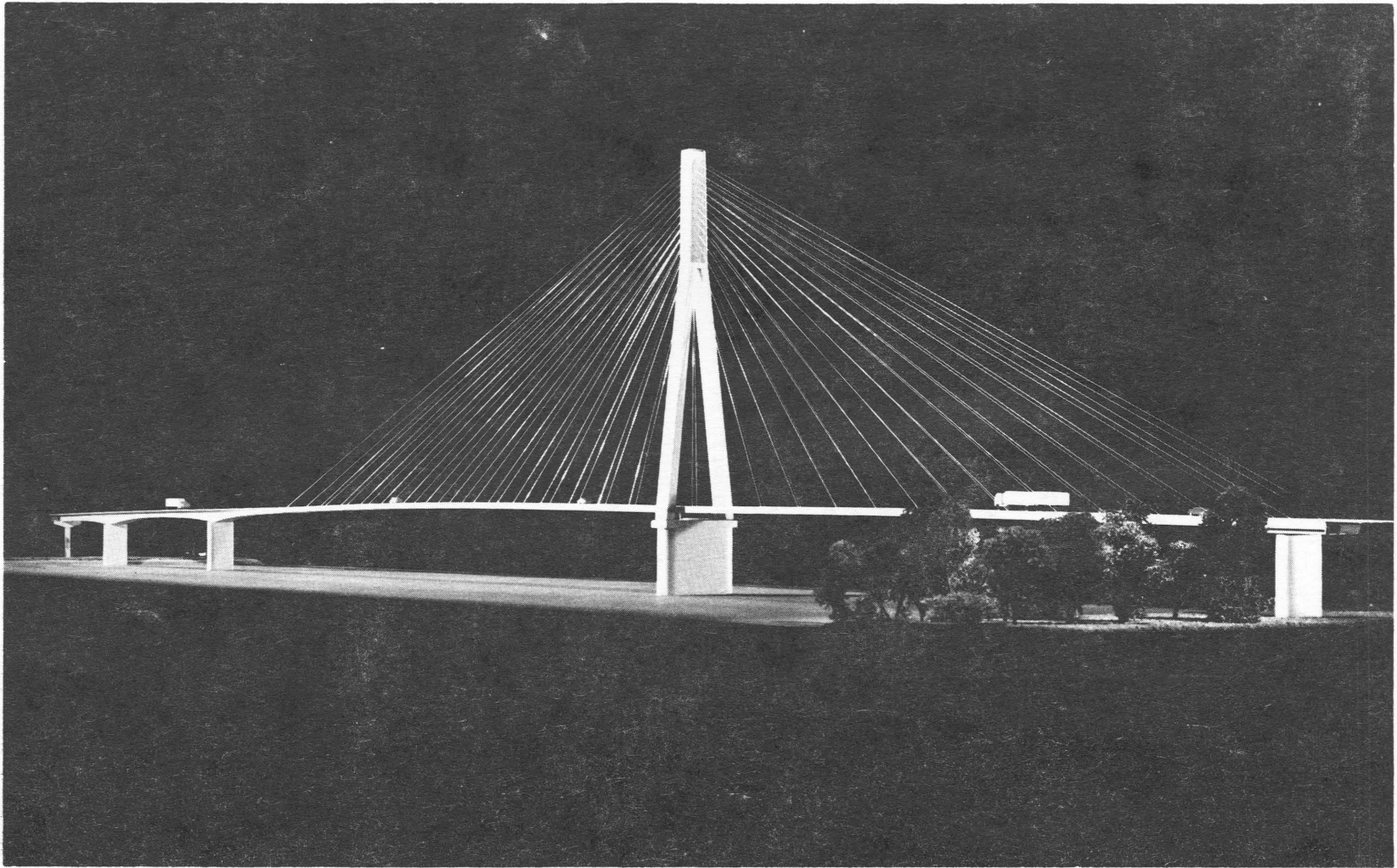
***Associate Professor, Fluid Mechanics and Wind Engineering
Program, Department of Civil Engineering

August 1980

CER80-81JEC-BB-JAP5



U18401 0075609



ABSTRACT

A section model of the proposed East Huntington Bridge (a concrete cable-stayed alternate) was used in the wind-tunnel study. The freely oscillating section model of the original bridge deck with and without railings (traffic barriers) was applied to evaluate the aerodynamic stability of the bridge. Basic aerodynamic derivatives were extracted in smooth flow and were used to estimate the prototype bridge critical wind speed for the one degree-of-freedom (torsional) flutter. Also the amplitude of the vortex-induced bridge oscillation was assessed.

The bridge section model response revealed one degree-of-freedom (torsional) flutter instability occurring at the critical wind speed dependent upon the value of mechanical damping of the model. The computed critical speed for the prototype bridge was about 240 mph for the assumed damping ratio-to-critical of the order of 2 percent and angles of attack in the range from -6 degrees to +6 degrees. Vortex-induced oscillation of the bridge section model (both in a vertical and a torsional degree-of-freedom) occurred at substantially lower speeds. The maximum amplitude of the corresponding prototype motion (higher for vertical oscillation) was estimated not to exceed 0.5 percent of B (where B is the width of the bridge deck) for the same damping level. The maximum vortex-induced response was predicted to be six times lower for the bridge deck with the railings removed. The minimum critical speed was reduced by approximately 17 percent for this new configuration.

ACKNOWLEDGMENTS

Support for this study was provided by Arvid Grant and Associates, Inc. Construction of the bridge section model was accomplished by personnel of the Engineering Research Center, Colorado State University. Data collection was facilitated by the assistance of Mr. Tom Aberle.

Discussions with Professor Fritz Leonhardt of Leonhardt und Andrä, Consulting Engineers, Stuttgart, West Germany, Mr. Arvid Grant and Mr. Conrad Bridges of Arvid Grant and Associates, Inc., and Dr. R. H. Scanlan of Princeton University were very helpful during initial formulation of the testing program for this study.

TABLE OF CONTENTS

<u>Chapter</u>	<u>Page</u>
LIST OF SYMBOLS	vi
LIST OF FIGURES	viii
LIST OF TABLES	xiii
1. INTRODUCTION	1
2. THEORETICAL BACKGROUND	3
2.1 Concept of Bridge Section Model	3
2.2 Similarity Requirements	3
2.3 Bridge Aerodynamic Stability	4
2.4 Vortex-Induced Response	8
3. WIND-TUNNEL FACILITY AND BRIDGE SECTION MODEL	12
3.1 Wind-Tunnel Facility	12
3.2 Bridge Section Model Description and Scaling	12
3.3 Model Construction and Details	13
3.4 Basic Experimental Configurations	14
4. TESTING PROCEDURES	15
4.1 Overall Bridge Section Model Response	15
4.2 Aerodynamic Derivatives	15
4.3 Vortex-Induced Response	16
5. INSTRUMENTATION	18
5.1 Flow Measurement	18
5.2 Measurement of the Bridge Section-Model Response	18
6. DATA ACQUISITION	19
6.1 Overall Bridge Section Model Response	19
6.2 Aerodynamic Derivatives and Stability	19
6.3 Vortex-Induced Response	21
7. RESULTS	23
7.1 Original Bridge Deck with Railings	23
7.1.1 Overall Bridge Section-Model Response	23
7.1.2 Aerodynamic Derivatives and Stability	24
7.1.3 Vortex-Induced Response	26
7.2 Original Bridge Deck without Railings	27
7.2.1 Aerodynamic Derivatives and Stability	27
7.2.2 Vortex-Induced Response	28
8. CONCLUSIONS	29
9. REFERENCES	32
10. FIGURES	33

TABLE OF CONTENTS (Cont.)

<u>Chapter</u>	<u>Page</u>
11. TABLES	102
12. APPENDICES	105
A. Full-Span Torsional Flutter for the Prototype Bridge . .	106
B. Full-Span Vortex-Induced Response in Torsion	108

LIST OF SYMBOLS

<u>Symbol</u>	<u>Description</u>
A (D)	cross-wind dimension of bridge deck with (without) railings
A_{oh} ($A_{o\alpha}$)	initial amplitude in vertical (torsional) degree-of-freedom
A_{nh} ($A_{n\alpha}$)	amplitude in vertical (torsional) degree-of-freedom after n cycles
B	width of bridge deck
C_L (C_M)	lift force (pitching moment) coefficient
$g, G = 32.17 \text{ ft-sec}^{-2}$	gravitational constant
h (α)	vertical (torsional) degree-of-freedom
h_o (α_o)	amplitude of steady-state response in vertical (torsional) degree-of-freedom associated with vortex-shedding
$h_1(t)[\alpha_1(t)]$	generalized coordinate for vertical [torsional] degree-of-freedom
H_i^* (A_i^*)	aerodynamic derivative for vertical (torsional) motion ($i=1,2,3$)
H_o^* (A_o^*)	aerodynamic derivative associated with vortex-shedding in vertical (torsional) degree-of-freedom
$K = \frac{B\omega}{U}$	reduced frequency
L	bridge span
L_b (M_b)	buffeting lift force (pitching moment)
L_{se} (M_{se})	self-excited lift force (pitching moment)
m (I)	mass (polar mass moment of inertia) per unit span
N	frequency in Hz
N_h (N_α)	natural frequency for h (α)--motion in Hz
N_v (N_T)	natural frequency for h (α)--motion in Hz

LIST OF SYMBOLS (Cont.)

<u>Symbol</u>	<u>Description</u>
St	Strouhal number
U	mean speed
U_c	critical speed for torsional flutter
β	angle of attack
$\gamma_h (\gamma_\alpha)$	damping ratio-to-critical for h (α)-- motion at a given wind speed
$\delta_h (\delta_\alpha)$	logarithmic decrement of damping for vertical (torsional) degree-of-freedom
$\zeta_h (\zeta_\alpha)$	damping ratio-to-critical for h (α)-- motion in still air
λ_I	moment of inertia scale
λ_L	geometrical scale
λ_m	mass scale
λ_N	frequency scale
λ_V	velocity scale
λ_ρ	density scale
ν	kinematic viscosity
ρ	air density
$\Psi_1 (x) [\Phi_1(x)]$	fundamental mode for vertical [torsional] degree-of-freedom
ω	circular frequency $\omega = 2\pi N$
$\omega_h (\omega_\alpha)$	circular frequency $\omega_h = 2\pi N_h$ ($\omega_\alpha = 2\pi N_\alpha$)
() _m	refers to bridge section model
() _p	refers to prototype bridge

LIST OF FIGURES

<u>Figure</u>		<u>Page</u>
1	Structural Aerodynamics Wind Tunnel	34
2	Bridge Section Model	35
3	Main Spans of East Huntington Bridge (Concrete Cable-Stayed Alternate)	36
4	Fundamental Modes in Bending and Torsion	37
5	Prototype Bridge Deck	38
6	Model Bridge Deck	39
7	Section Model of Bridge	40
8	Bridge Section Model in Wind Tunnel	41
9	Strain Gage Transducer and Electromagnet	42
10	Viscous Damper - General View	43
11	Viscous Damper - Details	44
12	Free Oscillation of Models in Still Air - Damping Level 1 ($\zeta_V=0.12\%$, $\zeta_T=0.17\%$)	45
13	Free Oscillation of Model in Still Air - Damping Level 2 ($\zeta_V=0.71\%$, $\zeta_T=0.75\%$)	46
14	Free Oscillation of Model in Still Air - Damping Level 3 ($\zeta_V=2.3\%$, $\zeta_T=2.1\%$)	47
15	Experimental Configurations	48
16	Basic Definitions	49
17	Basic Geometrical Dimensions	49
18	Arrangement for Aerodynamic Measurements	50
19	Instrumentation	51
20	General View of Some of the Instruments Used	52
21	Vertical Response of Section Model with Different Damping Levels at Angle of Attack $\beta = 0^0$	53

LIST OF FIGURES (Cont.)

<u>Figure</u>		<u>Page</u>
22	Torsional Response of Section Model with Different Damping Levels at Angle of Attack $\beta = 0^0$	54
23	Vertical Response of Section Model with Damping Level 2 at Different Angles of Attack	55
24	Torsional Response of Section Model with Damping Level 2 at Different Angles of Attack	56
25	Aerodynamic Derivative $-H_1^*$ Extracted for Model with Different Damping Levels at Angle of Attack $\beta = 0^0$	57
26	Aerodynamic Derivative A_2^* Extracted for Model with Different Damping Levels at Angle of Attack $\beta = 0^0$	58
27	Prototype Critical Wind Speed for Torsional Flutter, Angle of Attack $\beta = 0^0$	59
28	Aerodynamic Derivative $-H_1^*$, Angle of Attack $\beta = 0^0$	60
29	Aerodynamic Derivative A_2^* , Angle of Attack $\beta = 0^0$	61
30	Aerodynamic Derivative $-H_1^*$, Angle of Attack $\beta = +3^0$	62
31	Aerodynamic Derivative A_2^* , Angle of Attack $\beta = +3^0$	63
32	Prototype Critical Wind Speed for Torsional Flutter, Angle of Attack $\beta = +3^0$	64
33	Aerodynamic Derivative $-H_1^*$, Angle of Attack $\beta = -3^0$	65
34	Aerodynamic Derivative A_2^* , Angle of Attack $\beta = -3^0$	66
35	Prototype Critical Wind Speed for Torsional Flutter, Angle of Attack $\beta = -3^0$	67
36	Aerodynamic Derivative $-H_1^*$, Angle of Attack $\beta = +6^0$	68

LIST OF FIGURES (Cont.)

<u>Figure</u>		<u>Page</u>
37	Aerodynamic Derivative A_2^* , Angle of Attack $\beta = +6^\circ$	69
38	Prototype Critical Wind Speed for Torsional Flutter, Angle of Attack $\beta = +6^\circ$	70
39	Aerodynamic Derivative $-H_1^*$, Angle of Attack $\beta = -6^\circ$	71
40	Aerodynamic Derivative A_2^* , Angle of Attack $\beta = -6^\circ$	72
41	Prototype Critical Wind Speed for Torsional Flutter, Angle of Attack $\beta = -6^\circ$	73
42	Prototype Critical Wind Speed for Torsional Flutter for Different Angles of Attack	74
43	Aerodynamic Derivative $-H_1^*$ for Model with Froude Number Similarity Sustained and Relaxed, $\beta = 0^\circ$	75
44	Aerodynamic Derivative A_2^* for Model with Froude Number Similarity Sustained and Relaxed, $\beta = 0^\circ$	76
45	Prototype Critical Wind Speed, Froude Number Similarity Sustained and Relaxed, $\beta = 0^\circ$	77
46	Aerodynamic Derivative A_2^* for Model with Froude Number Similarity Sustained and Relaxed, $\beta = +3^\circ$	78
47	Prototype Critical Wind Speed, Froude Number Similarity Sustained and Relaxed, $\beta = +3^\circ$	79
48	Aerodynamic Derivative A_2^* for Model with Froude Number Similarity Sustained and Relaxed, $\beta = -3^\circ$	80
49	Prototype Critical Wind Speed, Froude Number Similarity Sustained and Relaxed, $\beta = -3^\circ$	81
50	Aerodynamic Derivative A_2^* for Model with Froude Number Similarity Sustained and Relaxed, $\beta = +6^\circ$	82
51	Prototype Critical Wind Speed, Froude Number Similarity Sustained and Relaxed, $\beta = +6^\circ$	83

LIST OF FIGURES (Cont.)

<u>Figure</u>		<u>Page</u>
52	Aerodynamic Derivative A_2^* for Model with Froude Number Similarity Sustained and Relaxed, $\beta = -6^\circ$	84
53	Prototype Critical Wind Speed, Froude Number Similarity Sustained and Relaxed, $\beta = -6^\circ$	85
54	Prototype Critical Wind Speed for Different Angles of Attack, Froude Number Similarity Relaxed	86
55	Prototype Vertical Vortex-Induced Response for Different Angles of Attack	87
56	Prototype Vertical Accelerations Associated with Vortex-Induced Response for Different Angles of Attack	88
57	Prototype Speed Associated with Maximum Vortex-Induced Vertical Response	89
58	Strouhal Number Based on Vertical Vortex-Induced Response	90
59	Prototype Maximum Vertical Deflections Associated with Torsional Vortex-Induced Response	91
60	Prototype Maximum Vertical Accelerations Associated with Torsional Vortex-Induced Response	92
61	Prototype Speed Associated with Maximum Vortex-Induced Torsional Response	93
62	Strouhal Number Based on Torsional Vortex-Induced Response	94
63	Aerodynamic Derivative A_2^* , Froude Number Similarity Relaxed, $\beta = 0^\circ$	95
64	Aerodynamic Derivative A_2^* , Froude Number Similarity Relaxed, $\beta = +3^\circ$	96
65	Aerodynamic Derivative A_2^* , Froude Number Similarity Relaxed, $\beta = -3^\circ$	97
66	Aerodynamic Derivative A_2^* , Froude Number Similarity Relaxed, $\beta = +6^\circ$	98

LIST OF FIGURES (Cont.)

<u>Figure</u>		<u>Page</u>
67	Aerodynamic Derivative A_2^* , Froude Number Similarity Relaxed, $\beta = -6^0$	99
68	Prototype Critical Wind Speed	100
69	Maximum Vortex-Induced Response	101

LIST OF TABLES

<u>Table</u>		<u>Page</u>
1	Parameters for Prototype and "Exact" Model (Original Bridge Deck with Railings)	103
2	Parameters of Actual Model (Original Bridge Deck with Railings)	104

1. INTRODUCTION

The aerodynamics of suspended-span and cable-stayed bridges has been recognized as an important element in analysis and design of such structures. Related problems are studied today mainly in wind tunnels. Two basic approaches are being used. One employs a full aeroelastic model of a given bridge and requires a relatively large wind tunnel. The other employs a typical section of the bridge (so called the bridge section model). The wind-tunnel tests in this case are simplified and can be conducted in a smaller wind tunnel. The results of these tests are then supplemented by analytical considerations and finally assessments are made with regard to the full-bridge aerodynamic stability.

In the wind-engineering study, reported herein, a bridge section model has been employed for the proposed East Huntington Bridge (a concrete cable-stayed alternate) over the Ohio River, Huntington, West Virginia and Proctorville, Ohio. The main purpose of the work was to evaluate the bridge aerodynamic stability for a given range of the assumed bridge damping. Of particular interest was the critical wind speed for flutter-type instability and the range of amplitudes of the anticipated vortex-induced bridge oscillation. Only the smooth flow conditions, believed to give conservative estimates, Scanlan [1], were considered in the study. The aerodynamic derivatives defined by Scanlan and Tomko [2] were obtained for different configurations and they formed the basis for further computations related to the bridge aerodynamic stability. Results of the measurements of the model response in the speed region where vortex-shedding controlled the bridge motion were used in estimating the similar prototype bridge response.

The present report describes the mentioned investigations. The theoretical background, experimental configurations, testing procedures, instrumentation and data acquisition are presented in the next chapters. Some supplementary material is included in Appendices.

2. THEORETICAL BACKGROUND

2.1 Concept of the Bridge Section Model

The most common procedure in the wind-tunnel study of bridge aerodynamics is use of the bridge section model. The model represents a relatively short, typical section of the bridge span, built rigidly and to model scale. It is mounted on springs and allowed to oscillate in two degrees of freedom (vertical and torsional). The bridge deck geometry, inertia, and elastic properties are scaled for the section model according to certain similarity requirements.

2.2 Similarity Requirements

The basic requirement is the geometrical length scale (model-to-prototype) ratio λ_L to which all geometrical bridge deck details should be scaled. For a given length scale λ_L the mass per unit span of the model should be scaled according to the mass scale

$$\lambda_m = \lambda_L^2 . \quad (1)$$

Accordingly, the polar mass moment of inertia per unit span for the model should be modeled as follows

$$\lambda_I = \lambda_L^4 . \quad (2)$$

The scalings (1) and (2) are valid if the mass density of the bridge deck and the model are equal, that is when the density scale is equal to

$$\lambda_\rho = 1 . \quad (3)$$

Since both the prototype bridge and the model are immersed in the same medium (air) the similarity requirement for the aerodynamic forces can be simplified to the following form, Simiu and Scanlan [3]:

$$\left(\frac{U}{NB}\right)_m = \left(\frac{U}{NB}\right)_p \quad (4)$$

This condition requires that the frequency scale be given by

$$\lambda_N = \lambda_V \cdot \lambda_L^{-1} \quad (5)$$

where λ_V is the velocity scale. If the Froude number similarity

$$\left(\frac{U^2}{Bg}\right)_m = \left(\frac{U^2}{Bg}\right)_p \quad (6)$$

where g is the gravitational constant, is assumed then the velocity scale λ_V is related to the length scale

$$\lambda_V = \lambda_L^{1/2} \quad (7)$$

and, as a consequence of the relation (5), the frequency scale λ_N is also directly associated with the length scale

$$\lambda_N = \lambda_L^{-1/2} \quad (8)$$

It can be easily checked that the Reynolds number similarity

$$\left(\frac{UB}{\nu}\right)_m = \left(\frac{UB}{\nu}\right)_p \quad (9)$$

where ν is the kinematic viscosity, cannot be attained in such situation. However, if the model Reynolds number is sufficiently high the aerodynamic forces acting on the (usually bluff) bridge do not vary significantly with Reynolds number and the similarity requirement (9) can be relaxed, Scanlan [1].

2.3 Bridge Aerodynamic Stability

Equations of motion for the bridge section model, assumed to be symmetrical about the vertical plane of the roadway centerline, can be written in the following form:

$$\begin{aligned}
 m \left[\ddot{h} + 2\zeta_h \omega_h \dot{h} + \omega_h^2 h \right] &= L \\
 I \left[\ddot{\alpha} + 2\zeta_\alpha \omega_\alpha \dot{\alpha} + \omega_\alpha^2 \alpha \right] &= M
 \end{aligned} \tag{10}$$

where

- m = model mass per unit span,
 I = model polar mass moment of inertia per unit span,
 $h(\alpha)$ = vertical (torsional) deflection of the model
 assumed uniform over the span,
 $\zeta_h(\zeta_\alpha)$ = damping ratio-to-critical for vertical (torsional)
 degree-of-freedom,
 $\omega_h(\omega_\alpha)$ = circular natural frequency for vertical (torsional)
 degree-of-freedom, and
 $L(M)$ = lift force (pitching moment) per unit span.

It is a common practice to assume that the right-hand sides of equation (10) can be written as the following linear combination

$$\begin{aligned}
 L &= L_{se} + L_b \\
 M &= M_{se} + M_b
 \end{aligned}$$

where

- $L_b(M_b)$ = lift force (pitching moment) induced through
 buffeting by turbulence and
 $L_{se}(M_{se})$ = self-excited lift force (pitching moment) induced
 by oscillation of the model.

In a smooth flow only the self-excited terms are retained and in a linearized model proposed by Scanlan and Tomko [2] they are expressed as follows:

$$L_{se} = \frac{1}{2} \rho U^2 (2B) [KH_1^* \frac{\dot{h}}{U} + KH_2^* \frac{B\dot{\alpha}}{U} + K^2 H_3^* \alpha]$$

and

(11)

$$M_{se} = \frac{1}{2} \rho U^2 (2B^2) [KA_1^* \frac{\dot{h}}{U} + KA_2^* \frac{B\dot{\alpha}}{U} + K^2 A_3^* \alpha] ,$$

where

ρ = air density,

U = oncoming wind velocity,

B = deck width of the model,

$K = \frac{B\omega}{U}$ = reduced frequency, ω being the actual oscillation circular frequency, $\omega = 2\pi N$, and

H_i^* and A_i^* = nondimensional aerodynamic derivatives, functions of K ($i=1,2,3$).

In a typical situation of unstreamlined bridge decks the self-excited oscillations occur in uncoupled modes leading in most cases to a one degree-of-freedom flutter instability. In this case only the derivatives H_1^* , A_2^* and A_3^* play an important role in equations (11). For some bridge decks (especially those with H-type geometrical shape) the magnitude of the derivative A_3^* is small in comparison with the contribution of the derivative A_2^* in equation (11). In such cases, after some rearrangements, equation (11) can be written as follows:

$$\ddot{h} + 2\zeta_h \omega_h \dot{h} + \omega_h^2 h = \frac{\rho B^2 \omega}{m} H_1^* \dot{h}$$

and

(12)

$$\ddot{\alpha} + 2\zeta_\alpha \omega_\alpha \dot{\alpha} + \omega_\alpha^2 \alpha = \frac{\rho B^4 \omega}{I} A_2^* \dot{\alpha} .$$

Equation (12) can be further modified to give

$$\ddot{h} + 2\gamma_h \omega_h \dot{h} + \omega_h^2 h = 0$$

and

$$\ddot{\alpha} + 2\gamma_\alpha \omega_\alpha \dot{\alpha} + \omega_\alpha^2 \alpha = 0 ,$$

(13)

where

$$\gamma_h = \zeta_h - \frac{\rho B^2}{2m} H_1^*$$

and

$$\gamma_\alpha = \zeta_\alpha - \frac{\rho B^4}{2I} A_2^* .$$

(14)

Now they describe free, damped oscillations in vertical and torsional degrees-of-freedom, mutually uncoupled, with damping being altered by the current value of the aerodynamic derivative, H_1^* and A_2^* , respectively. It is easy to observe from the relation (14) that measurements of damping γ_i ($i = h, \alpha$) of the freely oscillating model for one degree-of-freedom motion (h or α), when the mechanical damping of the model ζ_i ($i = h, \alpha$) is known, lead to determining the magnitude of the aerodynamic derivative H_1^* or A_2^* as a function of velocity U or, more generally, the reduced frequency K or, more commonly, the reduced velocity $\frac{U}{NB}$.

Unstreamlined bridge decks usually exhibit one degree-of-freedom flutter instability in torsion. The condition for this situation to occur can be stated for the bridge section model as follows:

$$\zeta_\alpha - \frac{\rho B^4}{2I} A_2^* = 0$$

(15)

or

$$A_2^* \left(\frac{U}{NB} \right) = \frac{2I}{\rho B^4} \zeta_\alpha .$$

(16)

The quantity on the right-hand side can be computed and equation (16) can be solved for the critical flutter speed if the aerodynamic derivative (being a function of the reduced velocity $\frac{U}{NB}$) is known. It can be easily shown (see Appendix A) that the same condition for the critical speed holds for the full-span of the bridge if only the fundamental mode of oscillation in torsion is taken into account and the inertial and geometrical properties of the bridge deck are uniform over the span.

2.4 Vortex-Induced Response

Vortex-induced motion of the bridge deck occurs at fairly low wind speeds. The maximum amplitude of uncoupled harmonic oscillation in the vertical or torsional degree-of-freedom is attained when the frequency of vortex-shedding coincides with the natural frequency of the vertical or torsional motion. Usually the fundamental frequency in h-motion is lower than in α -motion. Therefore, during wind-tunnel tests as wind speed is being increased the vortex-shedding induced oscillation usually occurs first in h-motion followed by a weaker oscillation in α -motion at higher speed.

The equation of motion for the vertical degree-of-freedom (12) of the bridge section model can be modified as follows in presence of the vortex-induced oscillation, Scanlan [1]:

$$m[\ddot{h} + 2\zeta_h \omega_h \dot{h} + \omega_h^2 h] = \frac{1}{2} \rho U^2 (2B) [KH_0^* \frac{\dot{h}}{U} + C_L \sin \omega t] \quad (17)$$

where

H_0^* plays role similar to H_1^* in Equation (12),

C_L = lift coefficient, and

ω = vortex-shedding frequency ($\omega \approx \omega_h$).

Equation (17) can be rewritten in a slightly different form

$$m[\ddot{h} + 2\gamma_h \omega_h \dot{h} + \omega_h^2 h] = P_0 \sin \omega t \quad (18)$$

where

$$\gamma_h = \zeta_h - \frac{\rho B^2}{2m} H_0^*$$

and

$$P_0 = \rho U^2 B C_L .$$

The amplitude of the steady-state response of the oscillator described by Equation (18)

$$h_0 = \frac{P_0}{m[(\omega_h^2 - \omega^2)^2 + (2\gamma_h \omega \omega_h)^2]^{1/2}}$$

can be approximated as follows when $\omega \approx \omega_h$ and damping is low:

$$h_0 \approx \frac{P_0}{2m\gamma_h \omega_h^2} = \frac{\rho U^2 B C_L}{2m\gamma_h \omega_h^2} . \quad (19)$$

If the amplitude h_0 and the damping ratio-to-critical γ_h are measured, then the lift coefficient C_L can be estimated to be

$$C_L = \frac{2h_0 \gamma_h m \omega_h^2}{\rho U^2 B} . \quad (20)$$

Also the current value of the aerodynamic derivative H_0^* can be estimated--

$$H_0^* = (\zeta_h - \gamma_h) \frac{2m}{\rho B^2} . \quad (21)$$

Based on this data obtained from the wind-tunnel tests of the bridge section model, predictions can be made with regard to the full-span vortex-induced response. The reasoning is similar to that presented in Appendix A. The vertical displacement $h(x,t)$, where x is a spanwise coordinate and t is time, can be expressed in terms of the

vertical fundamental spanwise mode $\Psi_1(x)$ and the generalized coordinate $h_1(t)$ --

$$h(x,t) = h_1(t)\Psi_1(x) . \quad (22)$$

An equation of motion for the whole span, similar in form to equation (18), can be written

$$m(x)[\ddot{h}(x,t) + 2\gamma_h\omega_h\dot{h}(x,t) + \omega_h^2 h(x,t)] = P_0\sin\omega t$$

and modified by introducing expression (22), multiplying by $\Psi_1(x)$ and integrating along the span. This gives

$$m_1[h_1 + 2\gamma_h\omega_h\dot{h}_1 + \omega_h^2 h_1] = P_{01}\sin\omega t \quad (23)$$

where

$$m_1 = \int_0^L m(x)\Psi_1^2(x)dx$$

and

$$P_{01} = P_0 \int_0^L \Psi_1(x)dx .$$

The amplitude of the steady-state response of the oscillator (23) is similar to the expression (19)--

$$h_{01} \approx \frac{P_{01}}{2m_1\gamma_h\omega_h^2} = \frac{\rho U^2 BC_L \int_0^L \Psi_1(x)dx}{2m_1\omega_h^2 \gamma_h} . \quad (24)$$

The maximum of the vortex-induced full-span response can be computed from (22) and (24) to obtain

$$h_0(x) \Big|_{\max} \approx \frac{\rho U^2 BC_L \int_0^L \Psi_1(x)dx}{2m_1\omega_h^2 \gamma_h} \Psi_1(x) \Big|_{\max} . \quad (25)$$

When the bridge deck is uniform along the span this formula can be simplified to

$$h_0(x) \Big|_{\max} \approx \frac{\rho U^2 B C_L}{2 m \omega_h^2 \gamma_h} F_L \quad (26)$$

where

$$F_L = \frac{\int_0^L \psi_1(x) dx}{\int_0^L \psi_1^2(x) dx} \psi_1(x) \Big|_{\max} . \quad (27)$$

It should be pointed out that the estimate (26) is strongly conservative since perfectly correlated vortex-shedding over the whole span has been assumed. Similar considerations for the vortex-induced response in the torsional degree-of-freedom are summarized in Appendix B.

3. WIND-TUNNEL FACILITY AND BRIDGE SECTION MODEL

3.1 Wind-Tunnel Facility

The experiments reported herein were conducted in the structural aerodynamics wind tunnel located in the Fluid Dynamics and Diffusion Laboratory at Colorado State University.

The structural aerodynamics wind tunnel shown in Figure 1 is an open circuit facility driven by a constant-pitch propeller. The test section is nominally 3 ft square and approximately 12 ft long with flow entering through a contraction having a 4:1 contraction ratio. The mean velocity is adjustable continuously from 1 - 30 fps. The mean velocity is constant across the test section except very close to the wind-tunnel walls where the wall boundary layer extends up to approximately 1 inch. The background turbulence intensity is low and does not exceed 1.5 percent.

3.2 Bridge Section Model Description and Scaling

The concept of a bridge section model has been described in Chapter 2. A typical arrangement used in the wind-tunnel tests of the model is shown in Figure 2. The section model, suspended on eight vertical, helical springs, is supplied with end plates to ensure predominantly two-dimensional flow around the deck.

A general view of the East Huntington Bridge investigated in the present study is shown in Figure 3 and the Frontispiece. Figure 4 shows the fundamental modes of oscillation in bending and torsion and Figure 5 presents details of the bridge deck. Basic properties of the prototype bridge are gathered in Table 1. Initial considerations indicated that a 1:80 geometrical scale bridge section model would be optimal for the present study. The scaled geometry of the model is shown in Figure 6.

All the basic physical properties of the model were scaled according to the similarity requirements discussed in Chapter 2.2 and they are collected in Table 1 as the values for the "exact" model. During the initial series of the wind-tunnel tests the Froude number similarity was sustained and it is reflected in Table 1. Subsequently this requirement was relaxed as will be discussed later.

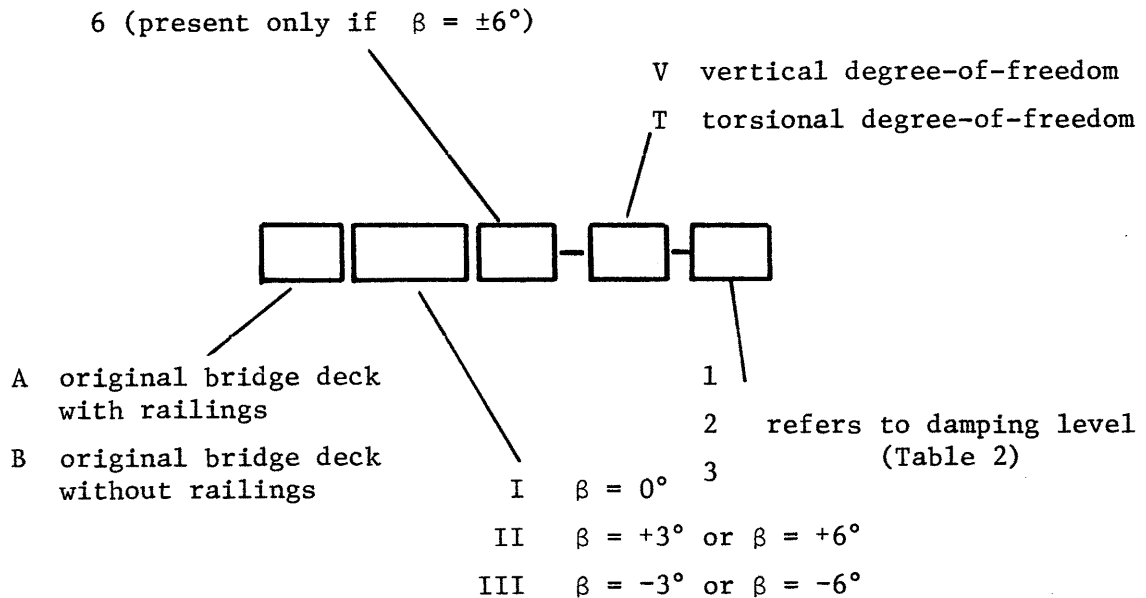
3.3 Model Construction and Details

Basically two materials were used to construct the bridge section model. The main body of the model corresponding to the concrete part of the prototype bridge deck was made of magnesium. The prototype H sections were modeled with plastic I-beams. The model was constructed in such a way that an angle of attack could be changed from -6 to $+6$ degrees. Elements of the model support were made of aluminum and light brass tubing. The overall length of the model was 35.5 in. An overall view of the model is shown in Figure 7 and the model placed in the wind tunnel is presented in Figure 8. Figure 9 shows a typical strain-gage transducer (a channel with a pair of strain gages to monitor strains of bending) and one of four electromagnets used for simultaneous release of the model to generate uniform harmonic oscillation of the model. The main geometrical and physical properties of the model listed in Table 2 under Model are compared with the target values of the "exact" model from Table 1. The remaining columns of Table 2 refer to the properties of the model at three different damping levels. The viscous damping was introduced by a series of thin vertical plates attached to both model supporting bars as shown in Figure 10. The plates, shown in detail in Figure 11, submerged in a hydraulic fluid, oscillated together with the model. The amount of damping introduced could be adjusted by

changing the number of plates. The damping level 1 defined in Table 2 refers to the bridge section model with the dampers containing only one plate each when oscillating in air. The damping levels 2 and 3 refer to the dampers with 1 and 3 plates oscillating in the hydraulic fluid. Figures 12, 13 and 14 show uncoupled decaying oscillation of the model in still air at the damping levels 1, 2 and 3.

3.4 Basic Experimental Configurations

The bridge section model has been tested at different angles of attack-- 0° , $\pm 3^\circ$ and $\pm 6^\circ$. Most of the tests were conducted for the original bridge deck with railings (traffic barriers); Configurations A in Figure 15. Some additional tests were performed with railings removed (original bridge deck with railings); Configurations B in Figure 15. Generally configurations were denoted in the following manner:



Finally, Figure 16 provides a definition of the angle of attack and the degrees-of-freedom of the model. The main geometrical dimensions of the model are shown in Figure 17.

4. TESTING PROCEDURES

4.1 Overall Bridge Section Model Response

An overall response of the bridge section model was measured for different configurations and a wide range of wind speeds. For a given wind speed the model was set at rest and then released. After a sufficiently long period of time (a few minutes) measurements of vertical and torsional model oscillations were taken. The velocity was then changed and the process repeated. In this way velocity regions of the vortex-induced oscillations and flutter instability were initially established.

4.2 Aerodynamic Derivatives

The aerodynamic derivatives considered in Chapter 2.3, formulas (14), express changes in total damping of the model.

$$H_1^* = (\zeta_h - \gamma_h) \frac{2m}{\rho B^2}$$

and

$$A_2^* = (\zeta_\alpha - \gamma_\alpha) \frac{2I}{\rho B^4}$$

(28)

where

ζ_h (ζ_α) is model damping ratio-to-critical in still air for vertical (torsional) degree-of-freedom; i.e., mechanical damping of the model

γ_h (γ_α) is model damping ratio-to-critical at a given wind speed for vertical (torsional) degree-of-freedom; i.e., mechanical plus aerodynamic damping.

In order to measure the model damping in uncoupled vertical or torsional motion at a given wind speed, the model was given an initial displacement in one degree-of-freedom (with the other degree restrained) and then released. The model was supported at four corners and simultaneously released using four electromagnets wired in series. Subsequent harmonic (decaying or divergent) model oscillation was recorded for

further analysis. A series of tests was conducted with different mechanical damping of the model in order to establish the optimal damping level for the most accurate damping measurements. Most of the measurements were taken with the Froude number similarity sustained. However this similarity requirement was relaxed later to obtain data for the higher velocity range necessary for flutter computations of the prototype bridge with higher damping.

4.3 Vortex-Induced Response

Estimation of the vortex-induced response for the prototype bridge was discussed in Chapter 2.4 and Appendix B. It follows that basically three experimental parameters for each degree of freedom are necessary for the analysis:

U_h, γ_h, h_o for vertical motion, and

$U_\alpha, \gamma_\alpha, \alpha_o$ for torsional motion

where

$U_h(U_\alpha)$ = speed at which the maximum vortex-induced oscillation in vertical (torsional) motion occurs,

$\gamma_h(\gamma_\alpha)$ = total damping ratio-to-critical for vertical (torsional) motion at $U_h(U_\alpha)$, and

$h_o(\alpha_o)$ = amplitude of the steady-state oscillation for vertical (torsional) motion at $U_h(U_\alpha)$.

In order to measure these parameters for each configuration the wind speed was gradually changed within the range established earlier from the measurements of the overall model response. Deflections of the model free to oscillate in one degree-of-freedom (with the other degree restrained) were monitored until the maximum amplitude of the steady-state oscillation was reached. Next the model was given an initial displacement in the degree-of-freedom considered. Finally the model

was released and its subsequent harmonic oscillations were recorded for further analysis.

5. INSTRUMENTATION

5.1 Flow Measurement

The flow characteristics (velocity and turbulence intensity profile) were measured using a cylindrical hot film in conjunction with a TSI constant-temperature anemometer. Current values of the mean wind speed during the bridge section-model tests were measured by a Prandtl tube connected to a differential manometer with a sufficiently high resolution.

5.2 Measurements of the Bridge Section-Model Response

The bridge section-model response was measured using four strain-gage transducers shown in Figure 18. Two of the transducers monitored vertical motion (analog signals from both of them were added) and the remaining two (with signals mutually subtracted) detected torsional deflection. The transducers were connected to a signal conditioner, Figure 19. Next the two signals (proportional to a vertical and torsional deflection of the model) underwent a secondary amplification with a low-pass filtering. The voltages obtained were monitored on a dual-beam oscilloscope, recorded on a two-channel strip-chart recorder and fed to a minicomputer as is schematically shown in Figure 19. Figure 20 shows basic instruments used in the measurements.

6. DATA ACQUISITION

6.1 Overall Bridge Section-Model Response

The overall bridge section-model response data was reduced using a minicomputer (HP-1000). During experiments the time histories of the vertical and torsional model oscillations were directly fed to the minicomputer on line. The mean values and the normalized root-mean-squares of the model deflections were then plotted versus reduced wind speed $\frac{U}{N_i B}$ ($i = h, \alpha$) for each configuration.

6.2 Aerodynamic Derivatives and Stability

Time series of the vertical and torsional oscillation of the bridge model, recorded on a strip-chart recorder, were used to compute the aerodynamic derivatives (28). Each record was divided into three sections. For each section the logarithmic decrement of damping

$$\delta_i = \frac{1}{n} \ln \left(\frac{A_{0i}}{A_{ni}} \right) \quad (i = h, \alpha) \quad (29)$$

where

A_{0i} = initial amplitude of motion, and

A_{ni} = amplitude of motion after n cycles

and the damping ratio-to-critical

$$\gamma_i \approx \frac{\delta_i}{2\pi} \quad (i = h, \alpha) \quad (30)$$

were computed. Since the damping considered was low, the approximate formula (30) was used instead of the exact expression

$$\gamma_i = \frac{1}{\sqrt{1 + \left(\frac{2\pi}{\delta_i} \right)^2}} \quad (i = h, \alpha). \quad (31)$$

Mean values of γ_i (taken over three record sections) were employed in computations. The aerodynamic derivatives (28) were computed using physical properties $\zeta_h, \zeta_\alpha, m, I, B$ of the model

$$H_1^* = \left(\zeta_{hm} - \gamma_{hm} \right) \frac{2m}{\rho B_m^2}$$

and

$$A_2^* = \left(\zeta_{\alpha m} - \gamma_{\alpha m} \right) \frac{2I_m}{\rho B_m^4} \quad (32)$$

where

()_m refers to the model.

The nondimensional derivatives (32) were plotted versus nondimensional wind speed $\frac{U}{N_i B}$ ($i = h, \alpha$) where $N_h(N_\alpha)$ is the natural frequency for vertical (torsional) motion.

The one degree-of-freedom torsional flutter instability is expressed by condition (16). Estimation of the prototype bridge critical speed U_{cp} should be based on the physical properties of the prototype--

$$A_0^* \left(\frac{U_{cp}}{N_{\alpha p} B_p} \right) = \frac{2I_p}{\rho B_p^4} \zeta_{\alpha p} \quad (33)$$

where

()_p refers to the prototype bridge.

The requirement (33) and the aerodynamic derivative A_2^* (32) were used to compute the critical speed as a function of the assumed prototype bridge mechanical damping. The calculations were performed for the different bridge configurations.

6.3 Vortex-Induced Response

The experimental parameters U_h , γ_h , h_0 , U_α , γ_α and α_0 required for estimation of the vortex-induced response were specified in Chapter 4.3. Also the method of determining speeds U_h and U_α was discussed. The remaining four quantities referring to the model damping and amplitude of the model steady-state response were determined from the time histories of vertical and torsional harmonic oscillations at speeds U_h and U_α , respectively. Damping was estimated in a way similar to the technique described in Chapter 6.2 except for the computations of the logarithmic decrement. Due to the simultaneous presence of the steady and decaying oscillations the formula (29) should be modified as follows:

$$\delta_i = \frac{1}{n} \ln \left(\frac{A_{0i} - i_0}{A_{ni} - i_0} \right) \quad (i = h, \alpha) \quad (34)$$

where

$h_0(\alpha_0)$ is amplitude of the steady vertical (torsional) oscillation

Once the experimental parameters were estimated, further computations were performed in order to determine the prototype bridge vortex-induced oscillation. The general procedure for the response in vertical degree-of-freedom was described in Chapter 2.4. It should be stressed that the lift coefficient C_L (20) and the aerodynamic derivative H_0^* (21) were computed using the physical properties for the model as follows:

$$C_L = \frac{2h_0 \gamma_{hm}^m \omega_{hm}^2}{\rho U_{hm}^2 B_m} \quad (35)$$

and

$$H_0^* = \left(\zeta_{hm} - \gamma_{hm} \right) \frac{2m_m}{\rho B_m^2} \quad (36)$$

where

()_m refers to the bridge model.

The final prediction (26) was computed using physical properties for the prototype bridge

$$h_0(x) \Big|_{\max} \approx \frac{\rho U_{hp}^2 C_L}{2m_p \omega_{hp}^2 \gamma_{hp}} F_L \quad (37)$$

where

()_p refers to the prototype bridge.

The damping ratio γ_{hp} was computed for a given prototype mechanical damping ζ_{hp} from (21)

$$\gamma_{hp} = \zeta_{hp} - H_0^* \frac{\rho B_p^2}{2m_p} \quad (38)$$

The coefficient F_L given by (27) (computed by integration of the mode shown in Figure 4) is equal to 1.41.

Similar comments are valid for estimation of the prototype bridge vortex-induced response in torsion described in Appendix B. The coefficient F_M is equal to 1.39. Since the vortex-induced responses were harmonic

$$i = i_0 \sin \omega_i t \quad (i = h, \alpha) \quad (39)$$

the corresponding maximum amplitudes of accelerations a_i were also computed from

$$a_i = \omega_i^2 i_0 \quad (i = h, \alpha) . \quad (40)$$

7. RESULTS

The main purpose of this study was estimation of the aerodynamic stability and the vortex-induced response of the prototype original bridge deck with railings. The details of the bridge deck geometry are shown in Figure 6. Evaluation of the effects of presence of solid railings upon the aerodynamic stability of the bridge was the secondary goal. Therefore, most of the results refer to the bridge deck with railings.

7.1 Original Bridge Deck with Railings

7.1.1 Overall Bridge Section-Model Response

The overall bridge section-model response was measured for different configurations. Figures 21 and 22 show the response of the model with different mechanical damping:

damping level 1 (D.L.1)	$\zeta_v = 0.12\%$, $\zeta_T = 0.17\%$
damping level 2 (D.L.2)	$\zeta_v = 0.71\%$, $\zeta_T = 0.75\%$
damping level 3 (D.L.3)	$\zeta_v = 2.3 \%$, $\zeta_T = 2.1 \%$

The plots show a one degree-of-freedom torsional flutter instability for the model with low damping (D.L.1) at relatively high reduced velocity, and vortex-induced oscillations both in torsional and vertical motion at lower reduced wind speeds. The magnitude of the vortex-induced oscillation decreases with increasing damping. In addition the rolling motion of the model (oscillation about the central mode) was observed for the model with the lowest damping (D.L.1) as is shown in Figure 21. Evaluation of the effects of the angle of attack upon the model response is summarized in Figures 23 and 24. The study was conducted for the model with intermediate damping (D.L.2). It can be seen that the model aerodynamic stability and the vortex-induced response depends upon the angle of attack. The model proved to be torsionally

unstable at the angle of attack $\beta = -3^\circ$ while being stable for the remaining angles of attack $\beta = \pm 6^\circ, +3^\circ,$ and 0° in the range of wind speeds considered, Figure 24.

7.1.2 Aerodynamic Derivatives and Stability

On theoretical grounds aerodynamic derivatives should be independent of the level of the mechanical damping of the model tested, Scanlan [1,2]. Figures 25 and 26 experimentally confirm this statement. Some discrepancies between values of the aerodynamic derivatives $-H_1^*$ and A_2^* occur but they should be related to the accuracy of the damping estimation. A substantial departure of the aerodynamic derivative A_2^* based on the model tests with the highest mechanical damping (D.L.3) can be attributed to the errors in damping evaluation of the fast decaying harmonic oscillation, Bienkiewicz [4]. The prototype critical speed for the torsional flutter (angle of attack $\beta = 0^\circ$) plotted versus assumed mechanical damping of the prototype bridge is shown in Figure 27. It is seen that the results of computations based on the A_2^* derivative for D.L.1 and D.L.2 are close and can be approximated by a parabolic analytical expression. It was concluded that the most accurate damping estimation was obtained for the model with intermediate damping--D.L.2. Therefore, further wind-tunnel tests were conducted with the model having mechanical damping at such a level. Figures 28 and 29 show once more the aerodynamic derivatives $-H_1^*$ and A_2^* extracted from the tests of the model with damping level D.L.2. Results of the wind-tunnel tests and computations for different angles of attack $\beta = \pm 3^\circ, \pm 6^\circ$ are presented in Figures 30 to 41. Plots of the derivatives $-H_1^*$ and A_2^* are accompanied by graphs of the prototype critical wind speed plotted versus the assumed prototype bridge

mechanical damping. On some of those plots, namely for $\beta = 0^\circ$ and $\beta = -3^\circ$, the critical speed for the bridge section model measured in the wind tunnel was also marked. It can be seen that for these particular cases the experimental values for the bridge section model are close to the values computed for the prototype bridge. Figure 42 summarizes data referring to the bridge aerodynamic stability obtained for different values of the angle of attack. The results presented were based on the experimental data obtained from the wind-tunnel tests of the model with the Froude number similarity sustained. It can be seen from Figure 42 that for the prototype damping ratio-to-critical of the order of $\zeta_T = 0.5$ percent the bridge is the most unstable at the angle of attack $\beta = -6^\circ$. For the higher damping ($\zeta_T > 0.8$ percent) the most unstable configuration is at $\beta = -3^\circ$.

It was expected that the similar situation would hold for a damping ratio higher than $\zeta_T = 1$ percent. In order to compute the critical speed at higher mechanical damping more data points for the aerodynamic derivative A_2^* were needed at wind speeds higher than actually obtainable in the structural aerodynamics wind tunnel. Therefore, it was decided to change the velocity scale for the model by relaxing the Froude number similarity sustained in the previous tests. This similarity requirement can be treated as optional in the bridge section-model studies where gravitational effects are believed to be negligible, Scanlan [1,5]. The aerodynamic derivatives $-H_1^*$ and A_2^* obtained for the model with the Froude number similarity sustained and relaxed are compared in Figures 43 and 44 for the angle of attack $\beta = 0^\circ$. The agreement between the derivatives obtained is fairly good. Figure 45 shows a plot of the prototype bridge critical speed versus assumed

mechanical damping of the bridge, computed using the derivative A_2^* obtained with Froude number similarity relaxed. This time the damping range covered extends to values higher than considered previously when the Froude number similarity was sustained. Again the agreement between values for these two configurations is good. Similar data for the angles of attack $\beta = \pm 3^\circ, \pm 6^\circ$ are presented in Figures 46 to 53. The aerodynamic derivatives $-H_1^*$ and A_2^* with the Froude number similarity relaxed were extracted for higher wind speeds only. They are compared with the derivatives obtained previously when the similarity was sustained. The same comparison is done for the prototype bridge critical speeds. The summary of data related to the prototype bridge aerodynamic stability (similar to that presented in Figure 42) is shown in Figure 54. As anticipated earlier the prototype bridge with the damping ratio higher than 1 percent is the most unstable at the angle of attack $\beta = -3^\circ$ and $\beta = 0^\circ$. Increase of the bridge damping ratio above $\zeta_T = 0.9$ percent leads to a substantial increase of the bridge stability at the remaining angles of attack-- $\beta = +3^\circ$ and $\pm 6^\circ$. The lowest critical speed at the bridge damping ratio $\zeta_T = 2$ percent occurs at $\beta = -3^\circ$ and is equal to 240 mph.

7.1.3 Vortex-Induced Response

Estimation of the vortex-induced response was based on the experimental data obtained from the wind-tunnel tests of the model with the Froude number similarity sustained. Figure 55 shows the computed normalized amplitudes of the prototype bridge oscillation in vertical degree-of-freedom for various angles of attack ($\beta = 0^\circ, \pm 3^\circ, \pm 6^\circ$) and a wide range of the assumed prototype damping. The corresponding reduced accelerations (g is the acceleration of gravity) are presented

in Figure 56. It can be seen that the highest vortex-induced amplitudes of oscillation and acceleration occur at the angles of attack $\beta = -3^\circ$ and $\beta = -6^\circ$ for the bridge with the damping ratio-to-critical higher than 0.5 percent. The prototype wind speed corresponding to the maximum of the vortex-induced vertical response is plotted versus angle of attack in Figure 57. A similar plot for the Strouhal number is shown in Figure 58. The Strouhal number

$$St = \frac{N A}{U} \quad (39)$$

is based on the cross-wind bridge deck dimension A defined in Figure 17. Similar data for the torsional degree-of-freedom is presented in Figures 59-62.

The results show that the maximum amplitudes of the vortex-induced oscillation for the vertical motion do not exceed 0.5 percent of the width of the bridge deck B for the prototype bridge damping ratio higher than 1.5 percent. Equivalent linear amplitudes $\alpha \cdot B/2$ for the torsional motion are roughly 25 percent of the vertical amplitudes. The corresponding accelerations are lower than 2.5 percent of g ($g = 32.17 \text{ ft/sec}^{-2}$) in the vertical degree-of-freedom and less than 1 percent of g in torsion.

7.2 Original Bridge Deck without Railings

7.2.1 Aerodynamic Derivatives and Stability

Only the aerodynamic derivative A_2^* was extracted for the original bridge deck without railings. The angles of attack considered were the same as in the previous tests with the original bridge deck with railings ($\beta = 0^\circ, \pm 3^\circ, \pm 6^\circ$). The derivatives obtained are shown in Figures 63-67. Figure 68 summarizes results of computations of the

prototype bridge critical speed for the one degree-of-freedom torsional flutter of the bridge deck without railings. The effects of railings on the critical wind speed can be assessed comparing Figure 68 (the original bridge deck without railings) and Figure 54 (the original bridge deck with railings). It can be seen that the bridge without railings is more unstable for the higher damping level ($\zeta_T > 0.9$) than the bridge with the railings. The lowest critical speed over the range of damping considered occurs at different angles of attack for the two cases investigated. It is approximately 30 percent lower for the bridge deck without railings for the intermediate bridge damping--the bridge damping ratio-to-critical ζ_T in the range from 0.6 percent to 1.5 percent. This difference decreases to about 17 percent for higher damping--1.6 percent $< \zeta_T < 2.3$ percent.

7.2.2 Vortex-Induced Response

The vortex-induced response of the original bridge deck section without railings was much smaller than response of the model with railings. The largest deflections occurred for the vertical motion at the angle of attack $\beta = -6^\circ$. The corresponding maximum amplitude of the prototype bridge was computed for this case and it is shown in Figure 69. It can be seen (by comparing Figures 69 and 55) that the extreme vortex-induced amplitude of motion is approximately six times lower for the bridge deck without railings than for the deck with the railings.

8. CONCLUSIONS

- A. The wind-tunnel tests of the bridge section model with different mechanical damping confirmed that the aerodynamic derivatives were independent of the damping level used.
- B. Accuracy of the derived aerodynamic derivatives is affected by the magnitude of mechanical damping of the bridge-section models.
- C. Relaxation of the Froude number similarity parameter did not affect the experimental results.
- D. The bridge-section model exhibited (for the range of angles of attack $-6^\circ \leq \beta \leq +6^\circ$) one degree-of-freedom torsional flutter with the critical speed dependent upon mechanical damping of the model.
- E. The vortex-induced response for vertical and torsional degree-of-freedom ($-6^\circ \leq \beta \leq +6^\circ$) occurred at speeds much lower than the critical wind speed. The amplitude of oscillation was dependent on the damping level of the model.
- F. Estimation for the prototype bridge with railings showed that for the prototype torsional damping of about $\zeta_T = 0.5$ percent the bridge was the most unstable at the angle of attack $\beta = -6^\circ$. For higher damping ($\zeta_T > 0.8$ percent) the most unstable configuration was at $\beta = -3^\circ$.
- G. The lowest critical wind speed for the prototype bridge with railings at the bridge damping ratio (in torsion) $\zeta_T = 2$ percent was estimated to be 240 mph. For higher damping this value is expected to increase.

- H. The bridge deck without railings is more unstable for the higher damping level than the deck with railings.
- I. The minimum critical wind speed for the prototype bridge without railings is approximately 30 percent lower than for the bridge with railings at the intermediate damping level ($0.6 \text{ percent} < \zeta_T < 1.5 \text{ percent}$). This difference decreases to about 17 percent for higher damping ($1.6 \text{ percent} < \zeta_T < 2.3 \text{ percent}$).
- J. It follows from H and I that the presence of railings increases the critical wind speed for the torsional flutter.
- K. The vortex-induced oscillations for the vertical and torsional degrees-of-freedom were estimated to occur for the prototype bridge with railings at 12-15 mph and 40-45 mph, respectively, depending on the angle of attack ($-6^\circ \leq \beta \leq 6^\circ$).
- L. The maximum vortex-induced amplitudes of oscillation and acceleration occurred at the angles of attack $\beta = -3^\circ$ and $\beta = -6^\circ$ for the bridge deck with railings and torsional damping $\zeta_T > 0.5 \text{ percent}$.
- M. The highest amplitudes of vertical oscillation (estimated for the prototype bridge with railings) did not exceed 0.5 percent of the width of the bridge deck B for the damping ratio $\zeta_T > 1.5 \text{ percent}$. Equivalent linear amplitudes $\alpha \cdot \beta/2$ in torsion were roughly 25 percent of the vertical amplitudes.
- N. The corresponding accelerations were lower than 2.5 percent of g ($g = 32.17 \text{ ft/sec}^{-2}$) for the vertical degree-of-freedom and less than 1 percent of g in torsion.

- O. Removing of the railings substantially reduced the vortex-induced oscillations. The maximum response occurred at the same angle of attack as for the bridge with railings ($\beta = -6^\circ$, compare L) but its amplitude (in vertical motion) was reduced by a factor of about six. The response at the remaining configurations was much lower.
- P. Effects of removing the railings can be summarized for the prototype bridge with the mechanical damping $\zeta_T = 2$ percent as follows:
1. the minimum critical wind speed for the torsional flutter is reduced from approximately 240 mph to about 200 mph, and
 2. the maximum vortex-induced response is reduced by a factor of six.

9. REFERENCES

- [1] Scanlan, R. H., "Recent Methods in the Application of Test Results to the Wind Design of Long, Suspended-Span Bridges," Report No. FHWA-RD75-115, October 1975.
- [2] Scanlan, R. H. and Tomko, J. J., "Airfoil and Bridge Deck Flutter Derivatives," Jnl. Eng. Mech. Div., ASCE, Vol. 97, EM6, December 1971, pp. 1717-1737.
- [3] Simiu, E. and Scanlan, R. H., Wind Effects on Structures: An Introduction to Wind Engineering, John Wiley and Sons, Inc., 1978.
- [4] Bienkiewicz, B., "On Errors Involved in Damping Evaluation for Wind-Tunnel Tests of Bridge Section Models," Unpublished Notes, Fluid Mechanics and Wind Engineering Program, Colorado State University, Fort Collins.
- [5] Scanlan, R. H., "The Action of Flexible Bridges under Wind, Pt. I: Flutter Theory," Jnl. Sound and Vibration, Vol. 60, No. 2, 1978, pp. 187-199, "Pt. II: Buffeting Theory," Jnl. Sound and Vibration, Vol. 60, No. 2, 1978, pp. 201-211.

10. FIGURES

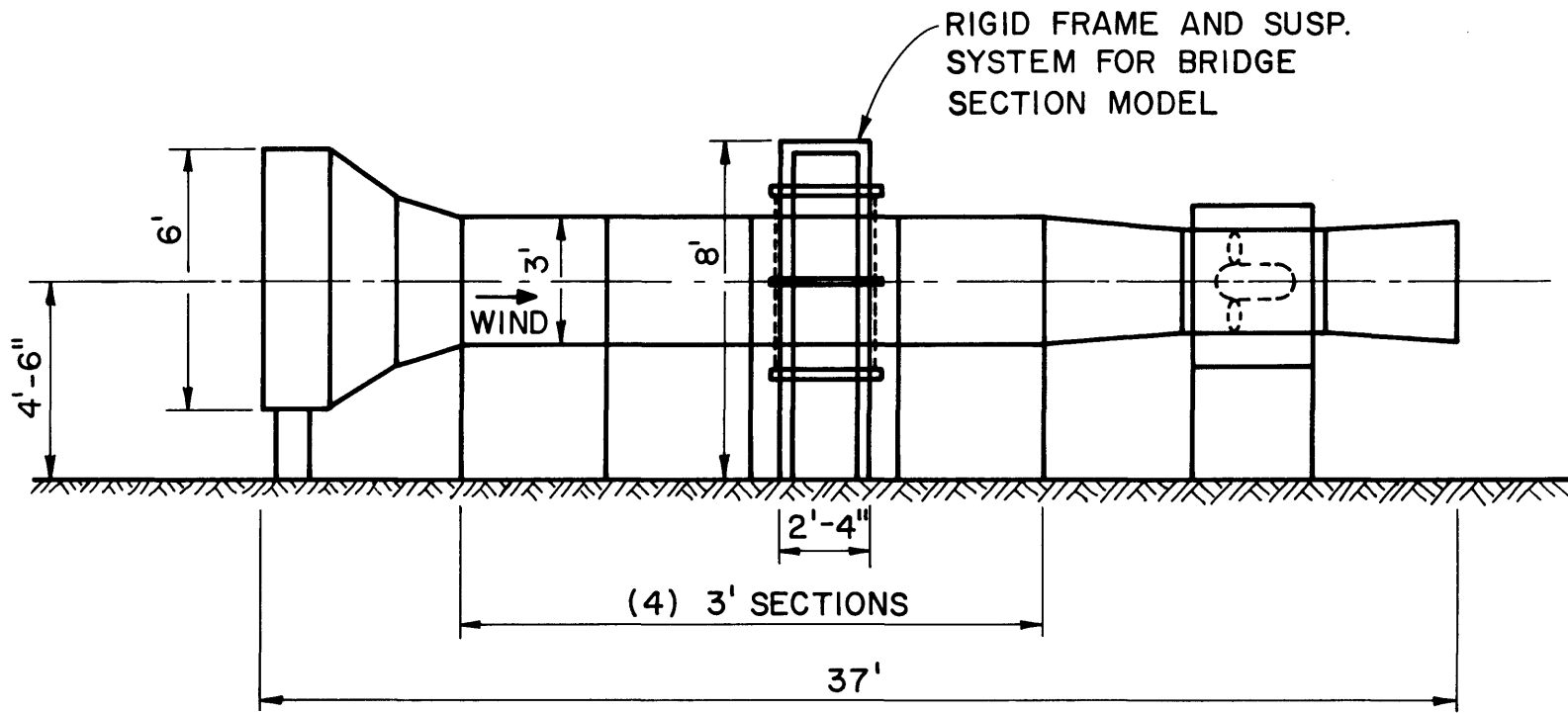


Figure 1. Structural Aerodynamics Wind Tunnel

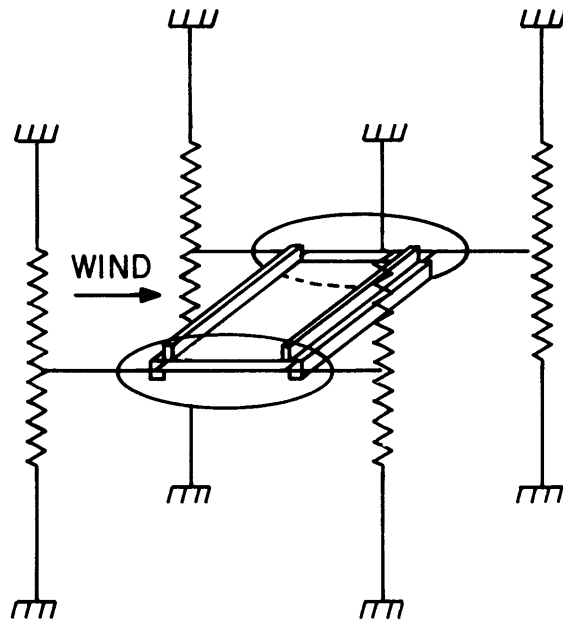
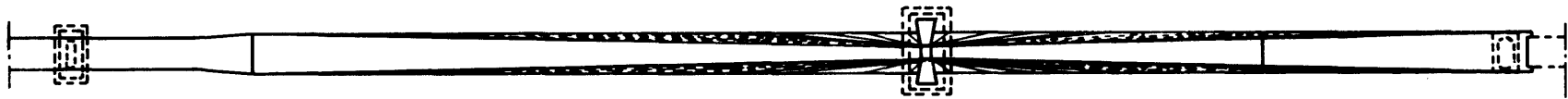
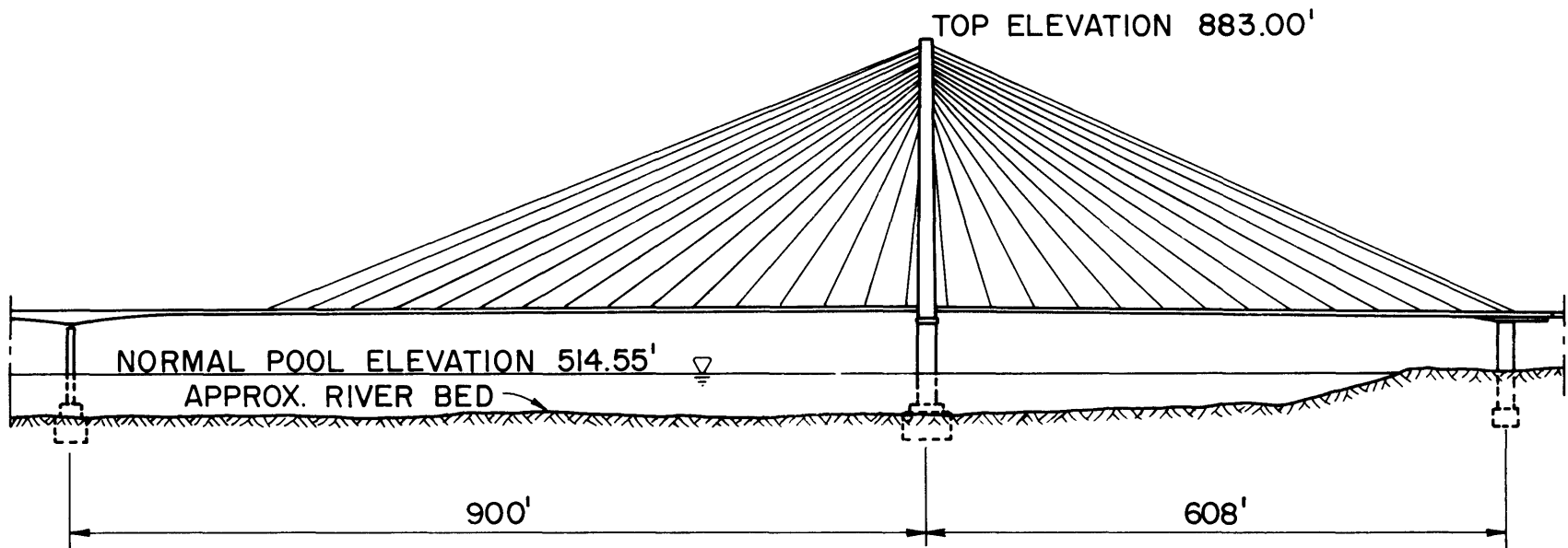


Figure 2. Bridge Section Model



PLAN



ELEVATION

Figure 3. Main Spans of East Huntington Bridge
(Concrete Cable-Stayed Alternate)

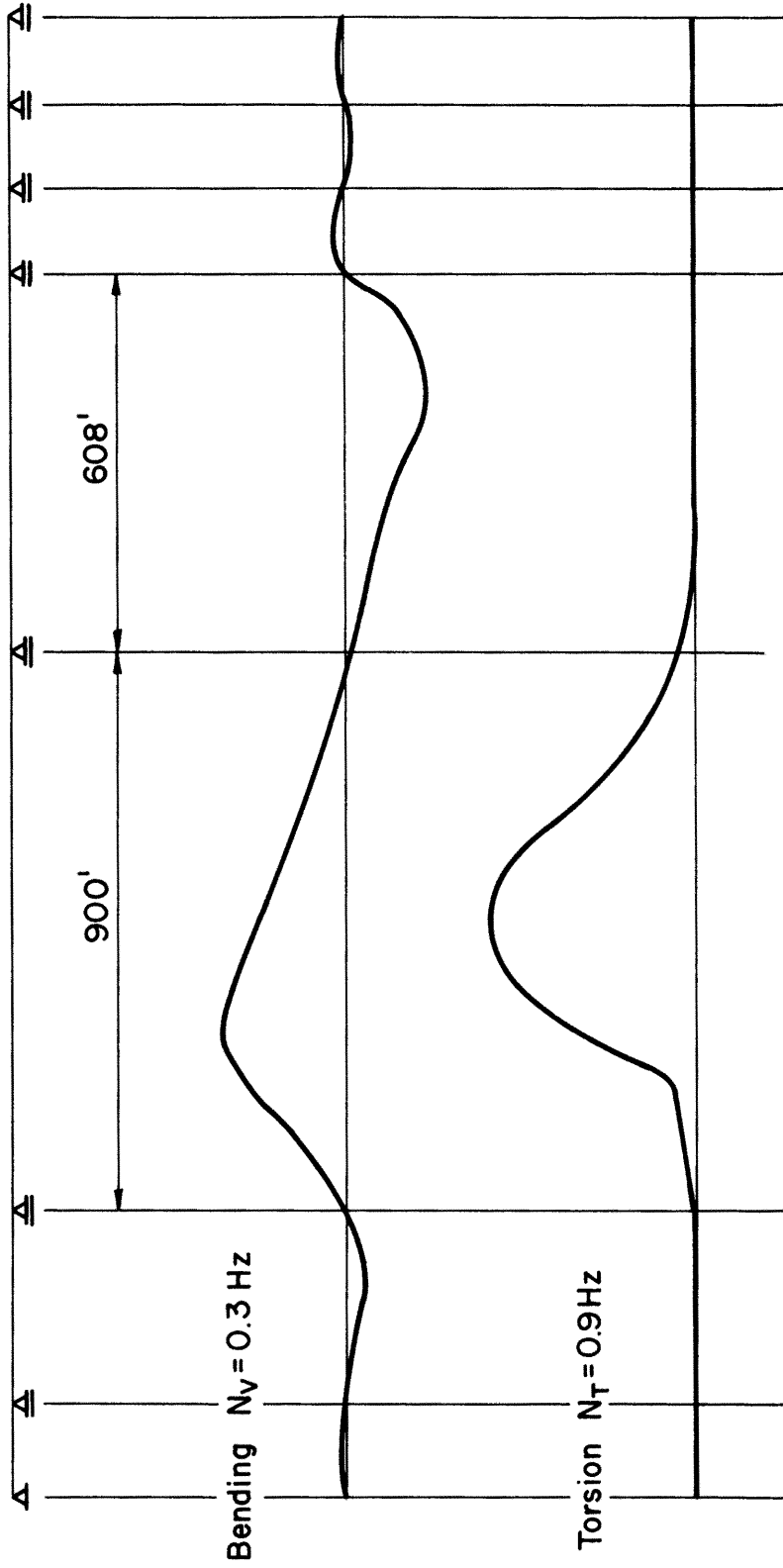


Figure 4. Fundamental Modes in Bending and Torsion

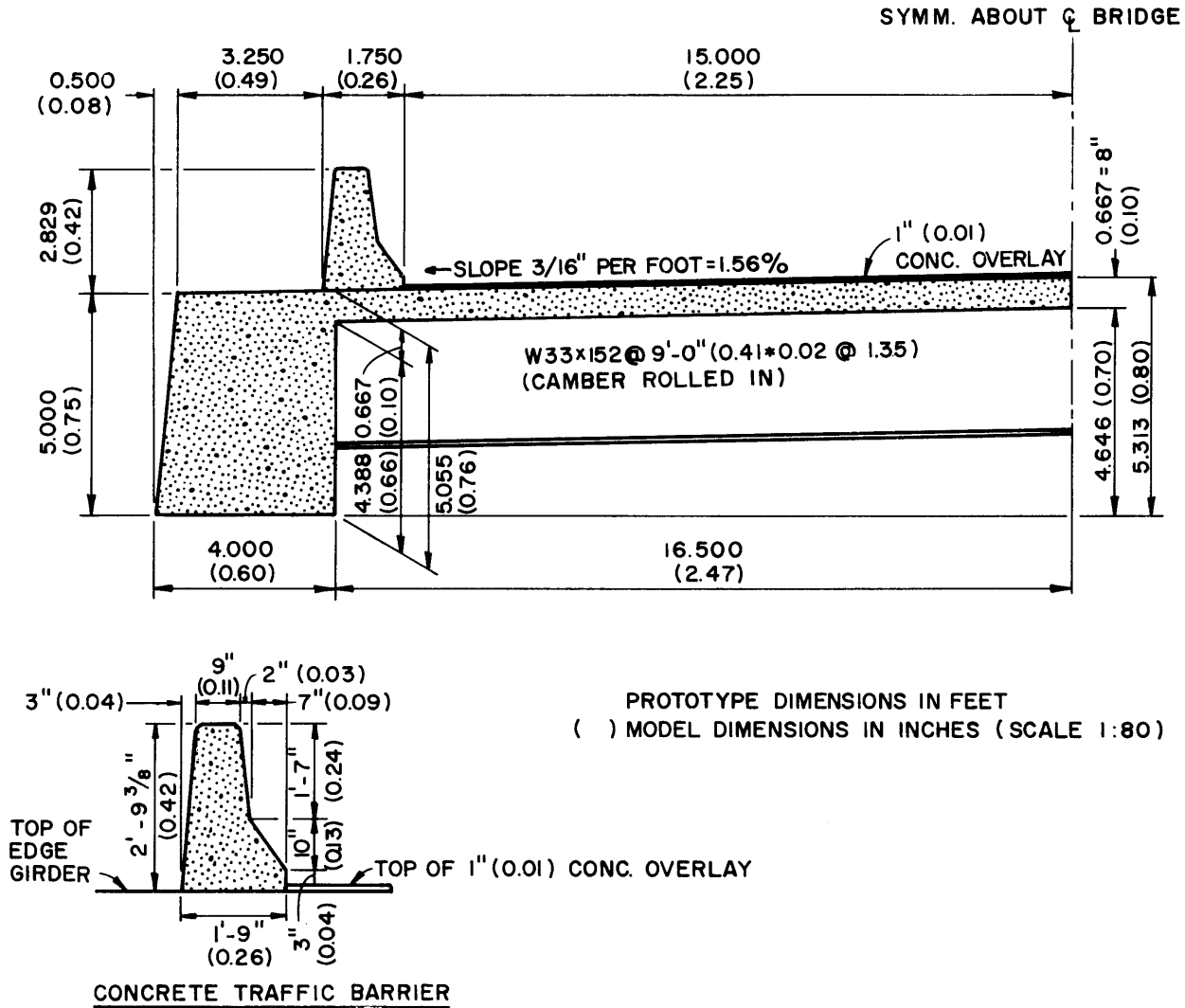
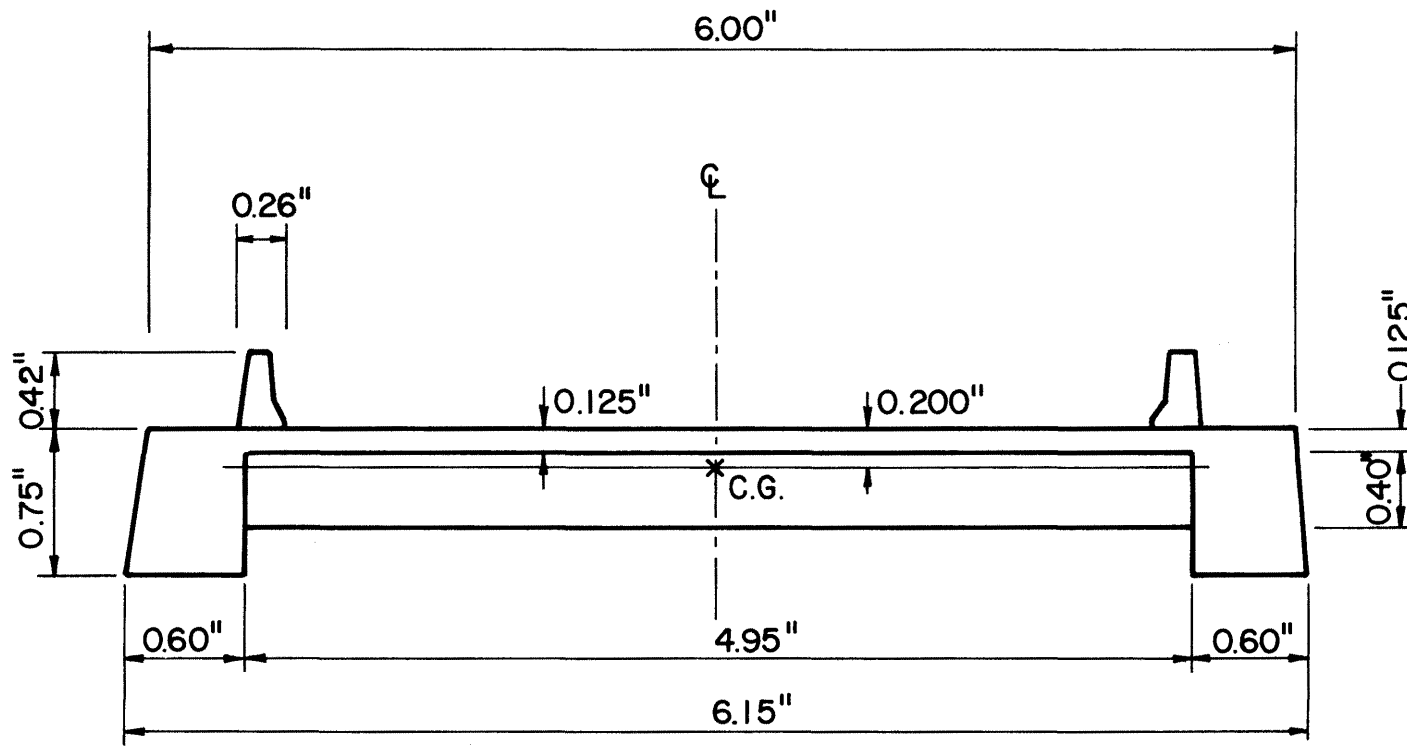


Figure 5. Prototype Bridge Deck



SCALE 1:80

Figure 6. Model Bridge Deck

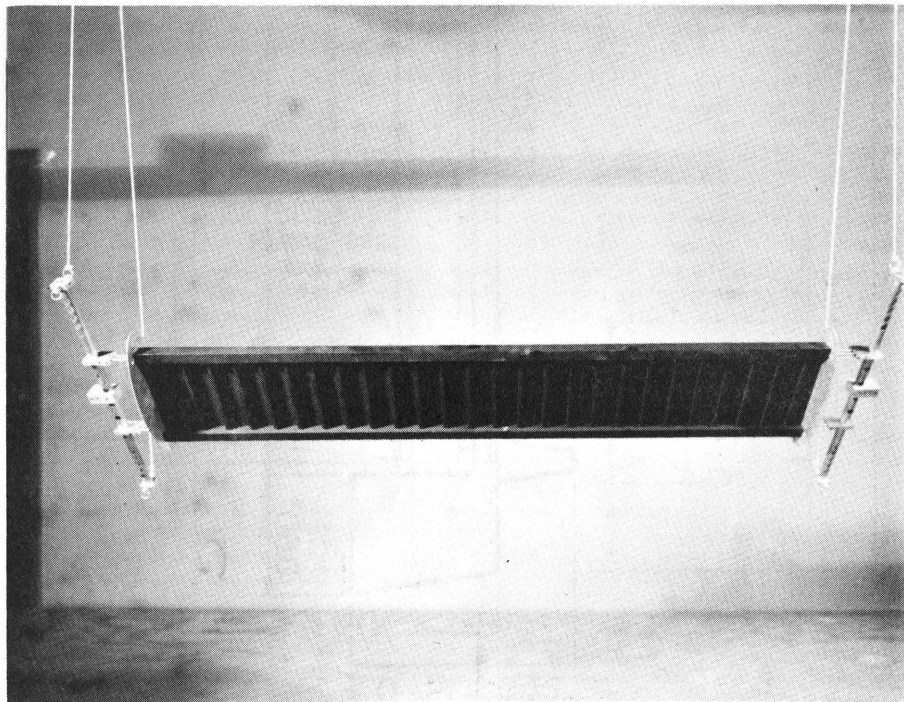
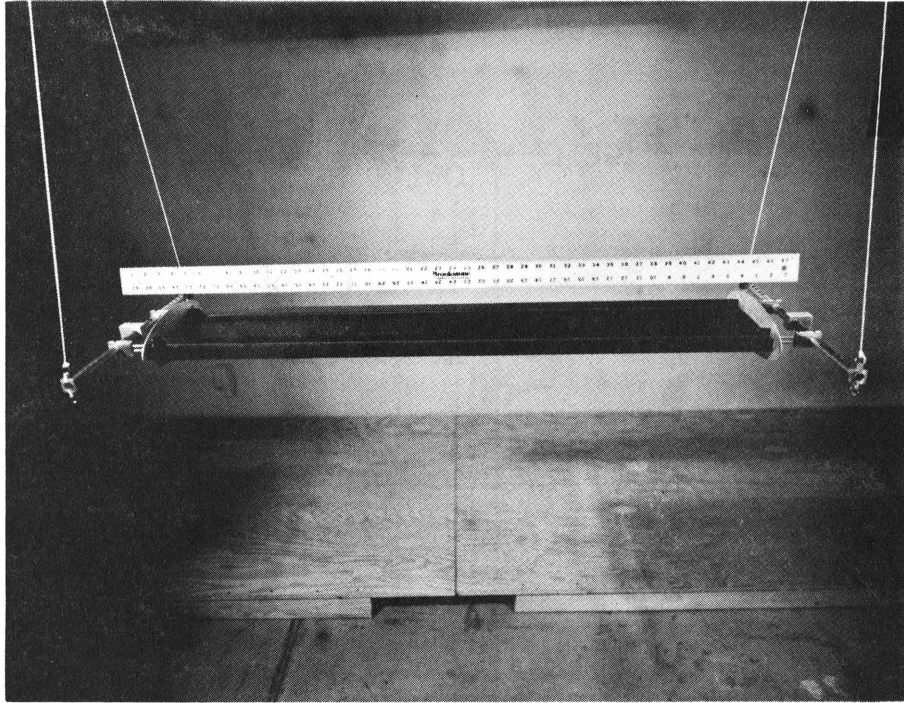


Figure 7. Section Model of Bridge

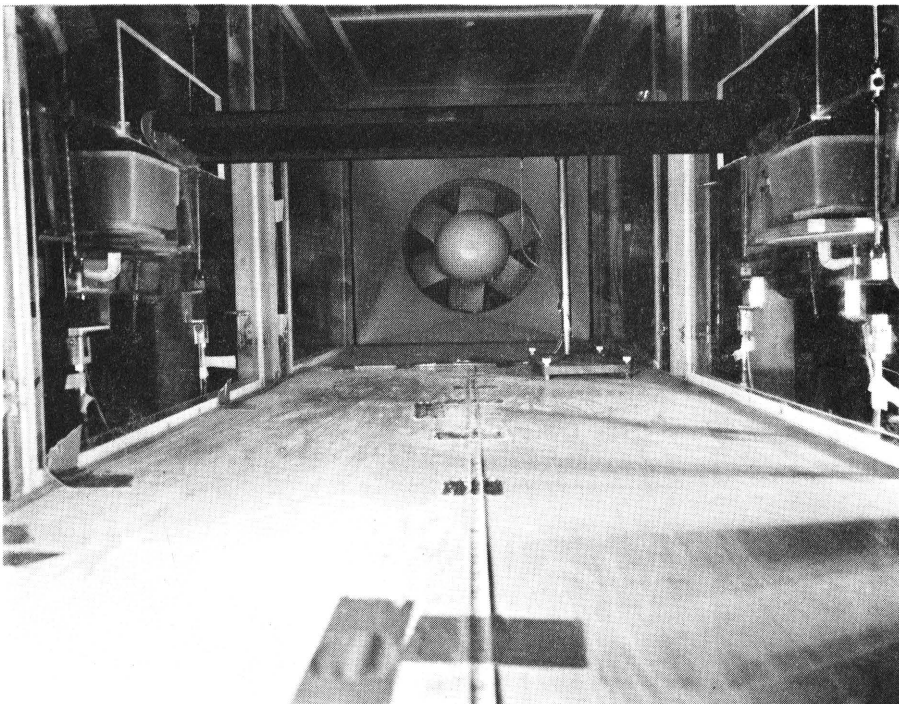
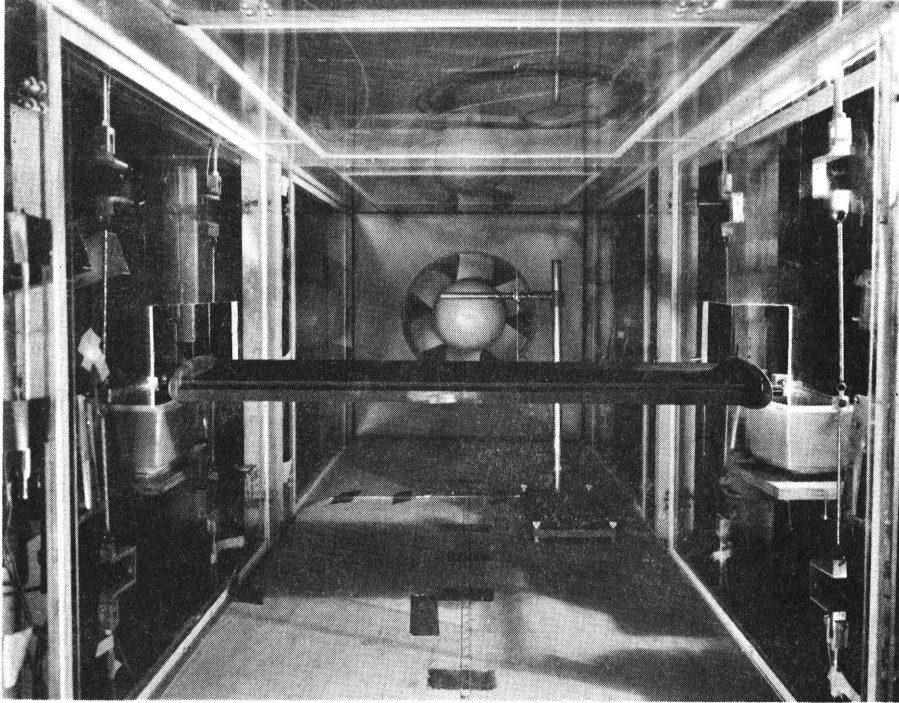


Figure 8. Bridge Section Model in Wind Tunnel

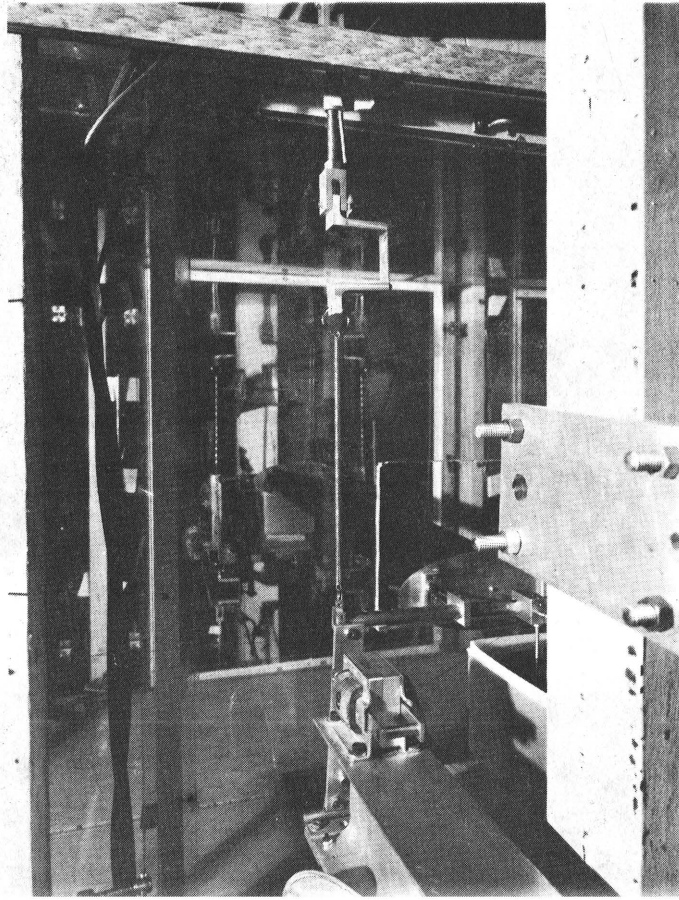


Figure 9. Strain Gage Transducer and Electromagnet

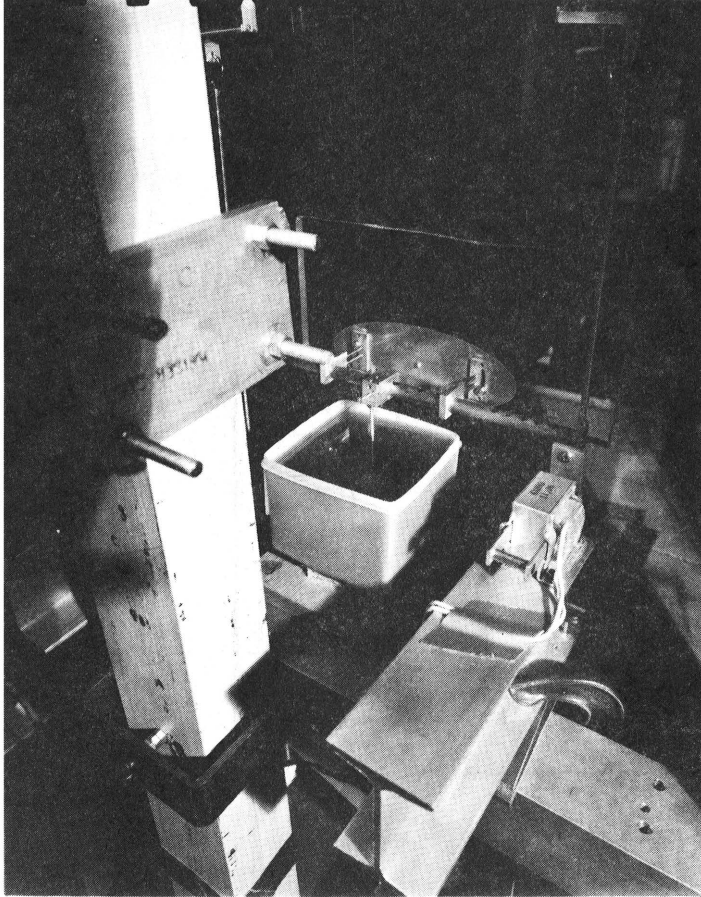


Figure 10. Viscous Damper - General View

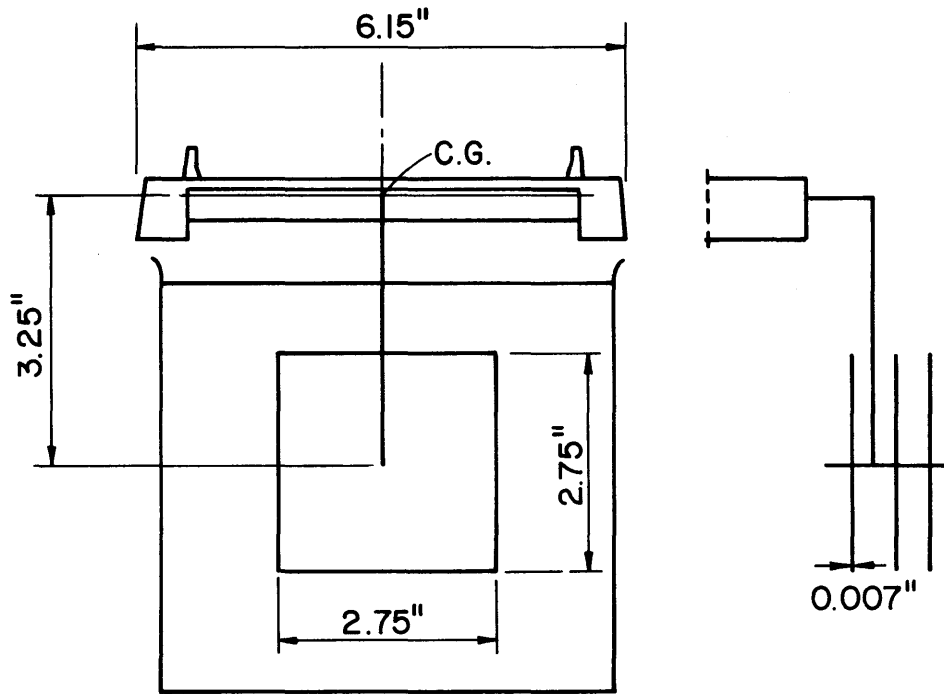


Figure 11. Viscous Damper - Details

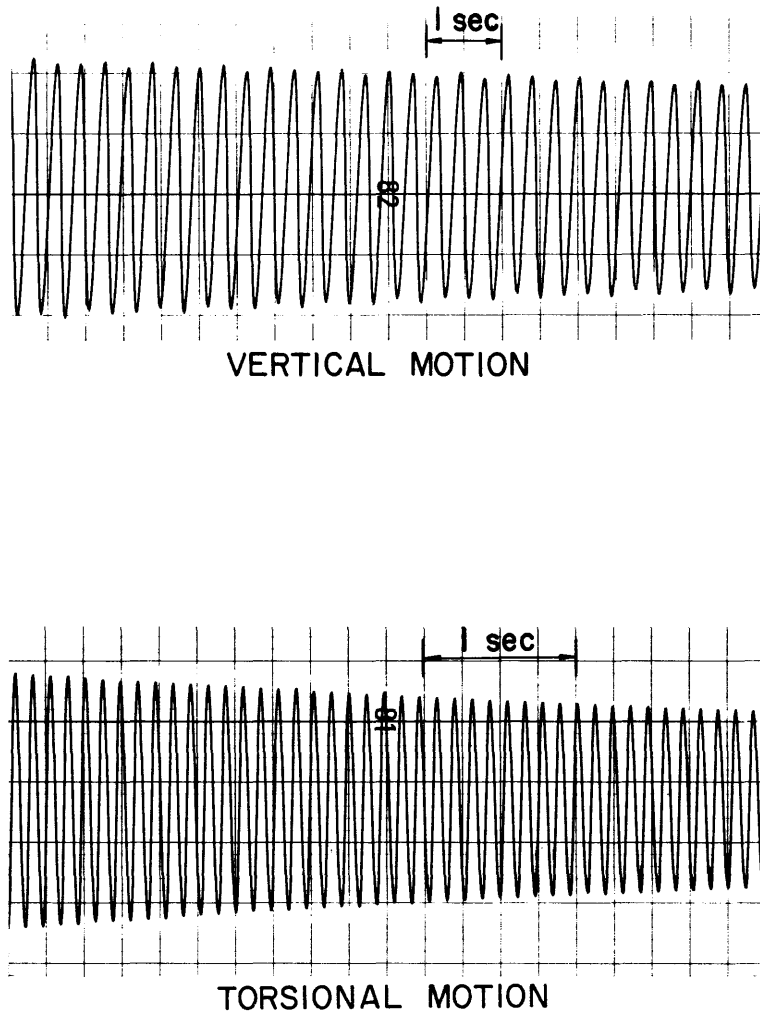


Figure 12. Free Oscillation of Models in Still Air -
Damping Level 1 ($\zeta_V = 0.12\%$, $\zeta_T = 0.17\%$)

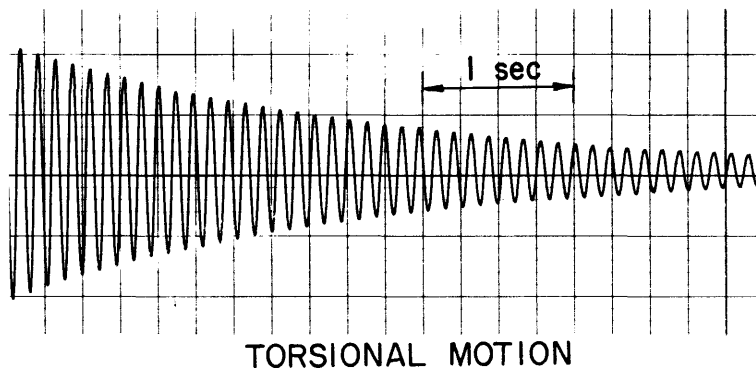
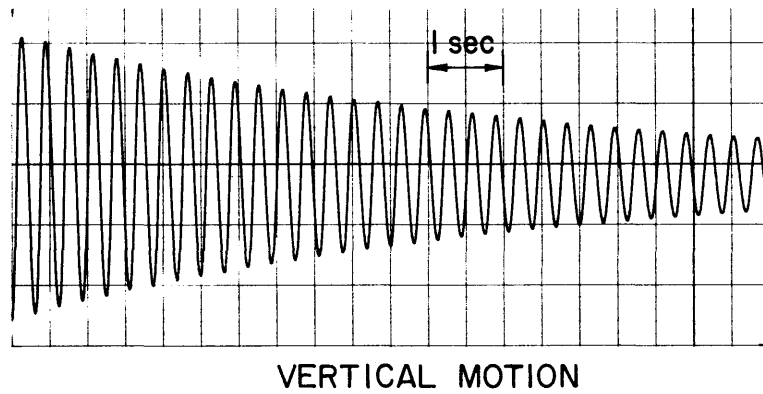


Figure 13. Free Oscillation of Model in Still Air -
Damping Level 2 ($\zeta_V = 0.71\%$, $\zeta_T = 0.75\%$)

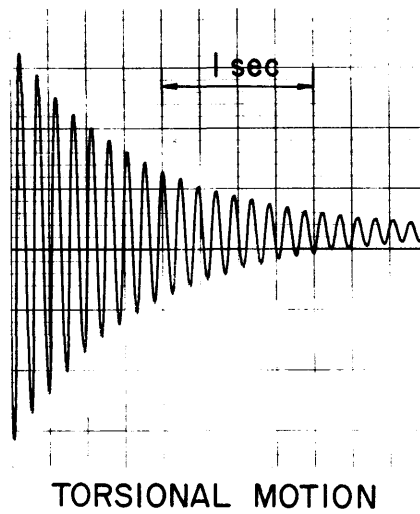
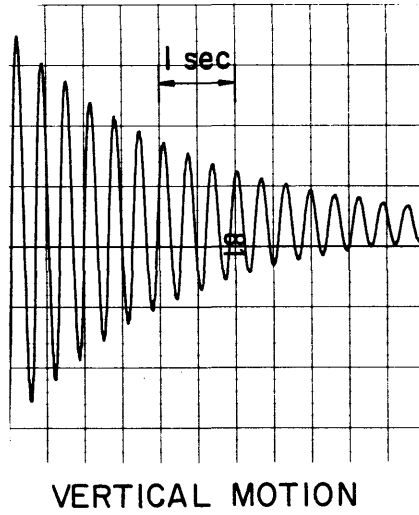


Figure 14. Free Oscillation of Model in Still Air -
Damping Level 3 ($\zeta_v = 2.3\%$, $\zeta_T = 2.1\%$)

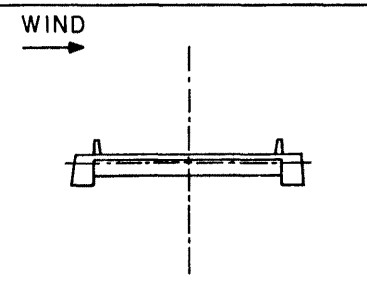
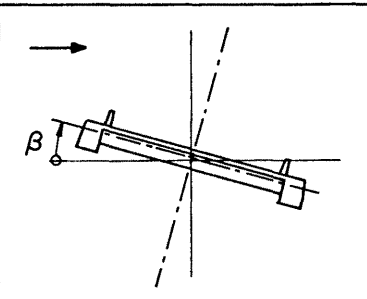
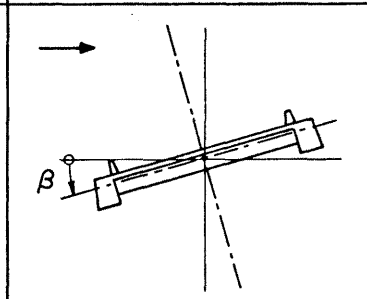
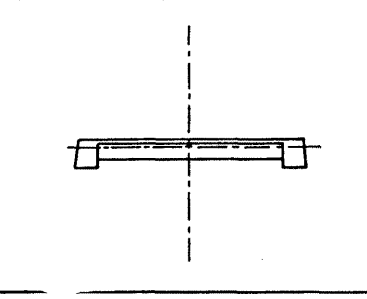
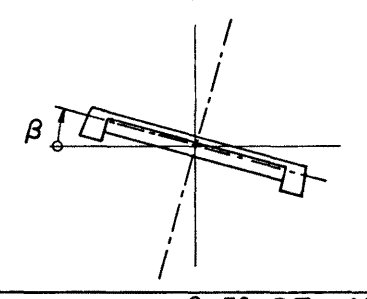
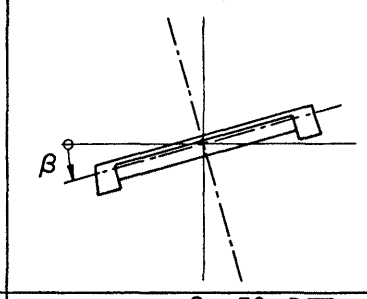
	I	II	III
A			
	VERTICAL AI-V	VERTICAL $\beta = 3^\circ$ AII-V $\beta = 6^\circ$ AII6-V	VERTICAL $\beta = -3^\circ$ AIII-V $\beta = -6^\circ$ AIII6-V
	TORSIONAL AI-T	TORSIONAL $\beta = 3^\circ$ AII-T $\beta = 6^\circ$ AII6-T	TORSIONAL $\beta = -3^\circ$ AIII-T $\beta = -6^\circ$ AIII6-T
B			
	VERTICAL BI-V	VERTICAL $\beta = 3^\circ$ BII-V $\beta = 6^\circ$ BII6-V	VERTICAL $\beta = -3^\circ$ BIII-V $\beta = -6^\circ$ BIII6-V
	TORSIONAL BI-T	TORSIONAL $\beta = 3^\circ$ BII-T $\beta = 6^\circ$ BII6-T	TORSIONAL $\beta = -3^\circ$ BIII-T $\beta = -6^\circ$ BIII6-T

Figure 15. Experimental Configurations

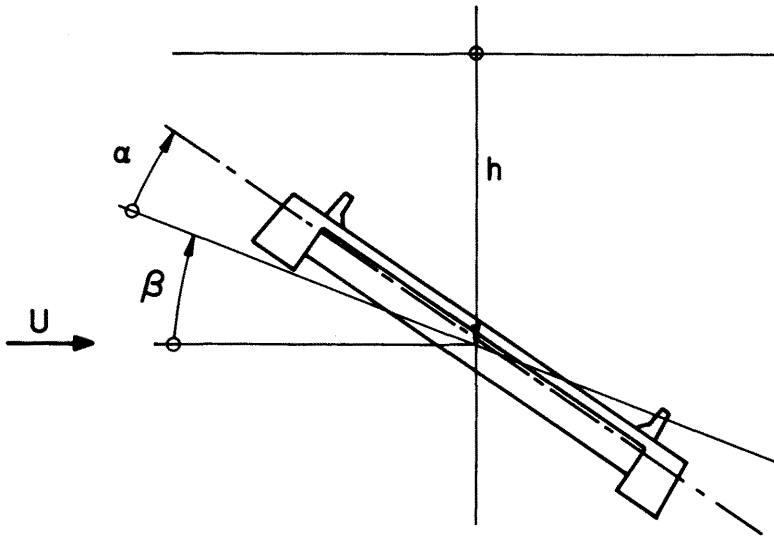


Figure 16. Basic Definitions

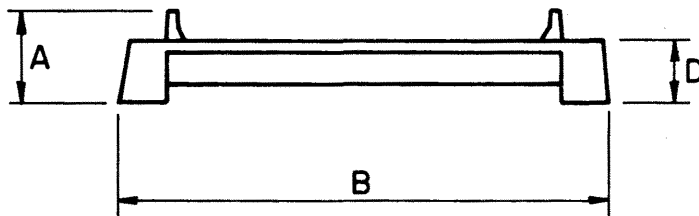
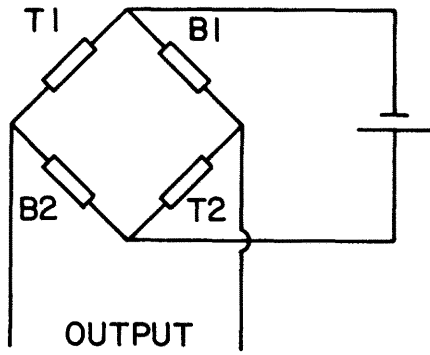


Figure 17. Basic Geometrical Dimensions

VERTICAL MOTION



TORSIONAL MOTION

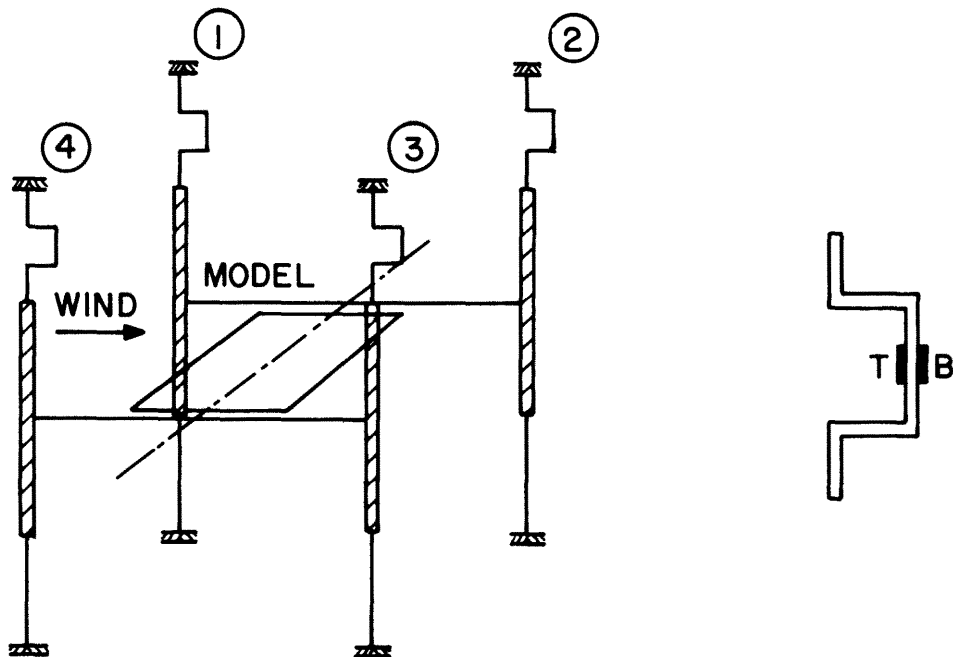
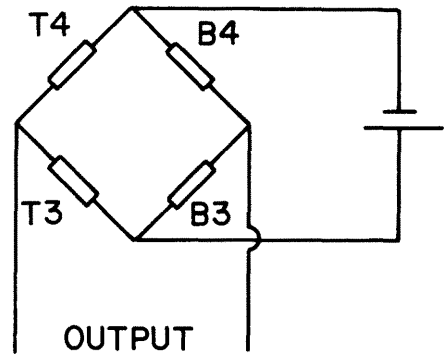


Figure 18. Arrangement for Aerodynamic Measurements

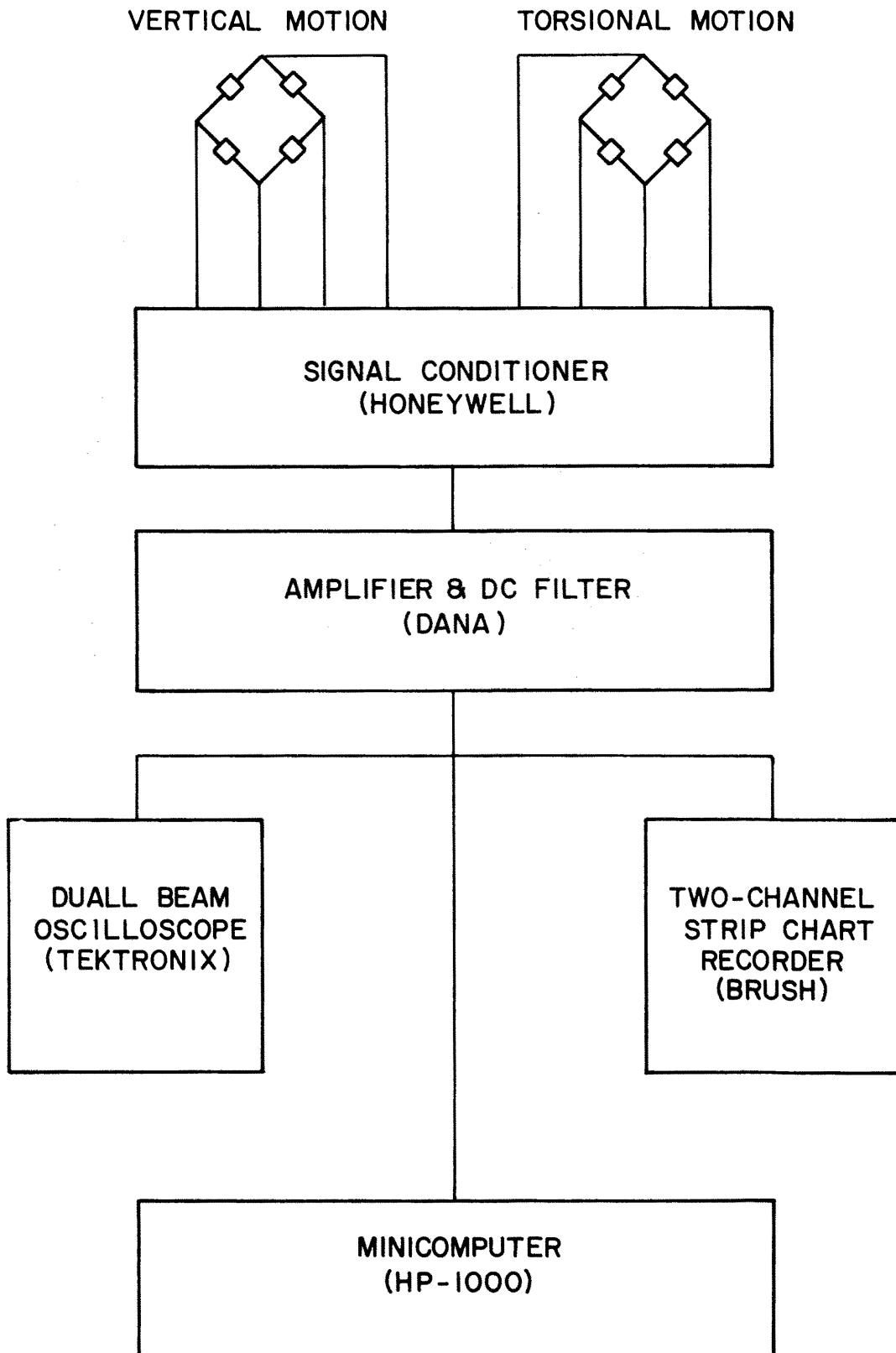


Figure 19. Instrumentation

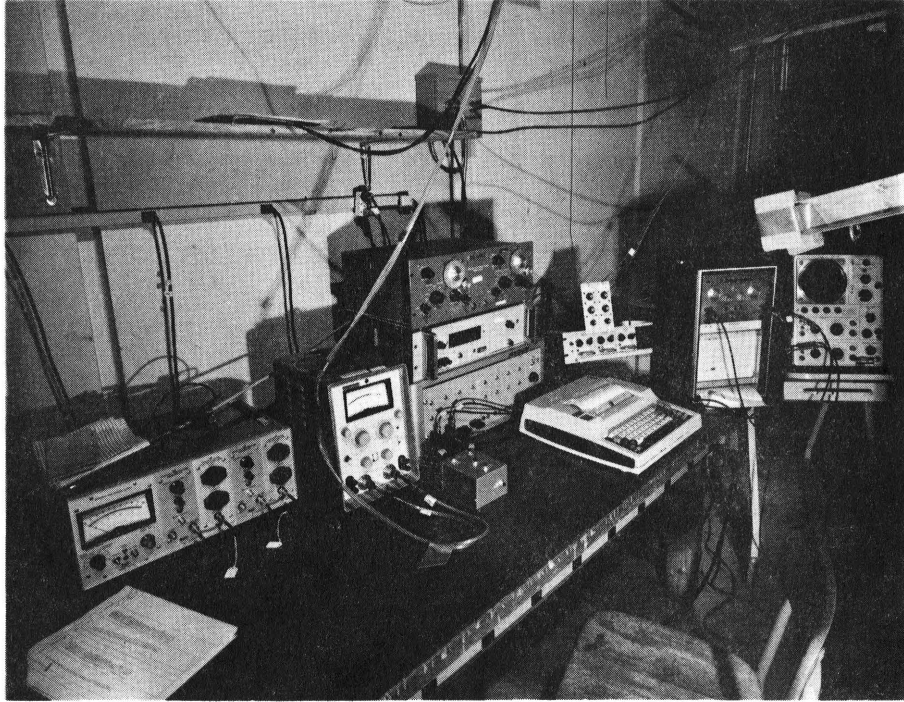


Figure 20. General View of Some of the Instruments Used

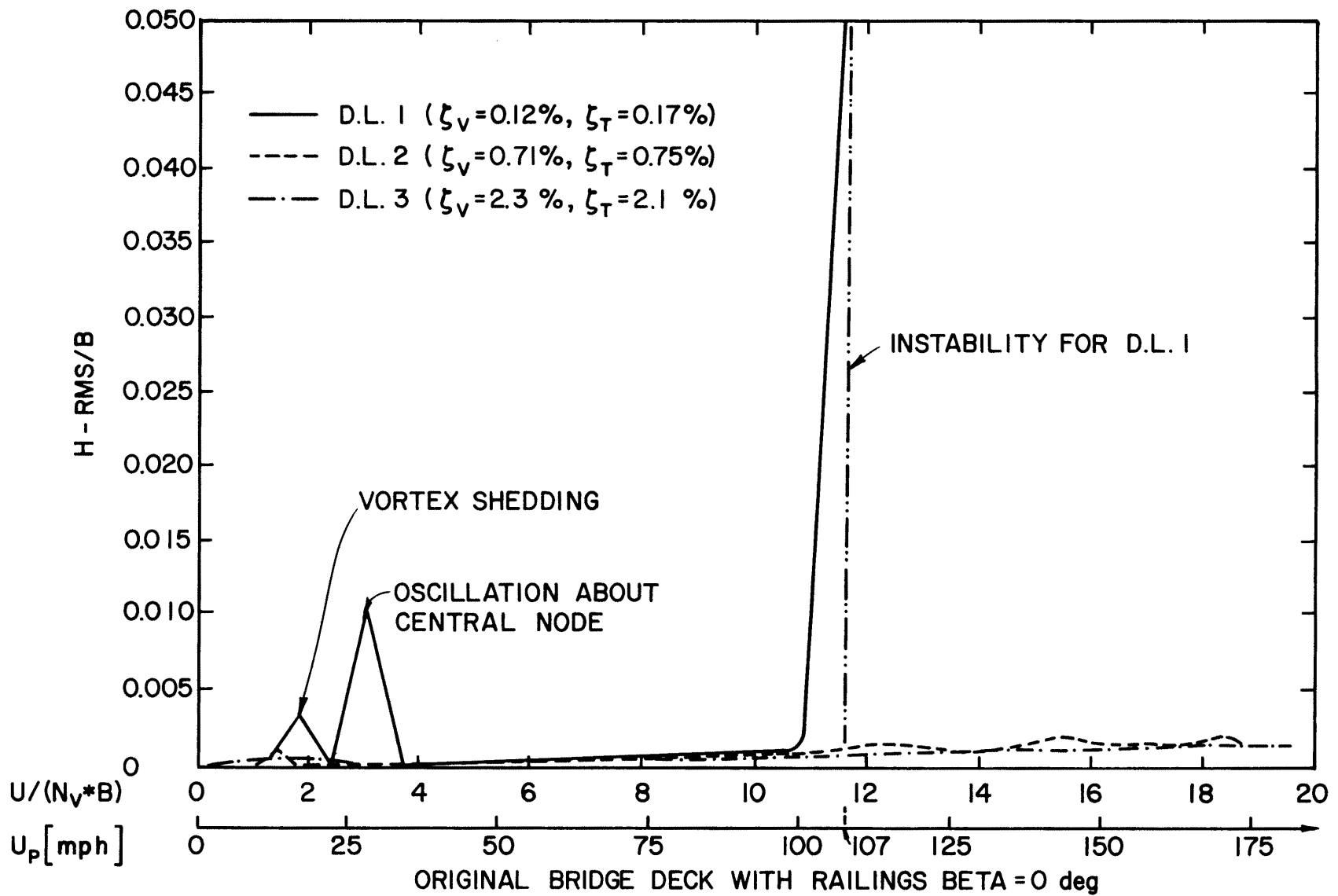
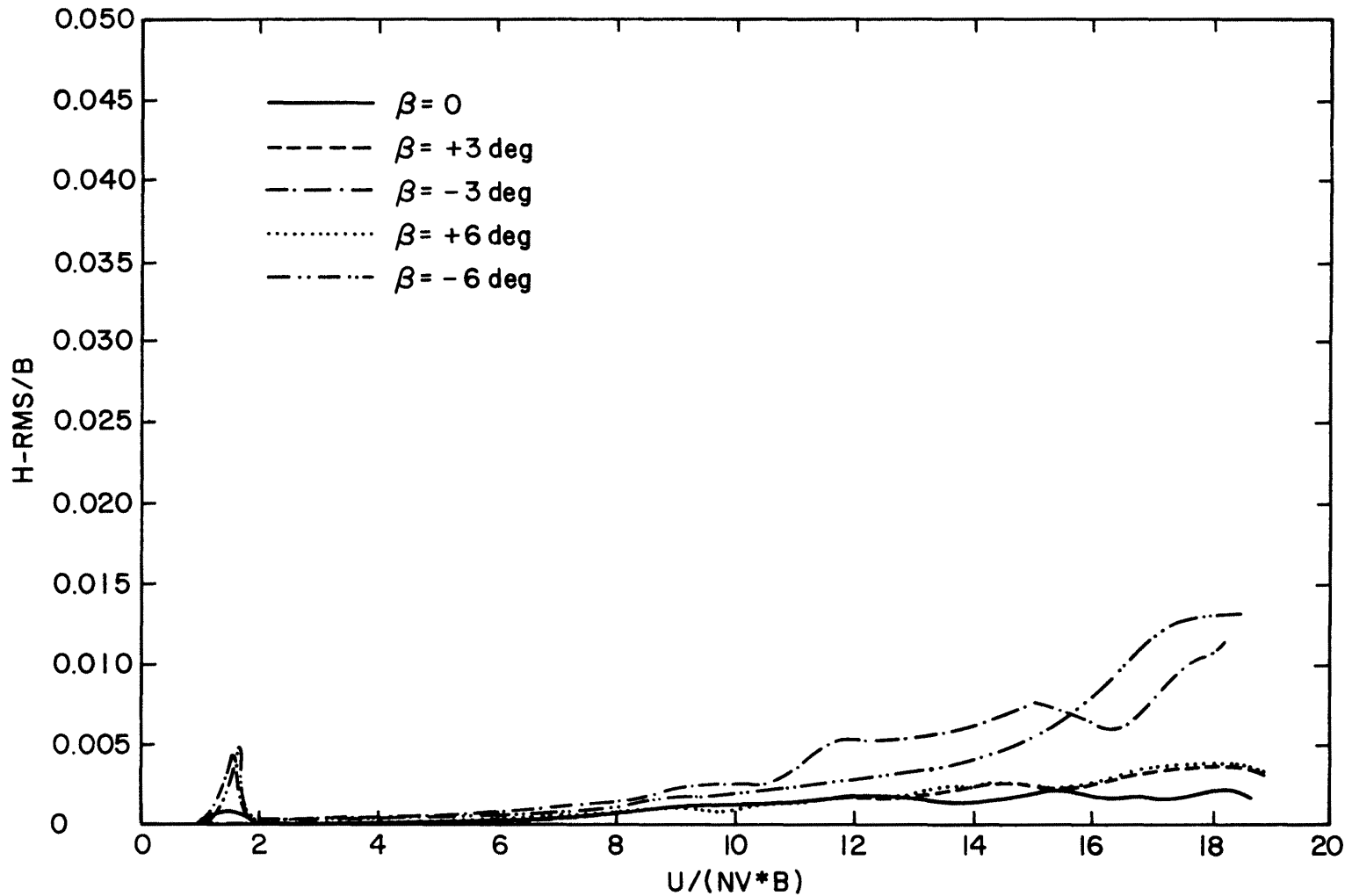


Figure 21. Vertical Response of Section Model with Different Damping Levels at Angle of Attack $\beta = 0^\circ$



ORIGINAL BRIDGE DECK WITH RAILINGS
 DAMPING LEVEL 2 ($\zeta_v = 0.71\%$, $\zeta_T = 0.75\%$)

Figure 23. Vertical Response of Section Model with Damping Level 2 at Different Angles of Attack

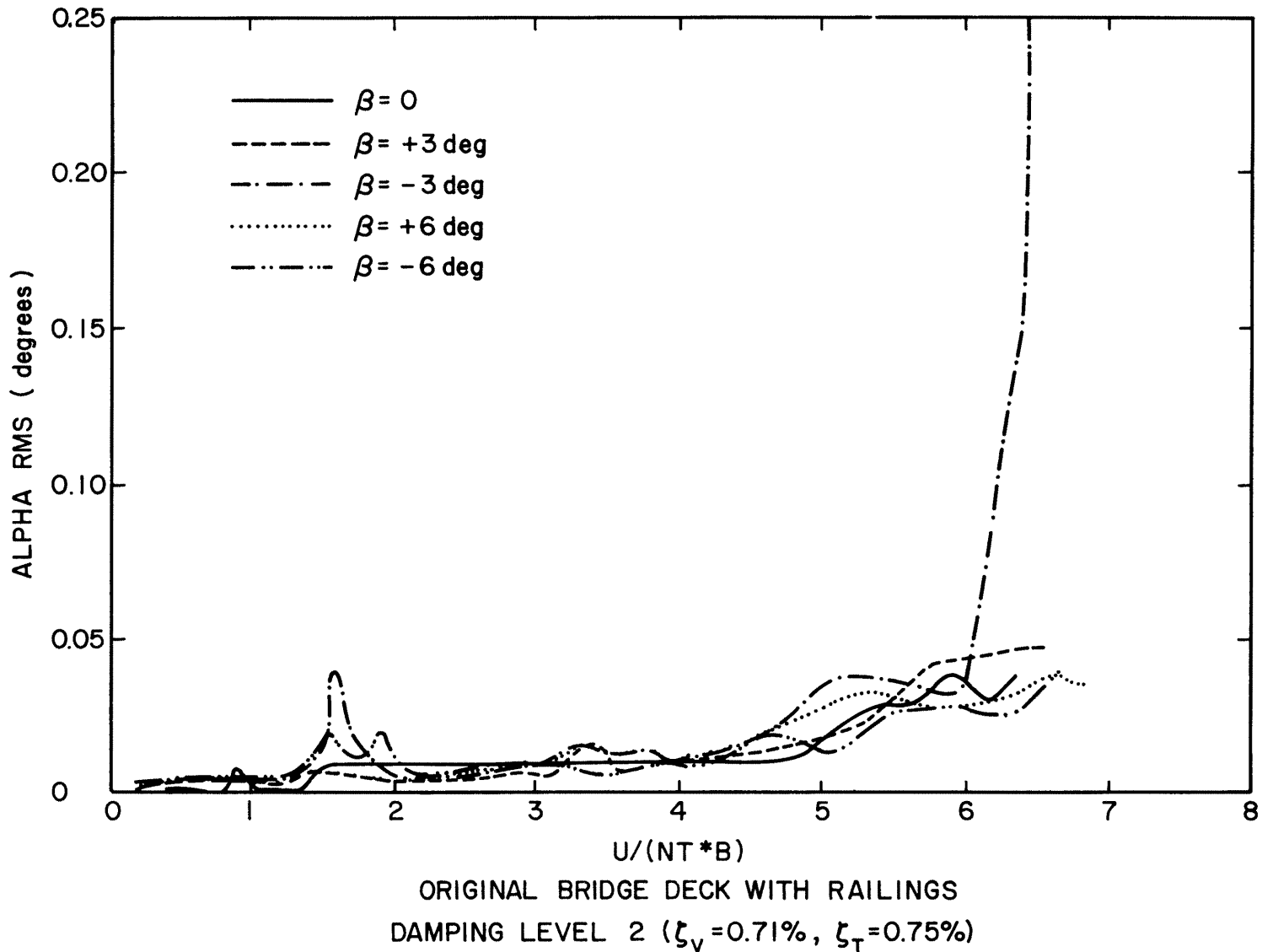


Figure 24. Torsional Response of Section Model with Damping Level 2 at Different Angles of Attack

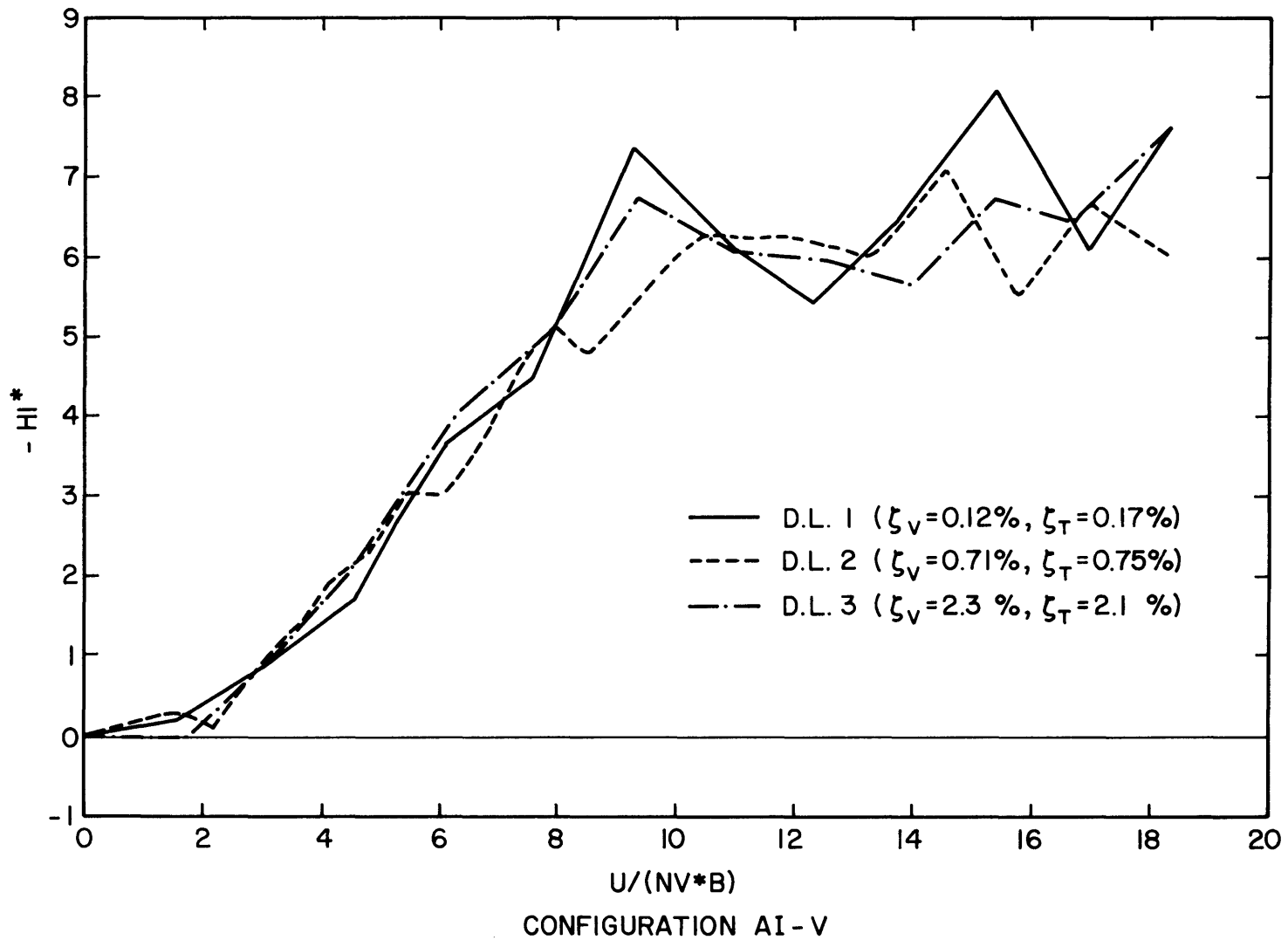


Figure 25. Aerodynamic Derivative $-H_1^*$ Extracted for Model with Different Damping Levels at Angle of Attack $\beta = 0^\circ$

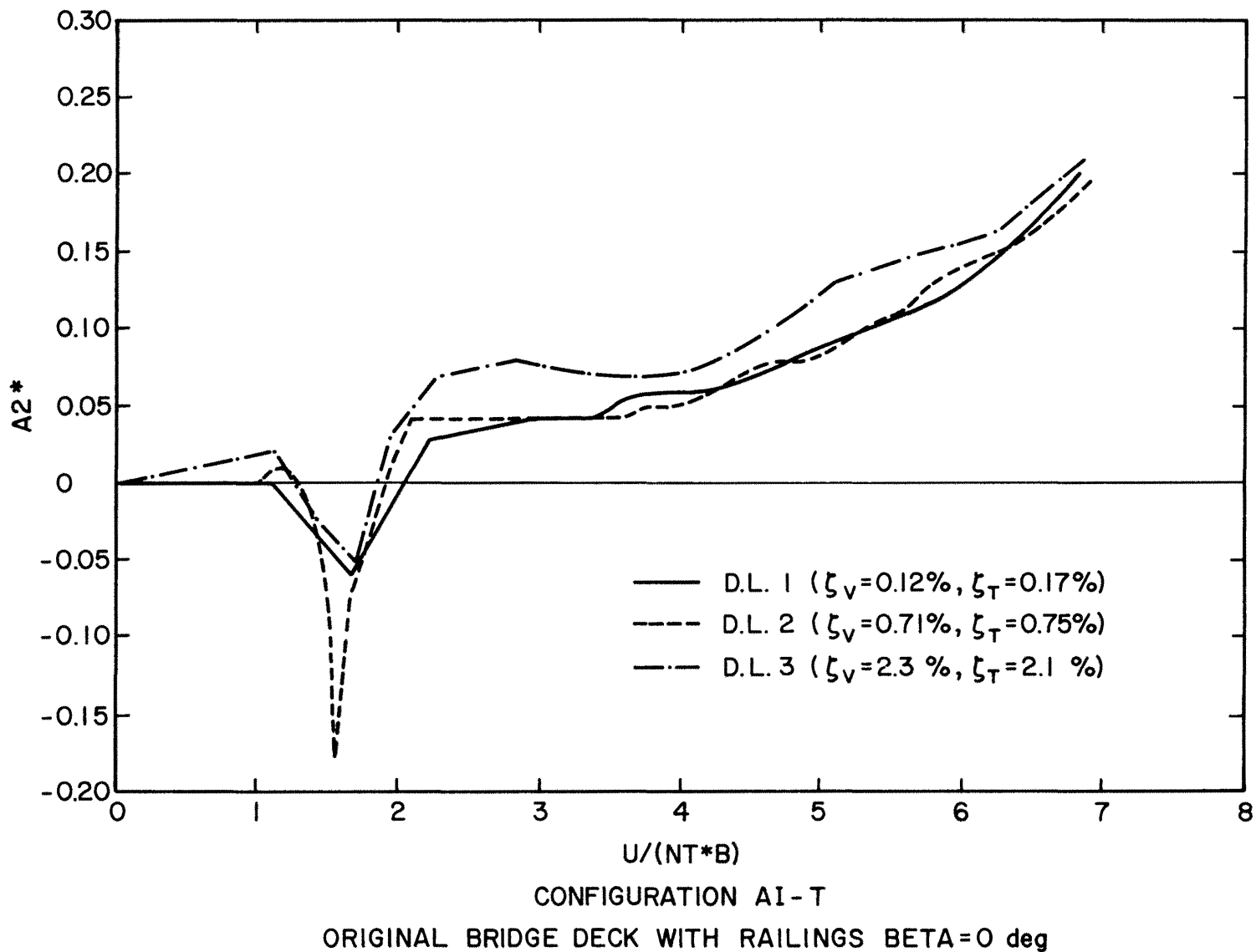


Figure 26. Aerodynamic Derivative A_2^* Extracted for Model with Different Damping Levels at Angle of Attack $\beta = 0^\circ$

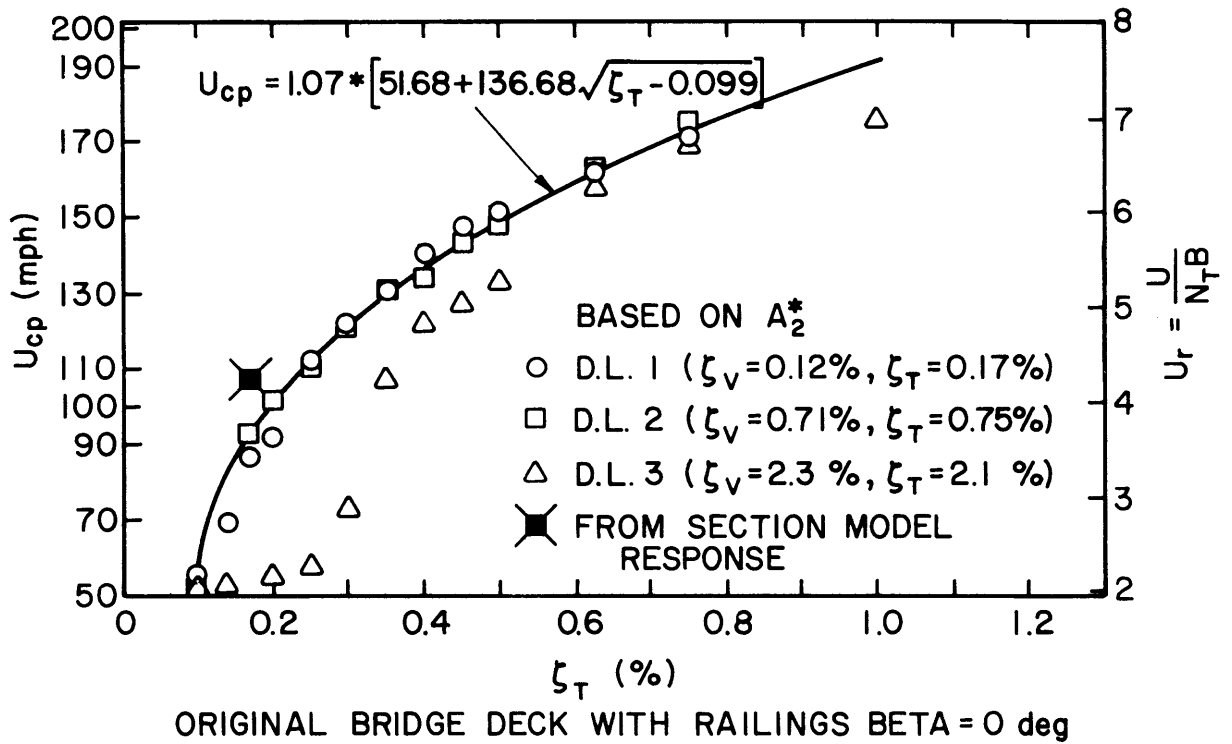
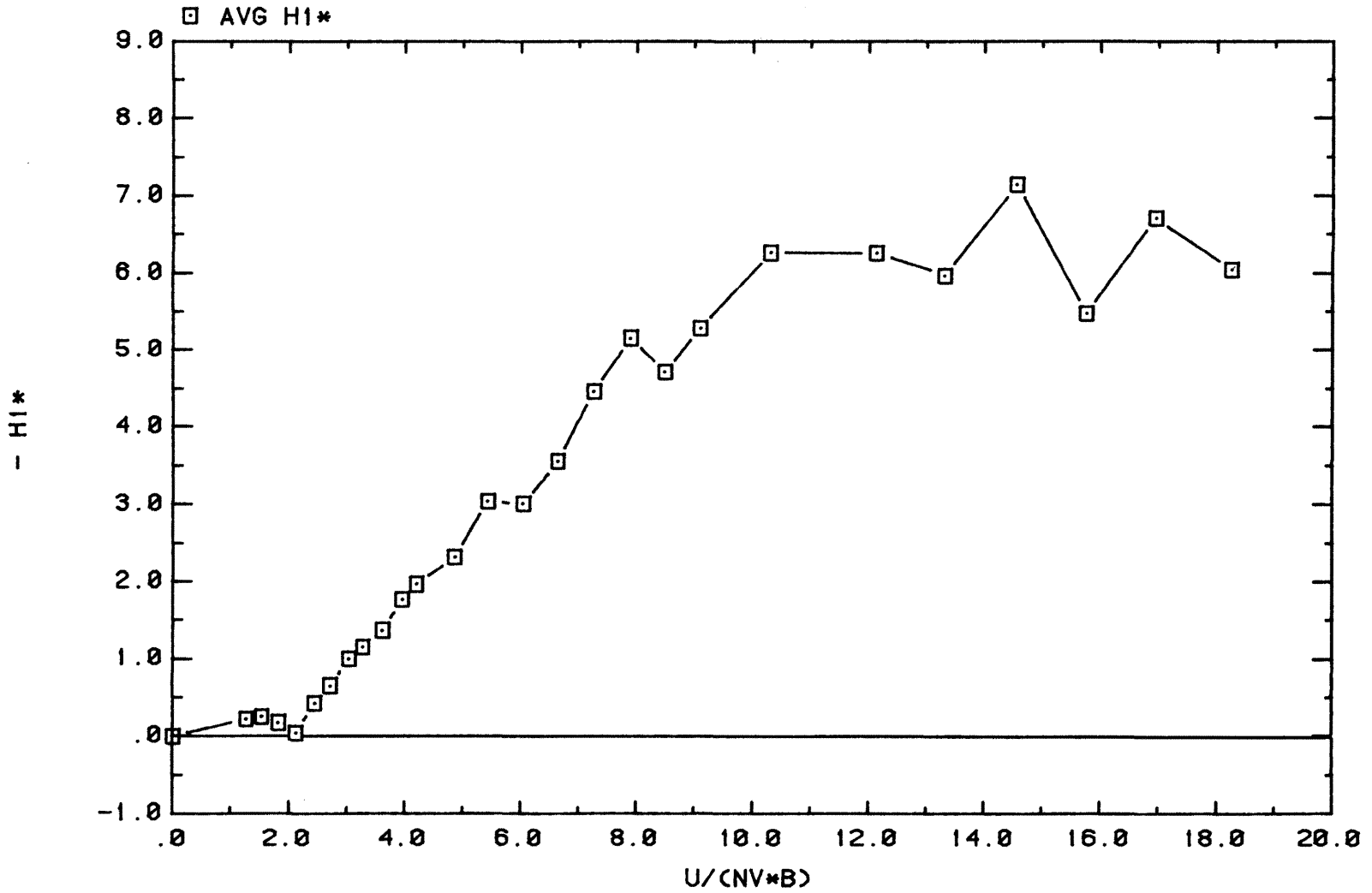


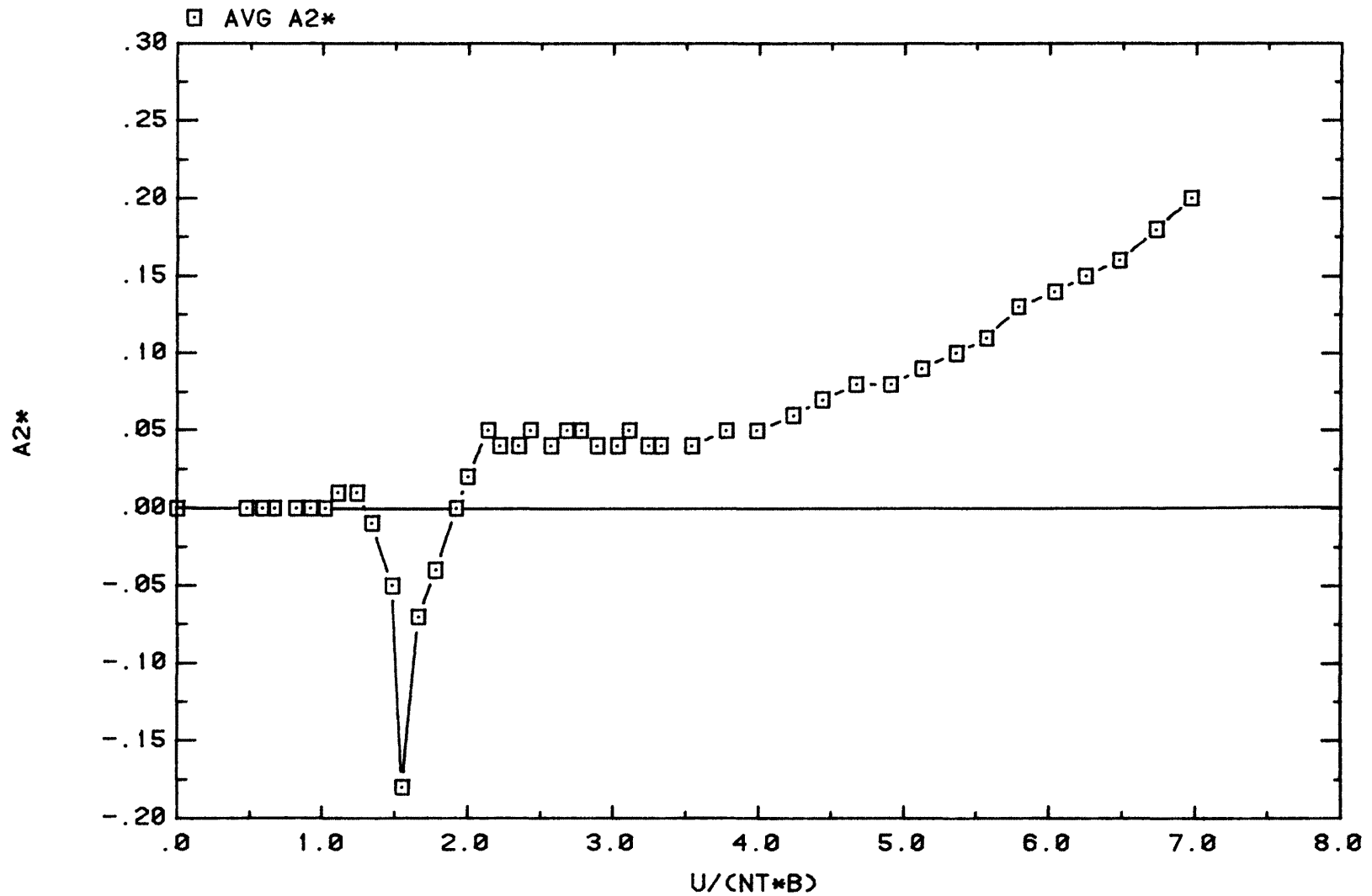
Figure 27. Prototype Critical Wind Speed for Torsional Flutter, Angle of Attack $\beta = 0^\circ$



CONFIGURATION AI-V-2

ORIGINAL BRIDGE DECK WITH RAILINGS BETA=0 DEG

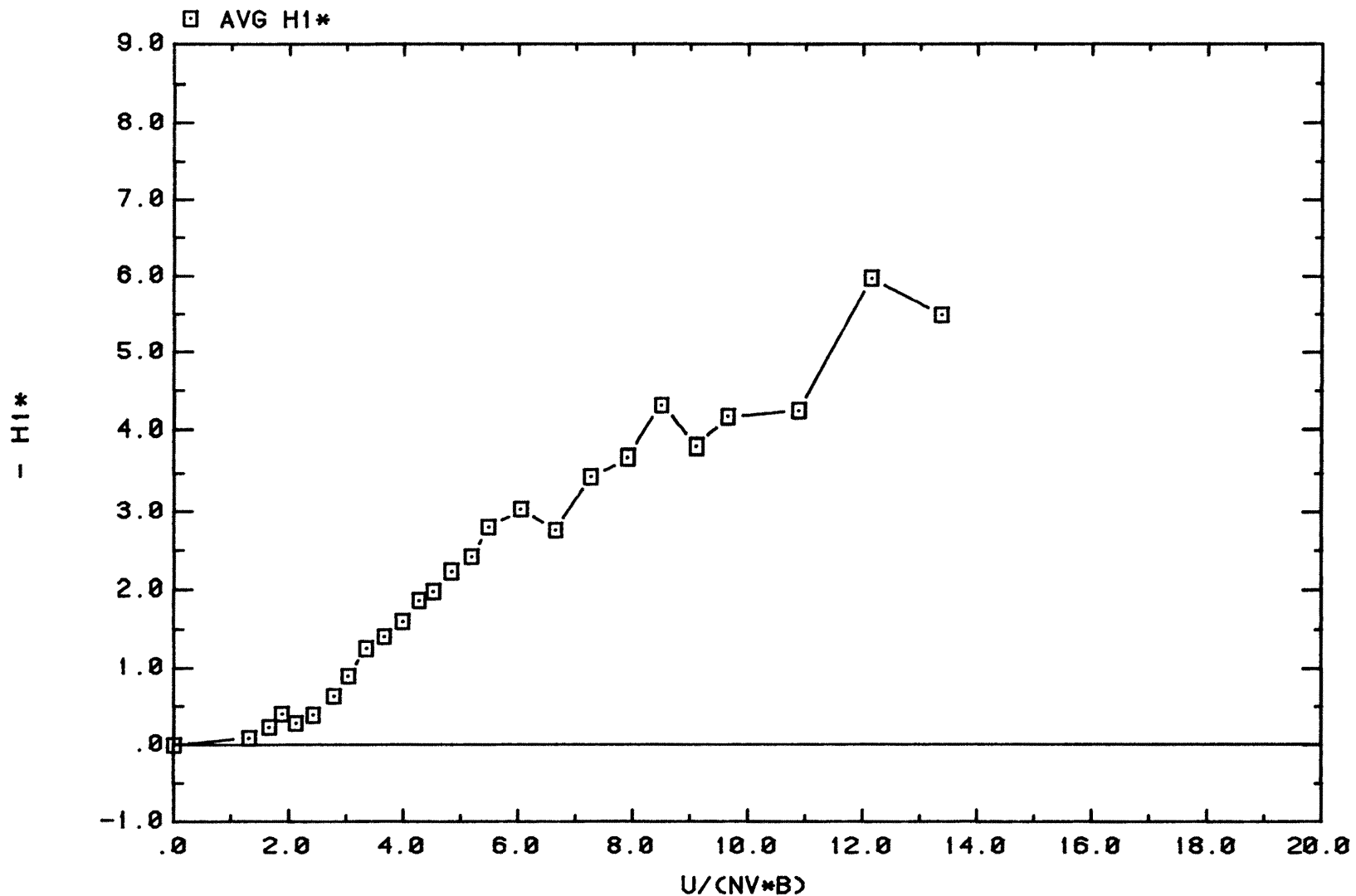
Figure 28. Aerodynamic Derivative $-H_1^*$, Angle of Attack $\beta = 0^\circ$



CONFIGURATION AI-T-2

ORIGINAL BRIDGE DECK WITH RAILINGS BETA=0 DEG

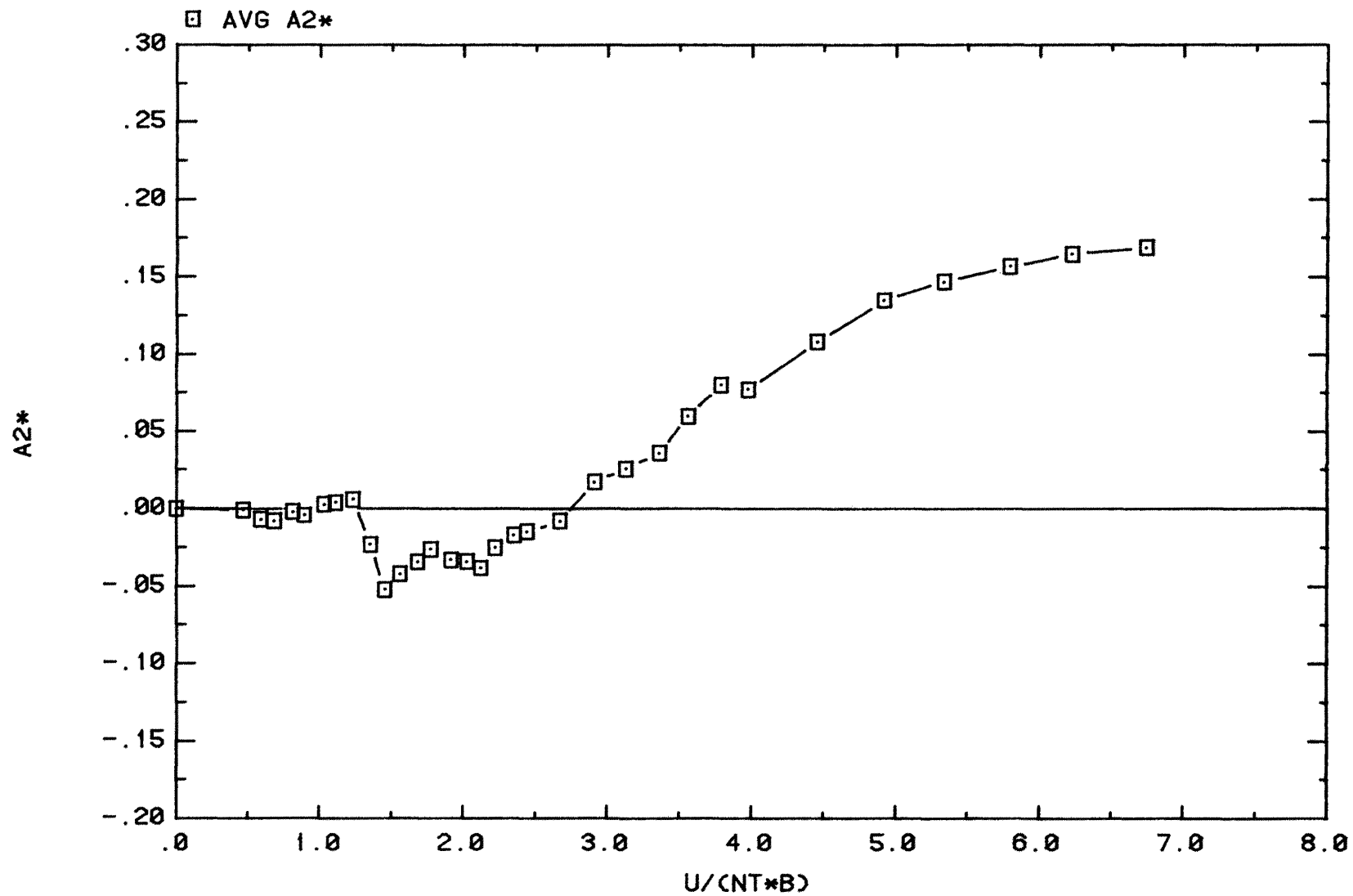
Figure 29. Aerodynamic Derivative A_2^* , Angle of Attack $\beta = 0^\circ$



CONFIGURATION AII-V-2

ORIGINAL BRIDGE DECK WITH RAILINGS BETA=+3 DEG

Figure 30. Aerodynamic Derivative $-H_1^*$, Angle of Attack $\beta = +3^\circ$



CONFIGURATION AII-T-2

ORIGINAL BRIDGE DECK WITH RAILINGS BETA=+3 DEG

Figure 31. Aerodynamic Derivative A_2^* , Angle of Attack $\beta = +3^\circ$

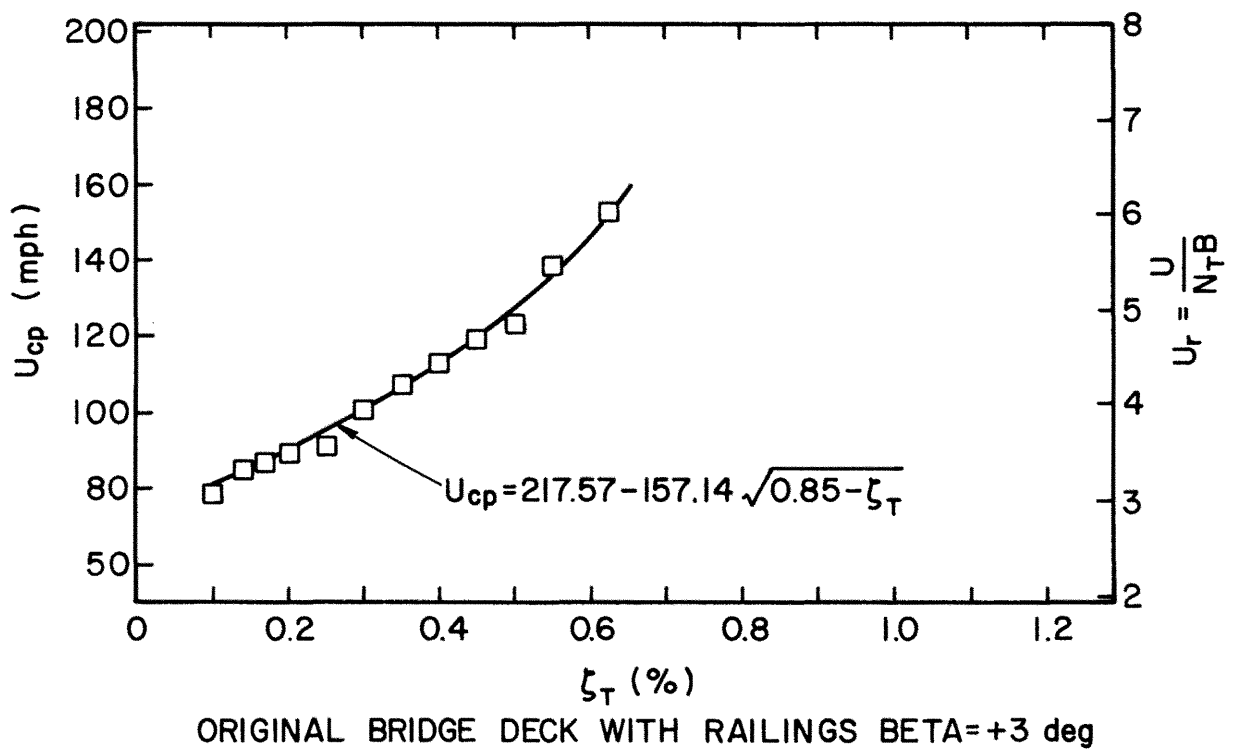
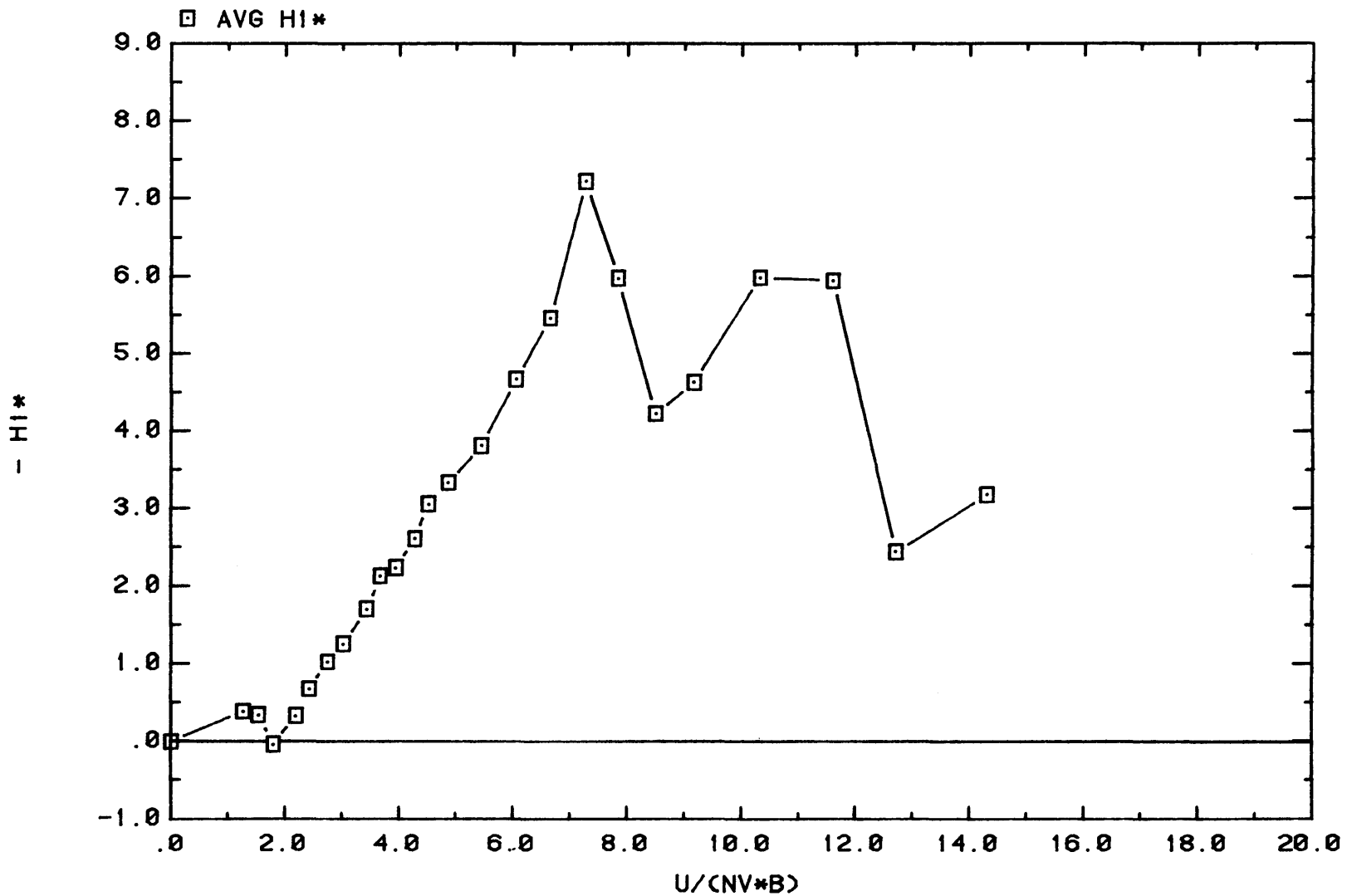


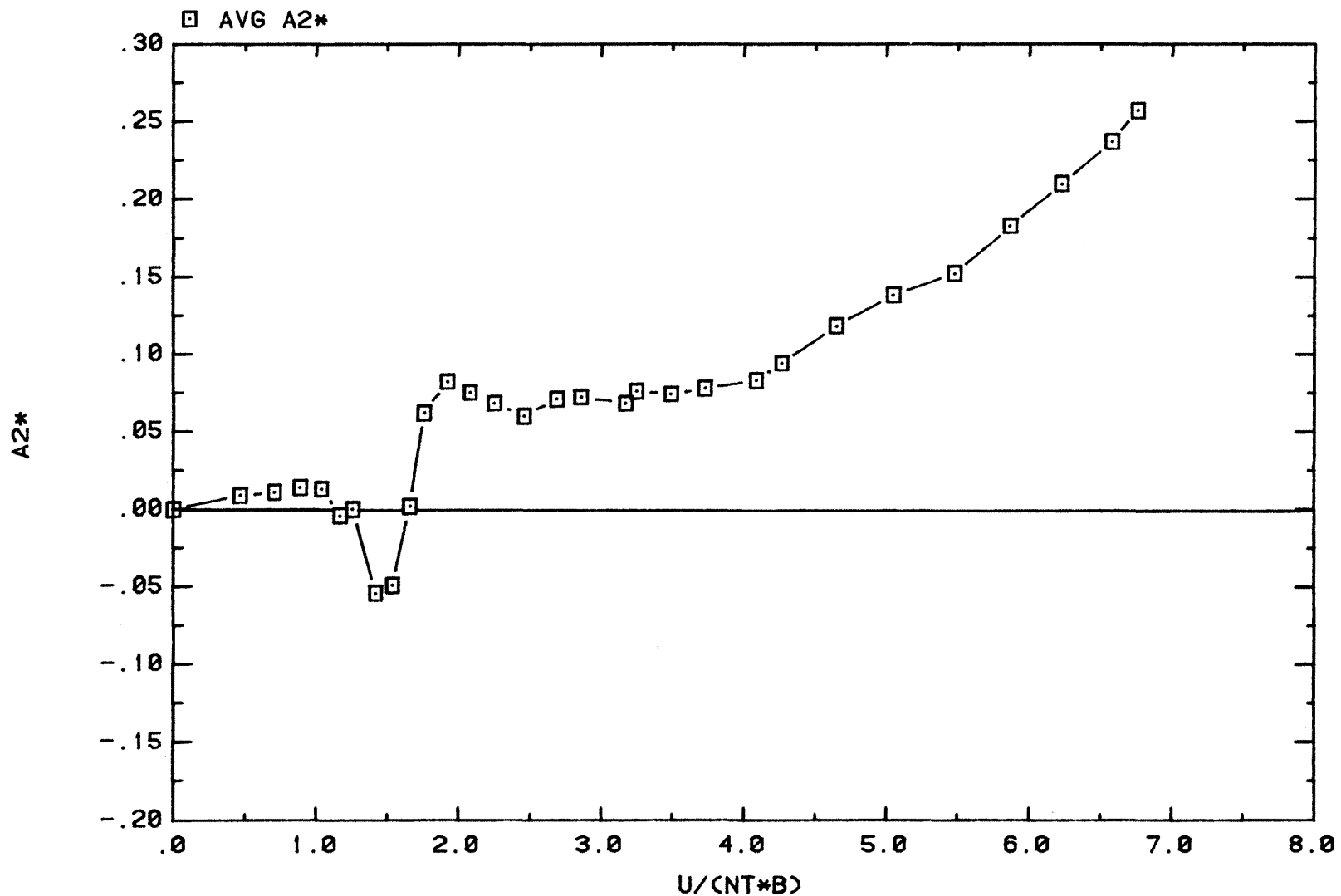
Figure 32. Prototype Critical Wind Speed for Torsional Flutter, Angle of Attack $\beta = +3^\circ$



CONFIGURATION AIII-V-2

ORIGINAL BRIDGE DECK WITH RAILINGS BETA=-3 DEG

Figure 33. Aerodynamic Derivative $-H_1^*$, Angle of Attack $\beta = -3^\circ$



CONFIGURATION AIII-T-2

ORIGINAL BRIDGE DECK WITH RAILINGS BETA=-3 DEG

Figure 34. Aerodynamic Derivative A_2^* , Angle of Attack $\beta = -3^\circ$

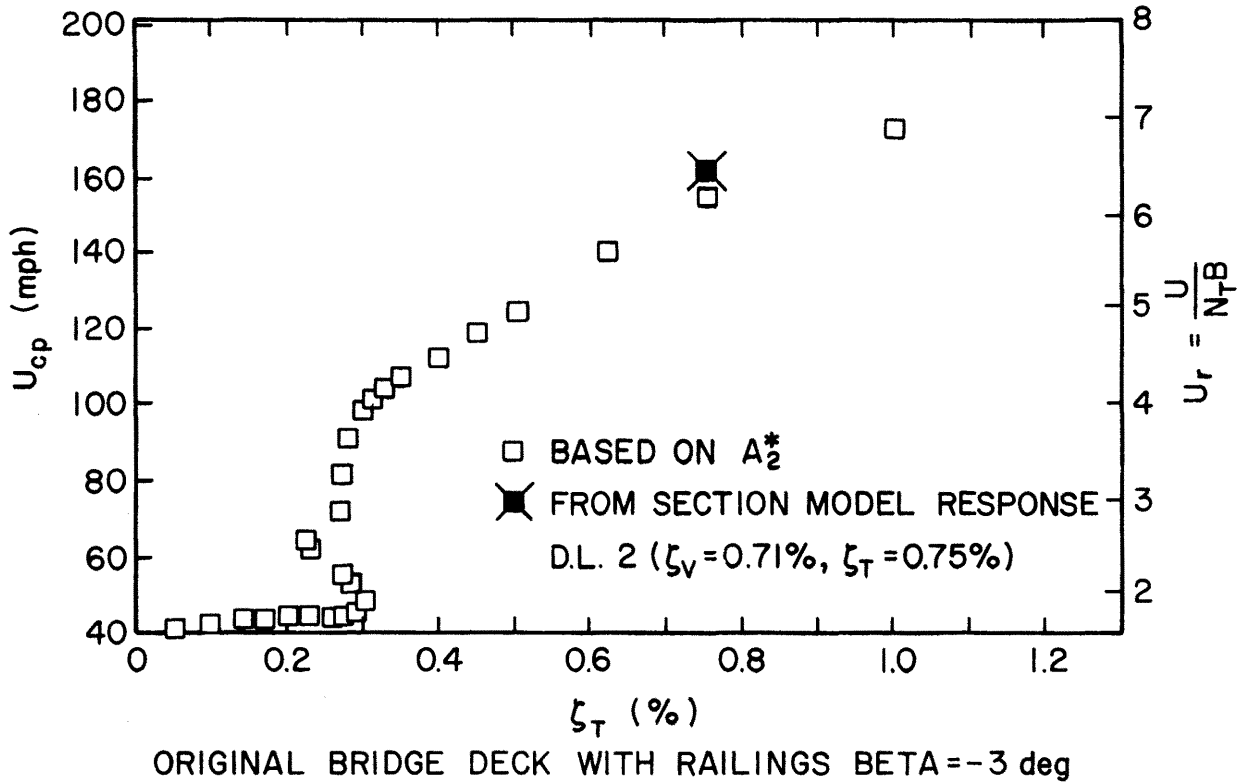
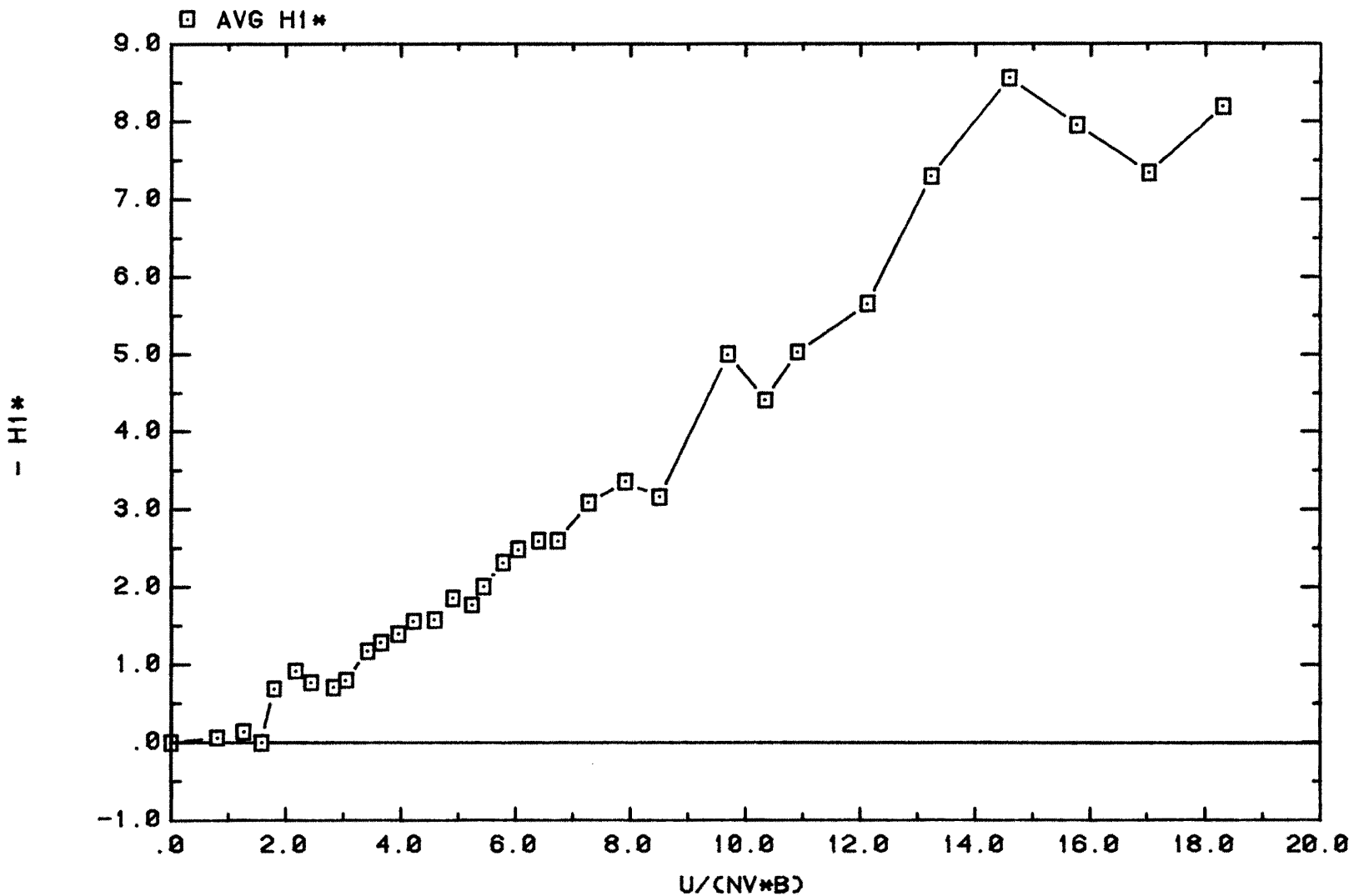
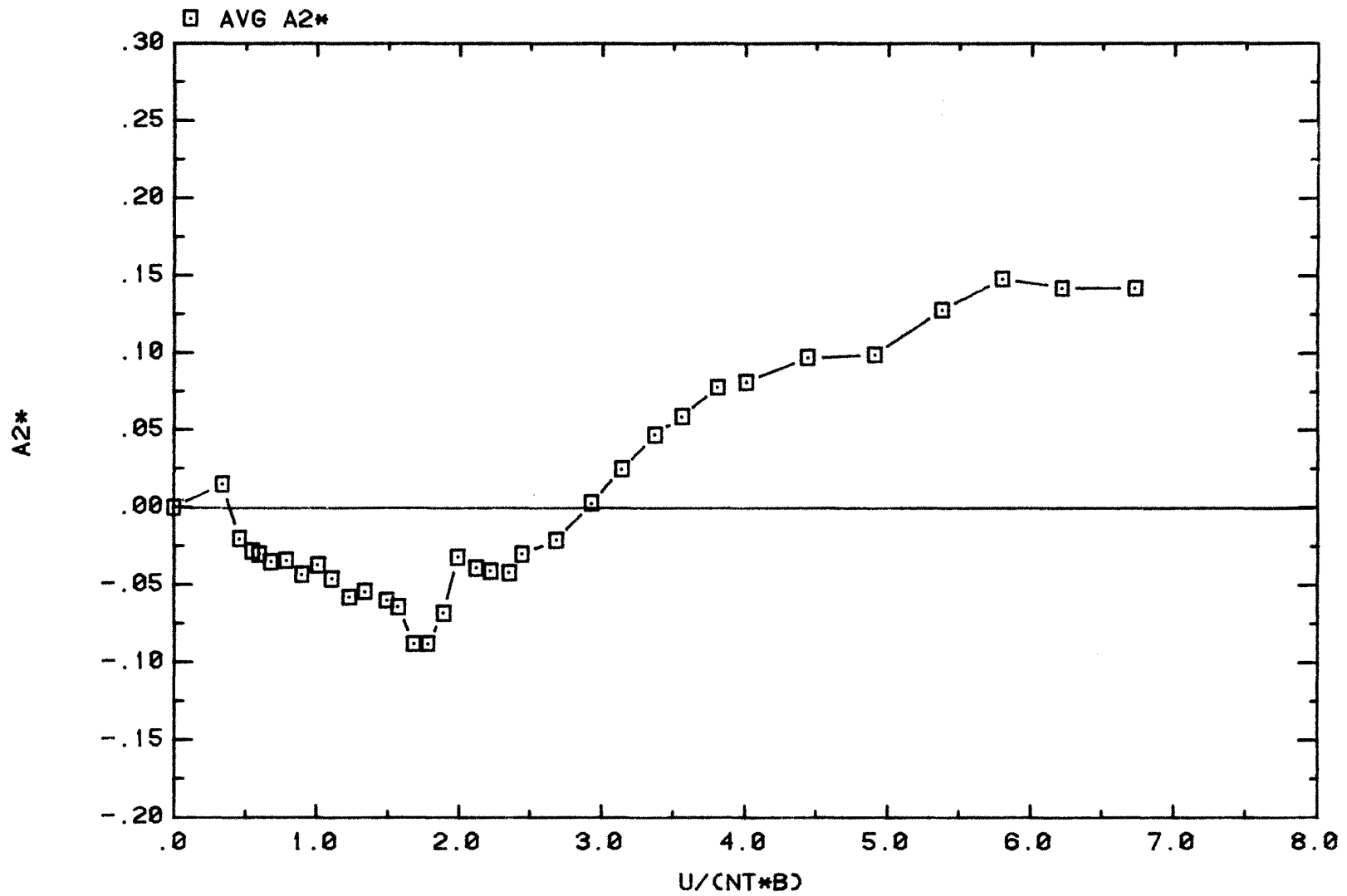


Figure 35. Prototype Critical Wind Speed for Torsional Flutter, Angle of Attack $\beta = -3^\circ$



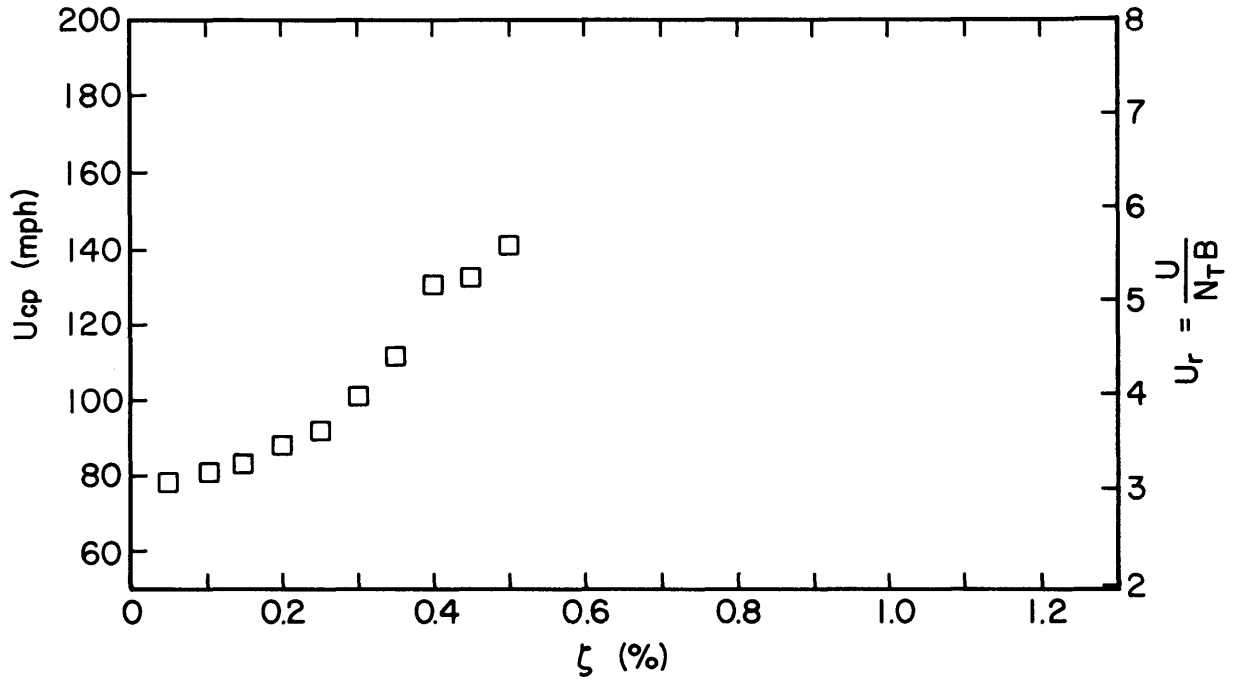
CONFIGURATION AII6-V-2
ORIGINAL BRIDGE DECK WITH RAILINGS BETA= 6 DEG
Figure 36. Aerodynamic Derivative $-H_1^*$, Angle of Attack $\beta = +6^\circ$



CONFIGURATION AII6-T-2

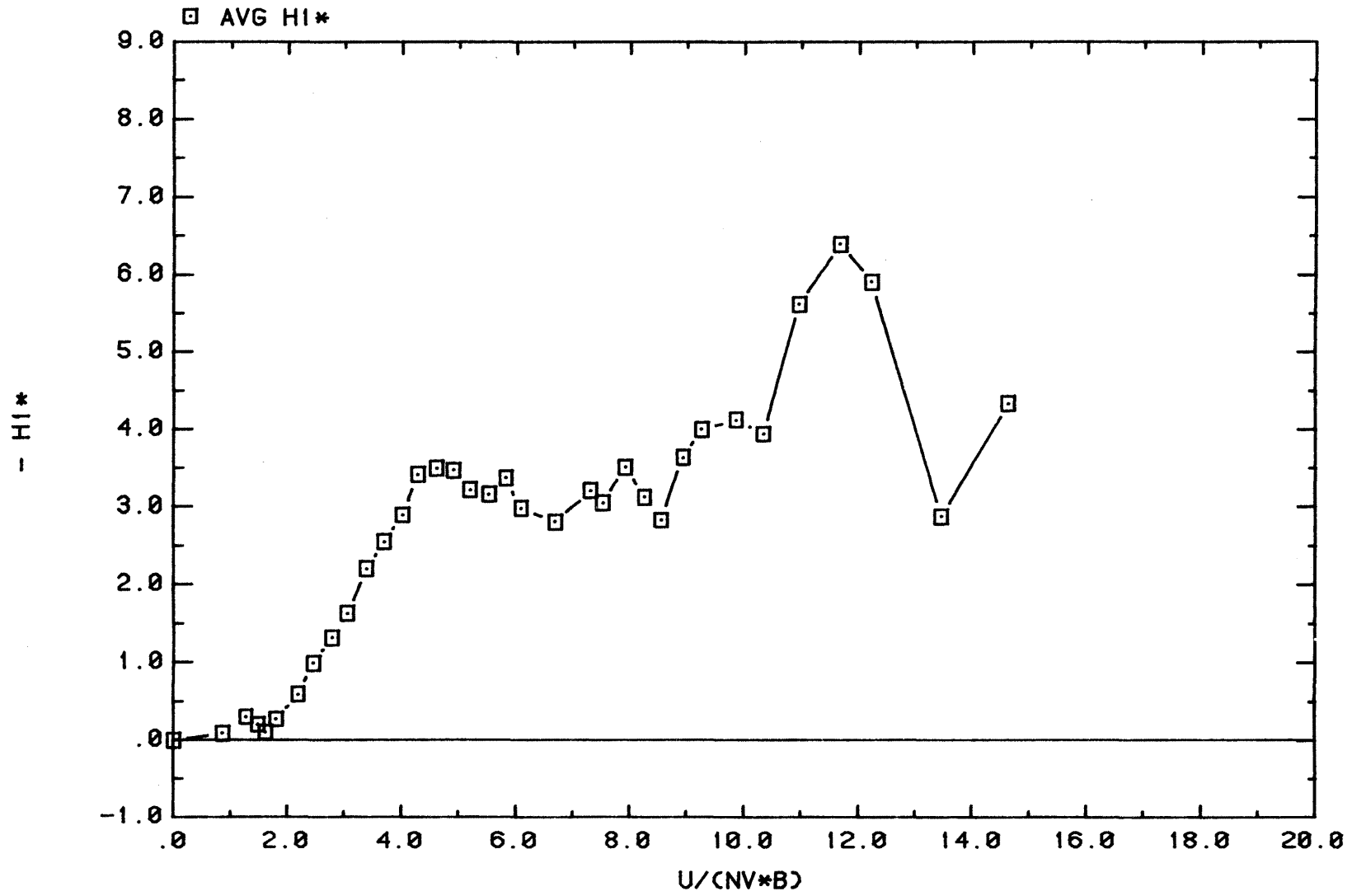
ORIGINAL BRIDGE DECK WITH RAILINGS BETA= 6 DEG

Figure 37. Aerodynamic Derivative A_2^* , Angle of Attack $\beta = +6^\circ$



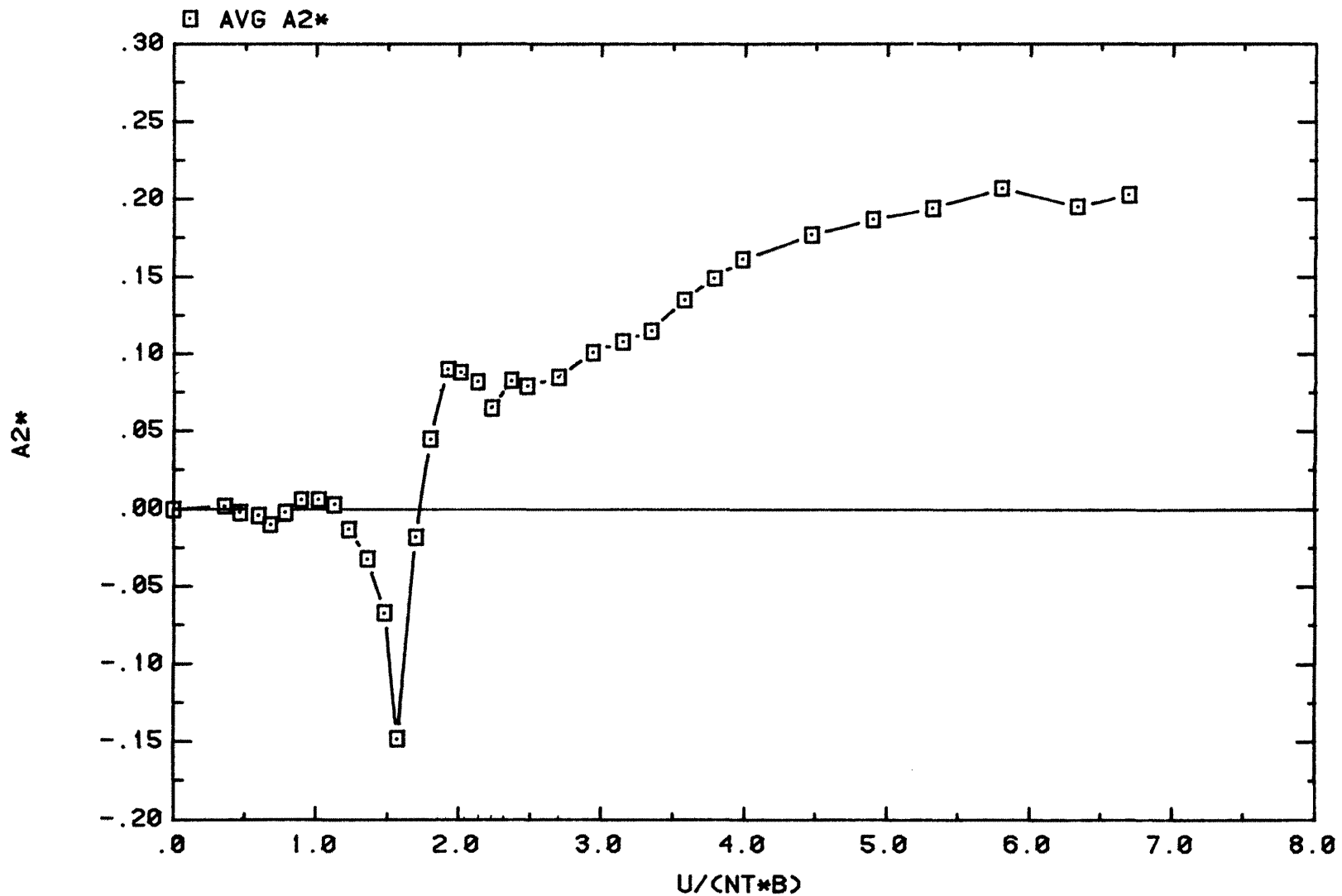
ORIGINAL BRIDGE DECK WITH RAILINGS BETA=+6 deg

Figure 38. Prototype Critical Wind Speed for Torsional Flutter, Angle of Attack $\beta = +6^\circ$



CONFIGURATION AIII6-V-2
 ORIGINAL BRIDGE DECK WITH RAILINGS BETA=-6 DEG

Figure 39. Aerodynamic Derivative $-H_1^*$, Angle of Attack $\beta = -6^\circ$



CONFIGURATION AIII6-T-2

ORIGINAL BRIDGE DECK WITH RAILINGS BETA=-6 DEG

Figure 40. Aerodynamic Derivative A_2^* , Angle of Attack $\beta = -6^\circ$

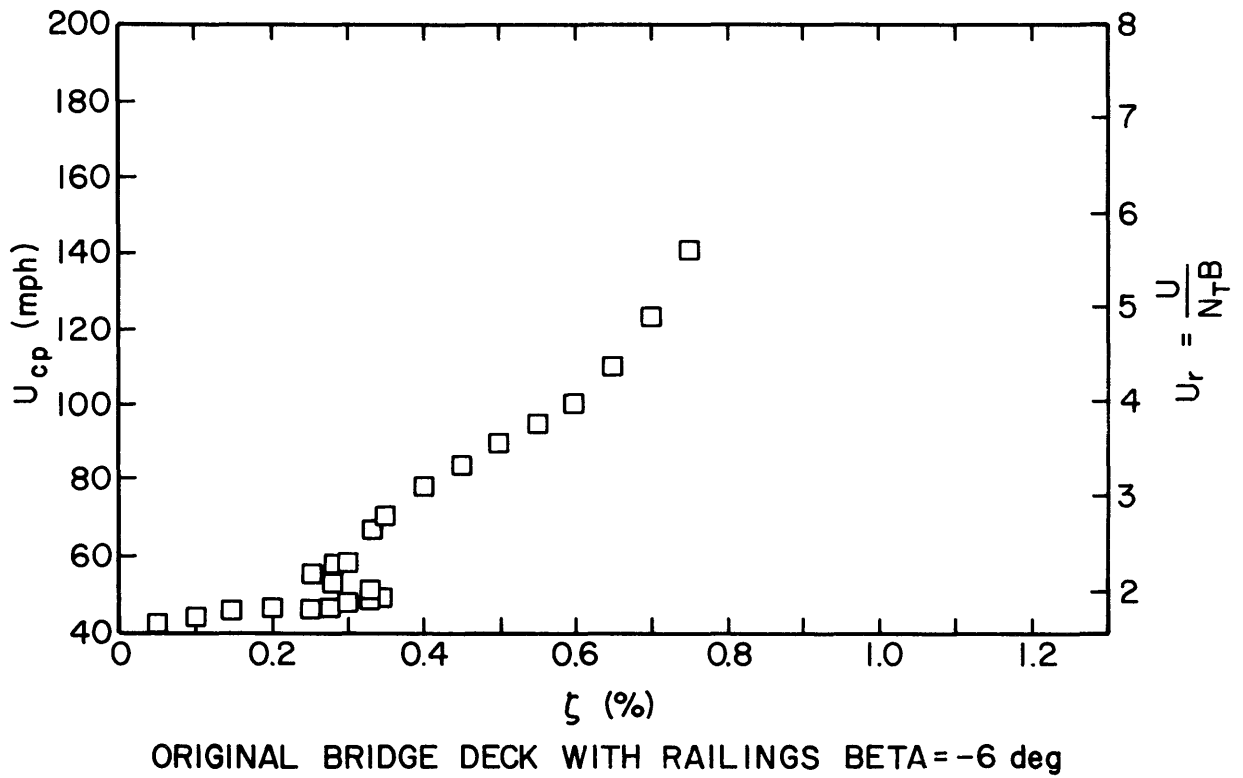


Figure 41. Prototype Critical Wind Speed for Torsional Flutter, Angle of Attack $\beta = -6^\circ$

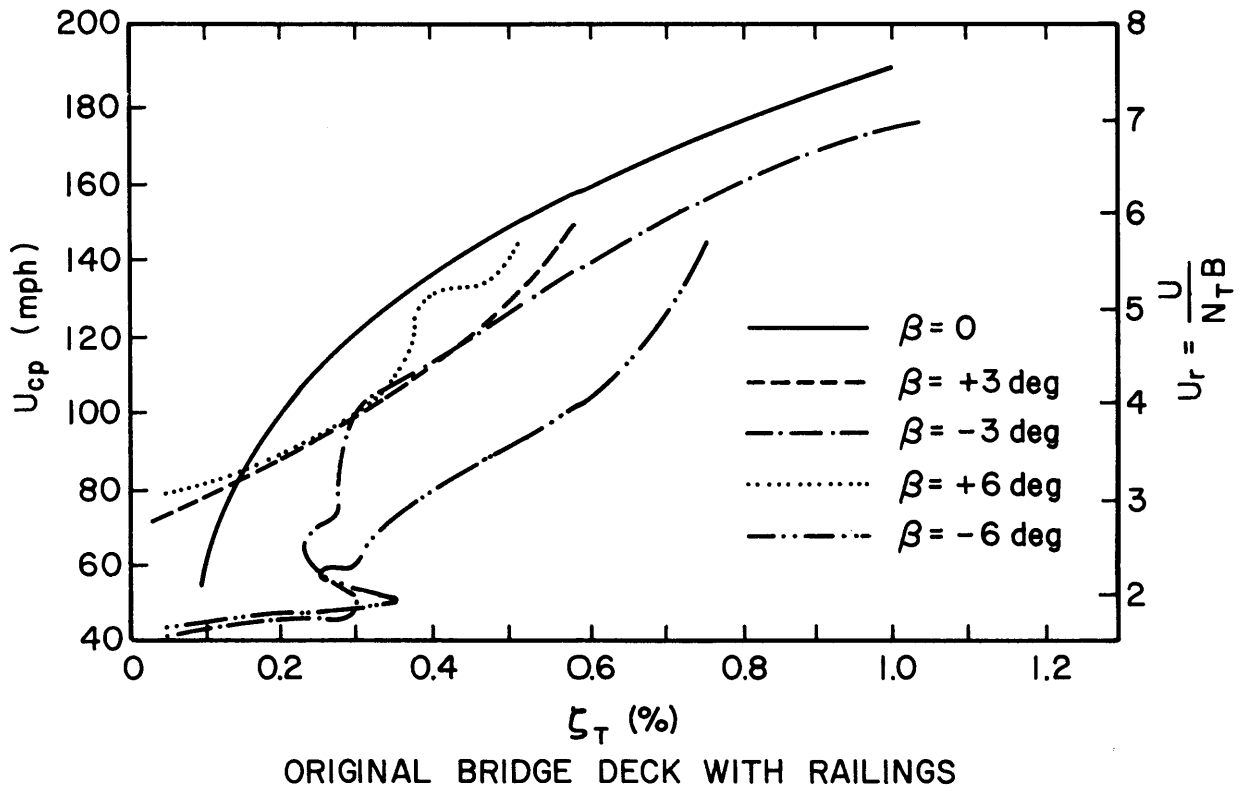
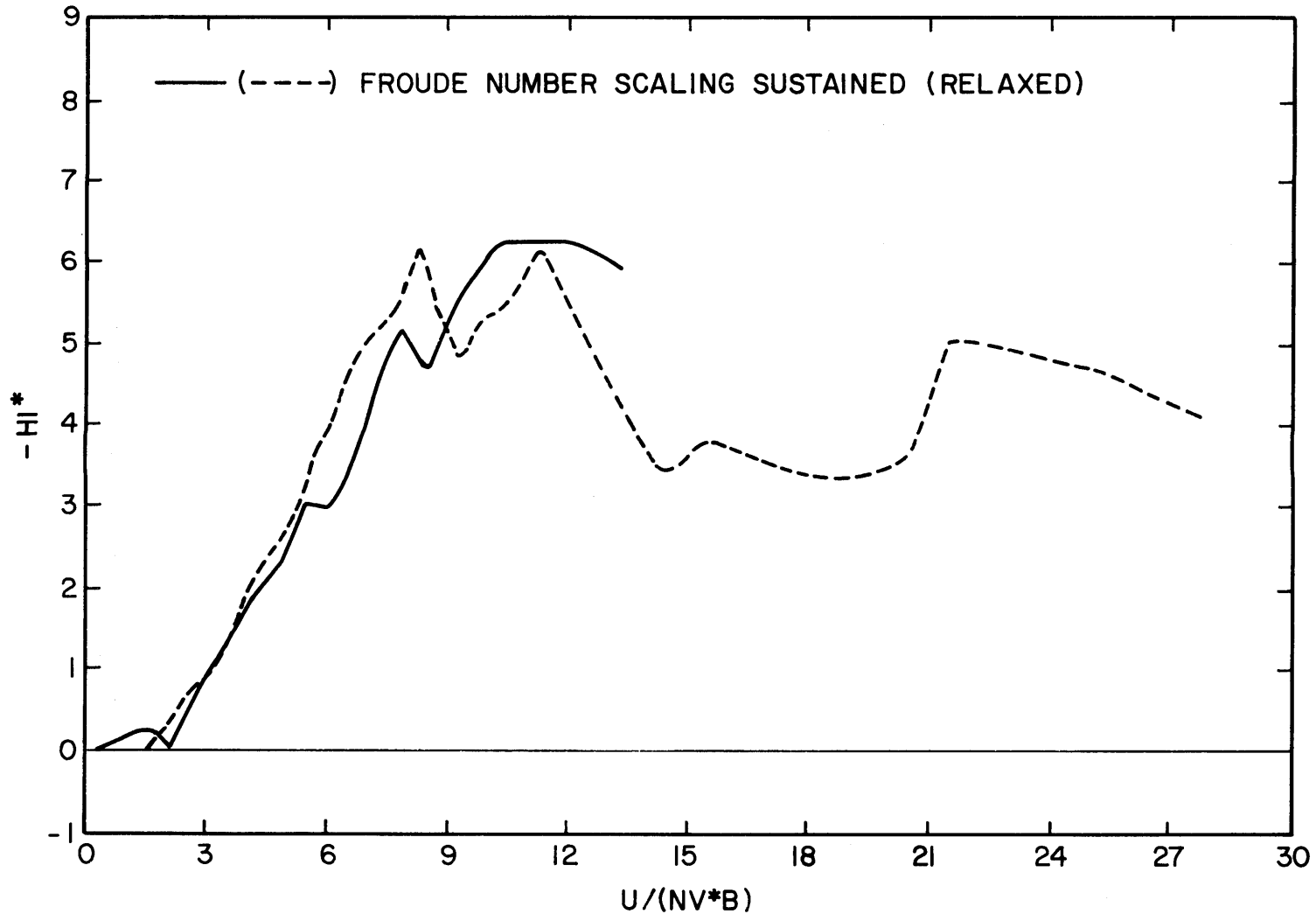
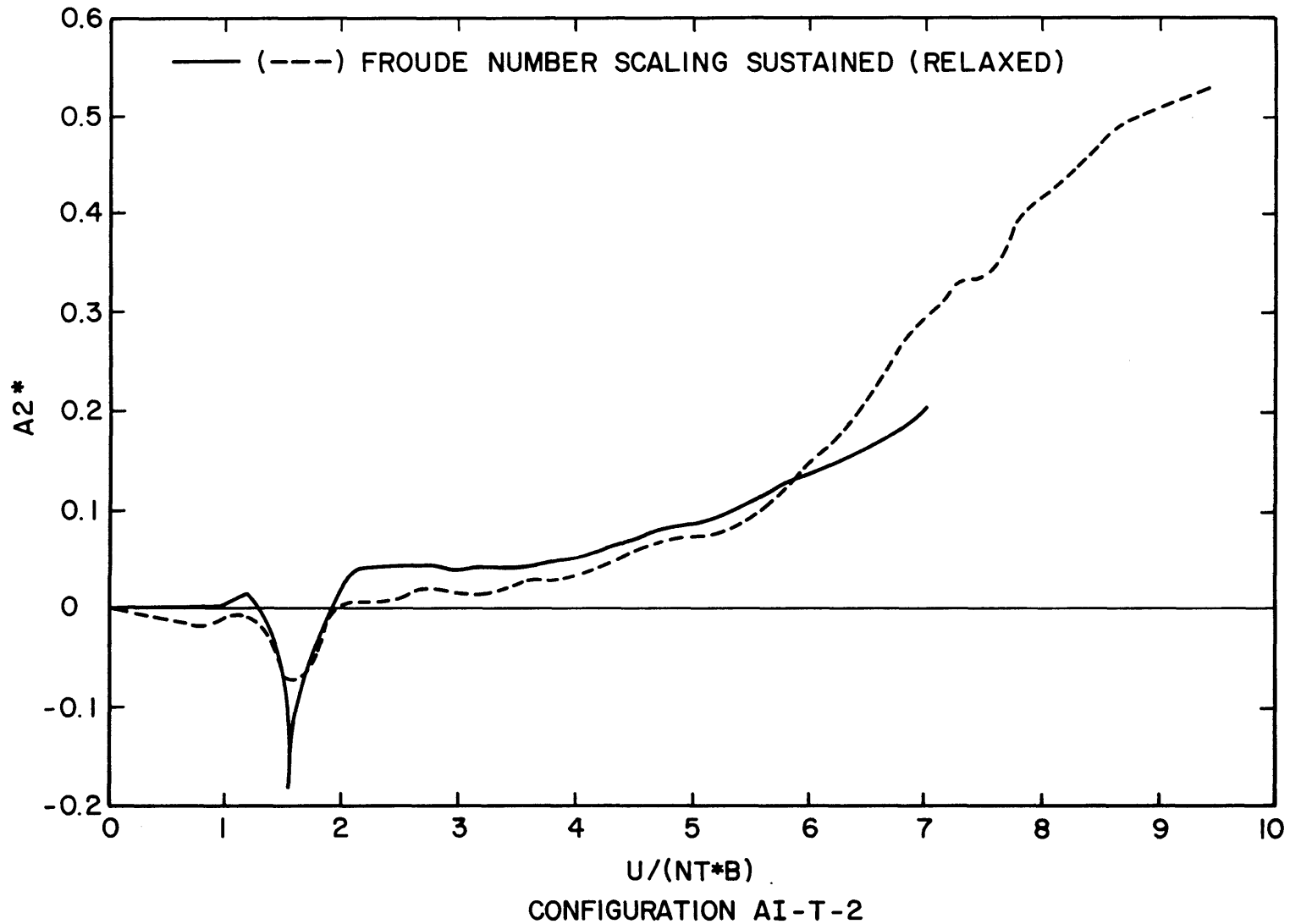


Figure 42. Prototype Critical Wind Speed for Torsional Flutter for Different Angles of Attack



CONFIGURATION AI-V-2
 ORIGINAL BRIDGE DECK WITH RAILINGS BETA = 0 deg

Figure 43. Aerodynamic Derivative $-H_1^*$ for Model with Froude Number Similarity Sustained and Relaxed, $\beta = 0^\circ$



ORIGINAL BRIDGE DECK WITH RAILINGS BETA = 0 deg

Figure 44. Aerodynamic Derivative A_2^* for Model with Froude Number Similarity Sustained and Relaxed, $\beta = 0^\circ$

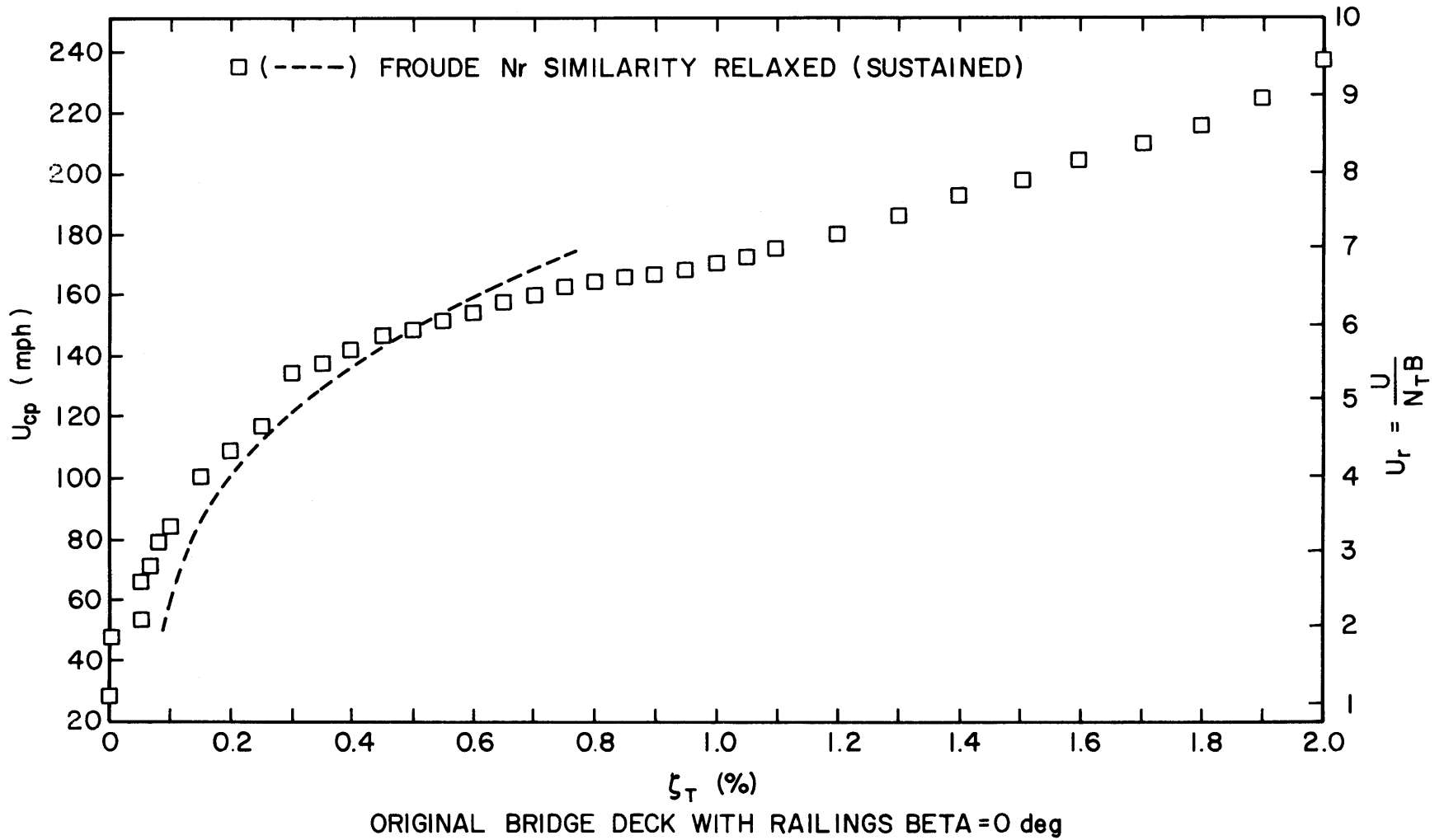
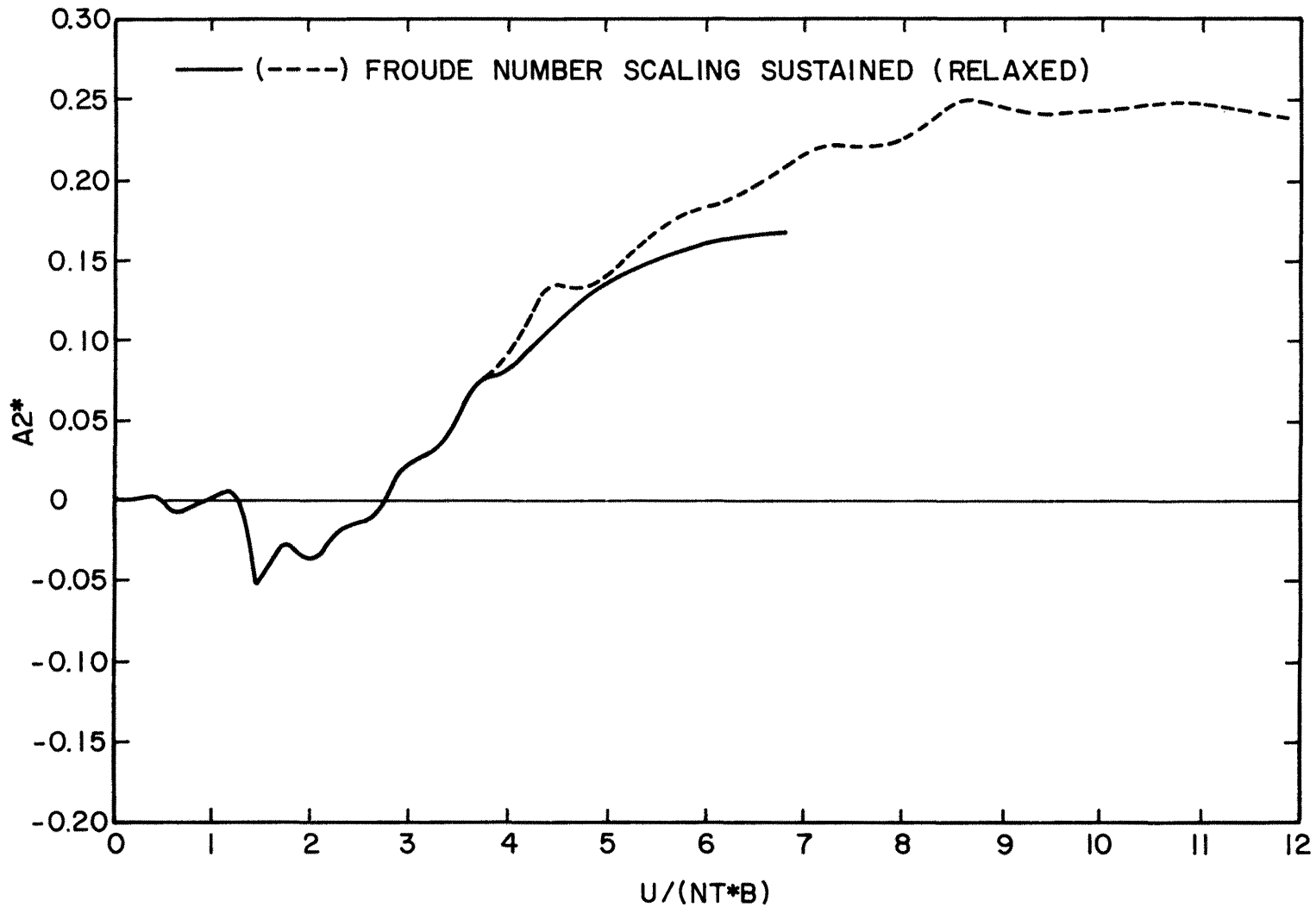


Figure 45. Prototype Critical Wind Speed, Froude Number Similarity Sustained and Relaxed, $\beta = 0^\circ$



CONFIGURATION AII-T-2
 ORIGINAL BRIDGE DECK WITH RAILINGS BETA = +3 deg

Figure 46. Aerodynamic Derivative A_2^* for Model with Froude Number Similarity Sustained and Relaxed, $\beta = +3^\circ$

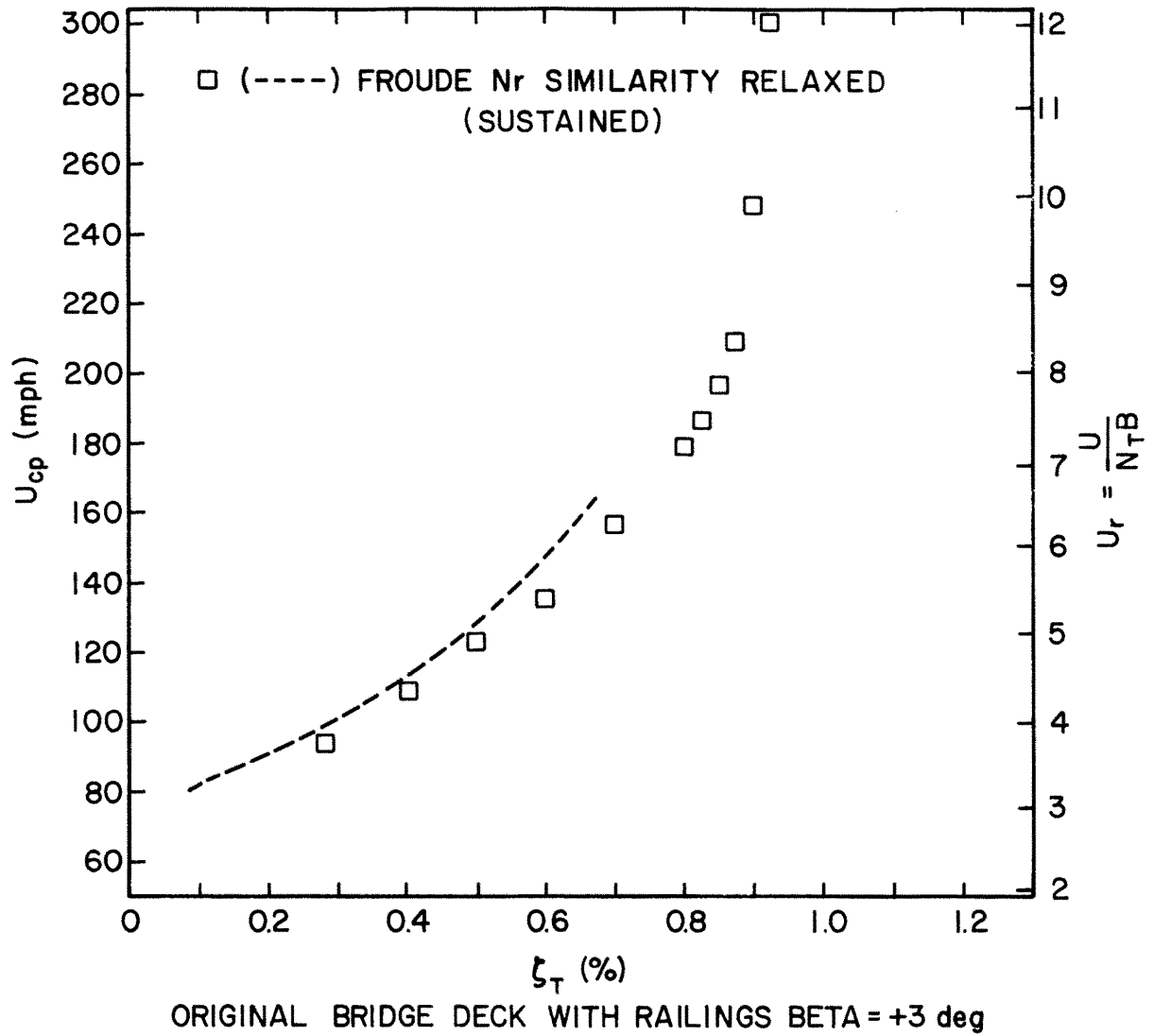
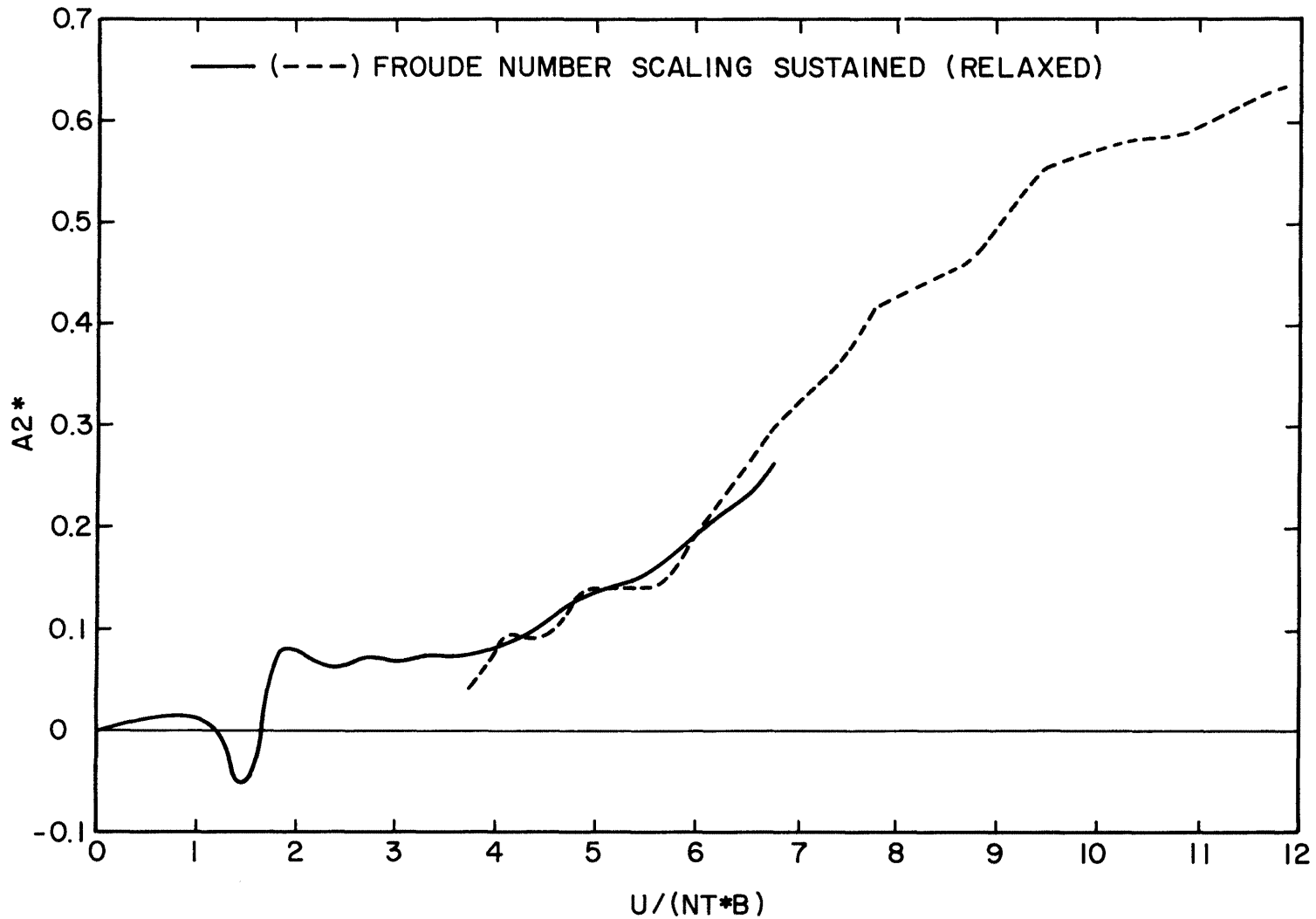


Figure 47. Prototype Critical Wind Speed, Froude Number Similarity Sustained and Relaxed, $\beta = +3^\circ$



U/(NT*B)
 CONFIGURATION AIII-T-2
 ORIGINAL BRIDGE DECK WITH RAILINGS BETA = -3 deg

Figure 48. Aerodynamic Derivative A_2^* for Model with Froude Number Similarity Sustained and Relaxed, $\beta = -3^\circ$

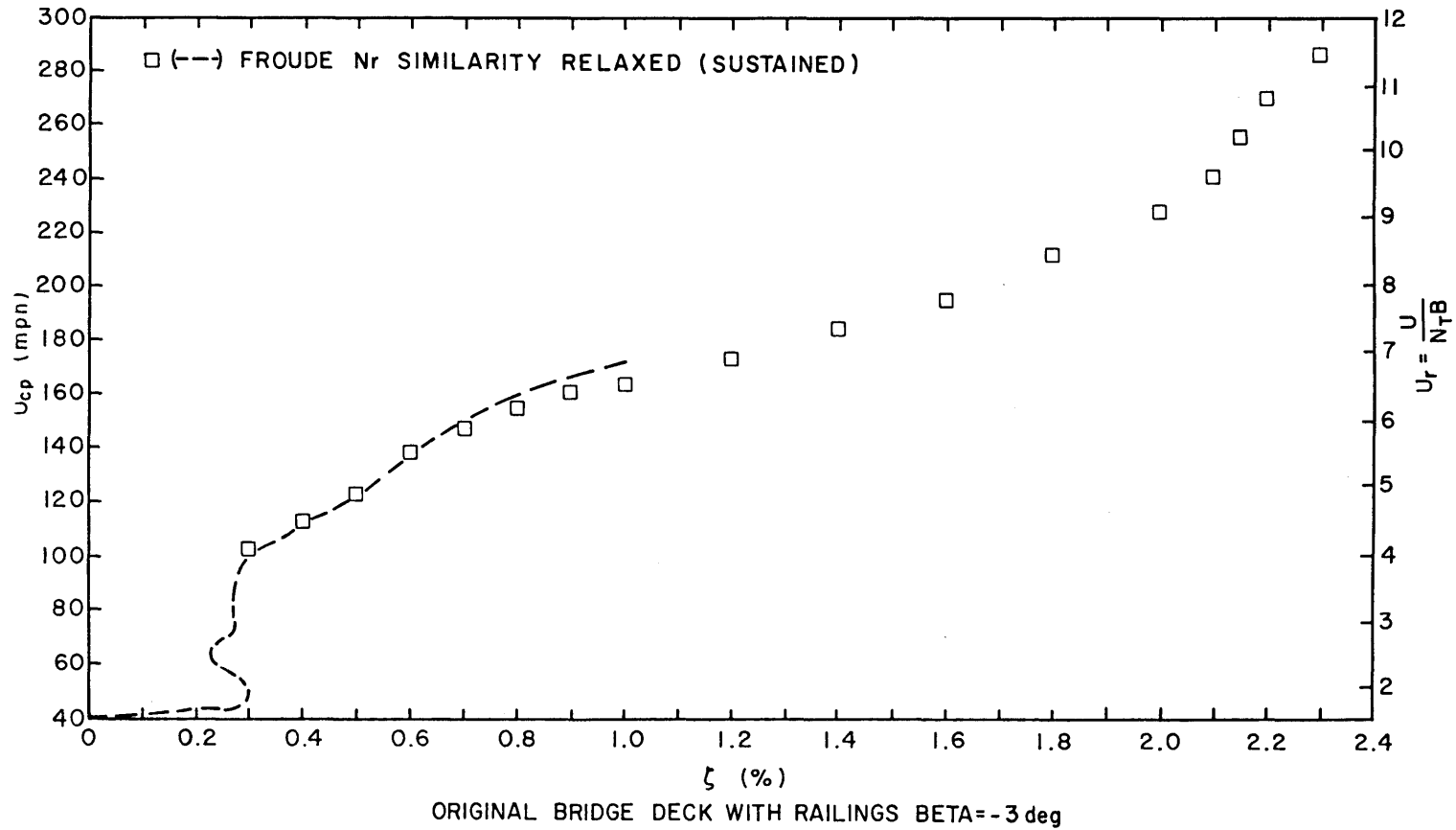
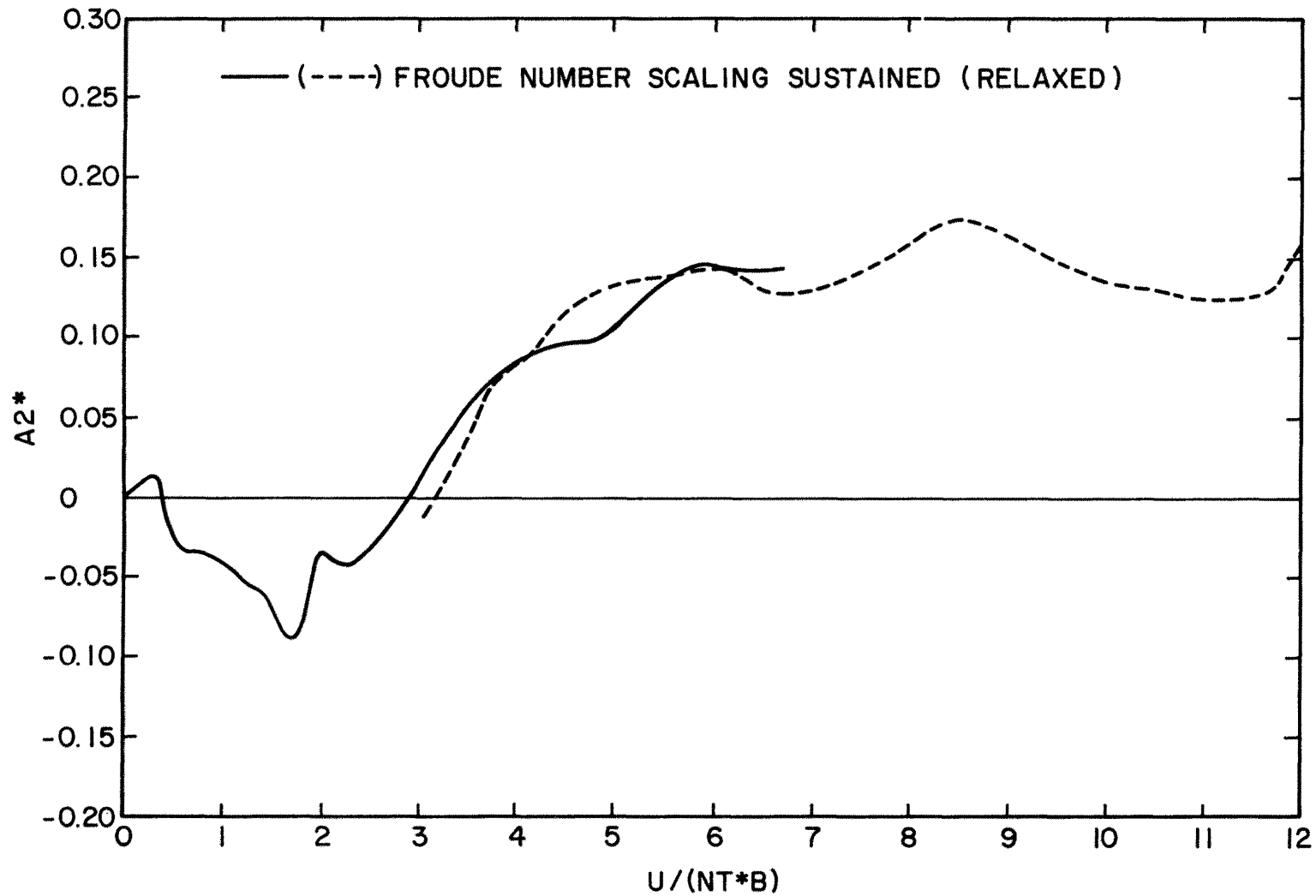


Figure 49. Prototype Critical Wind Speed, Froude Number Similarity Sustained and Relaxed, $\beta = -3^\circ$



CONFIGURATION AII6-T-2

ORIGINAL BRIDGE DECK WITH RAILINGS BETA = +6 deg

Figure 50. Aerodynamic Derivative A_2^* for Model with Froude Number Similarity Sustained and Relaxed, $\beta = +6^\circ$

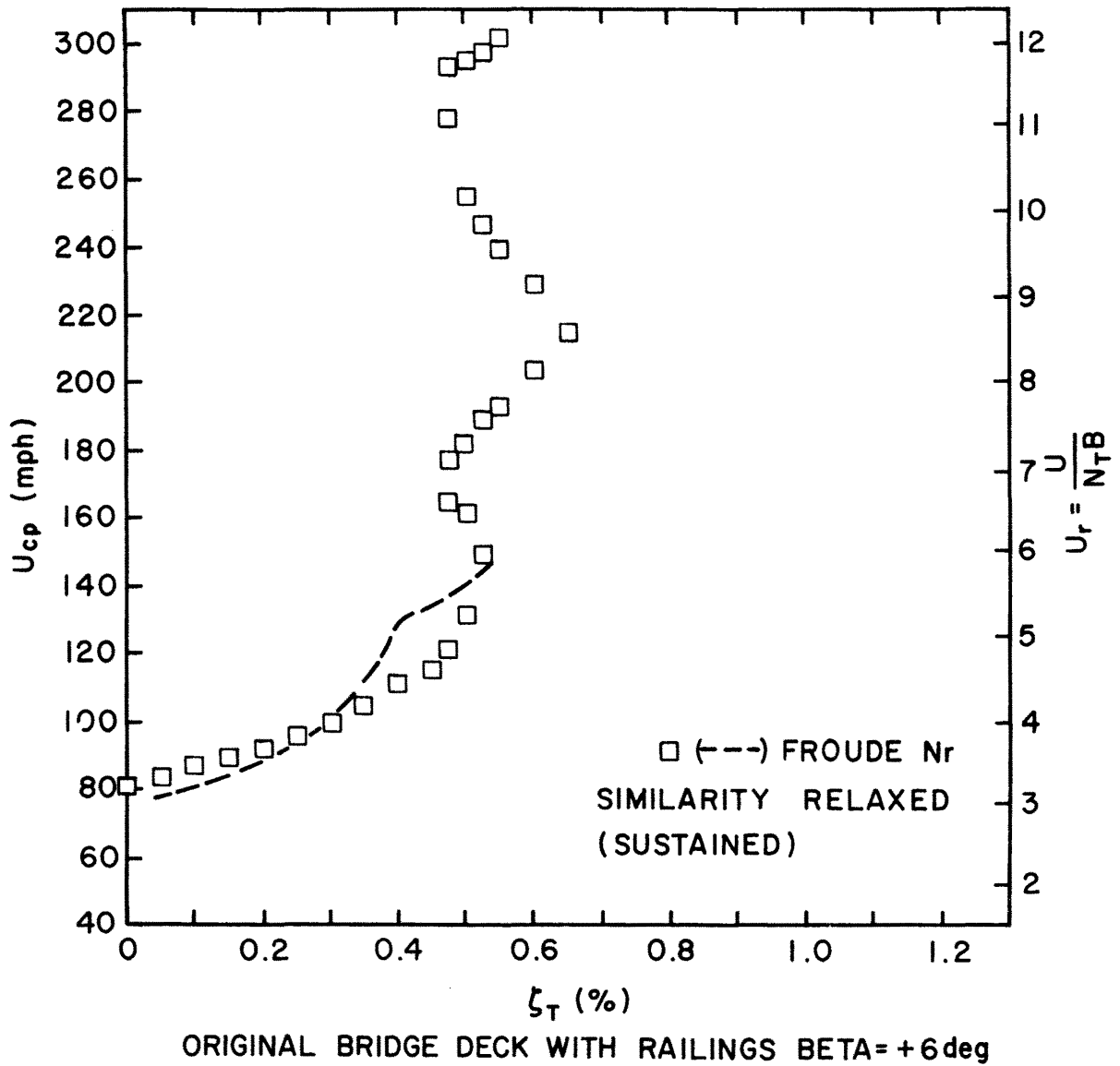
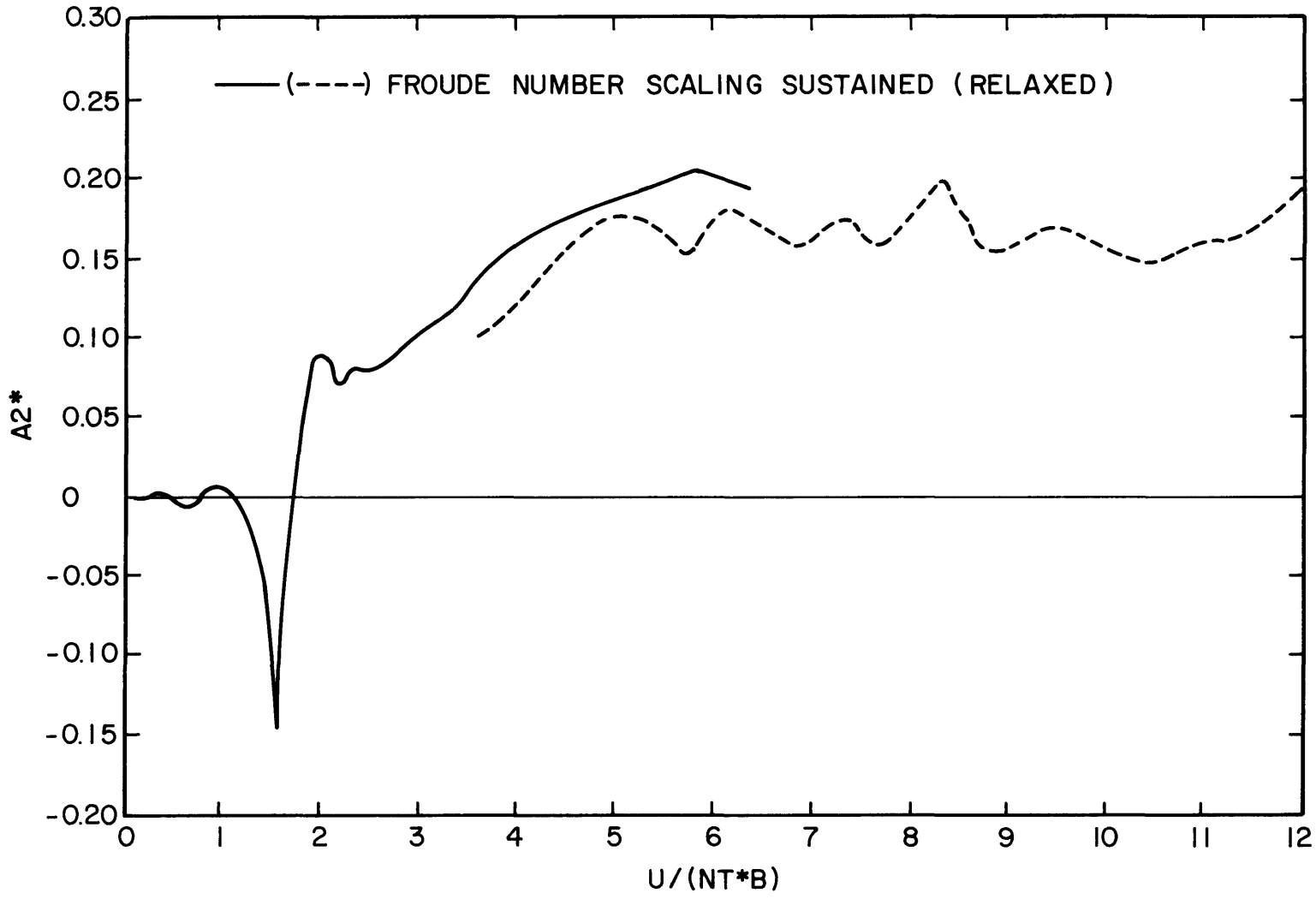


Figure 51. Prototype Critical Wind Speed, Froude Number Similarity Sustained and Relaxed, $\beta = +6^\circ$



CONFIGURATION AIII6-T-2
ORIGINAL BRIDGE DECK WITH RAILINGS BETA = -6 deg

Figure 52. Aerodynamic Derivative A_2^* for Model with Froude Number Similarity Sustained and Relaxed, $\beta = -6^\circ$

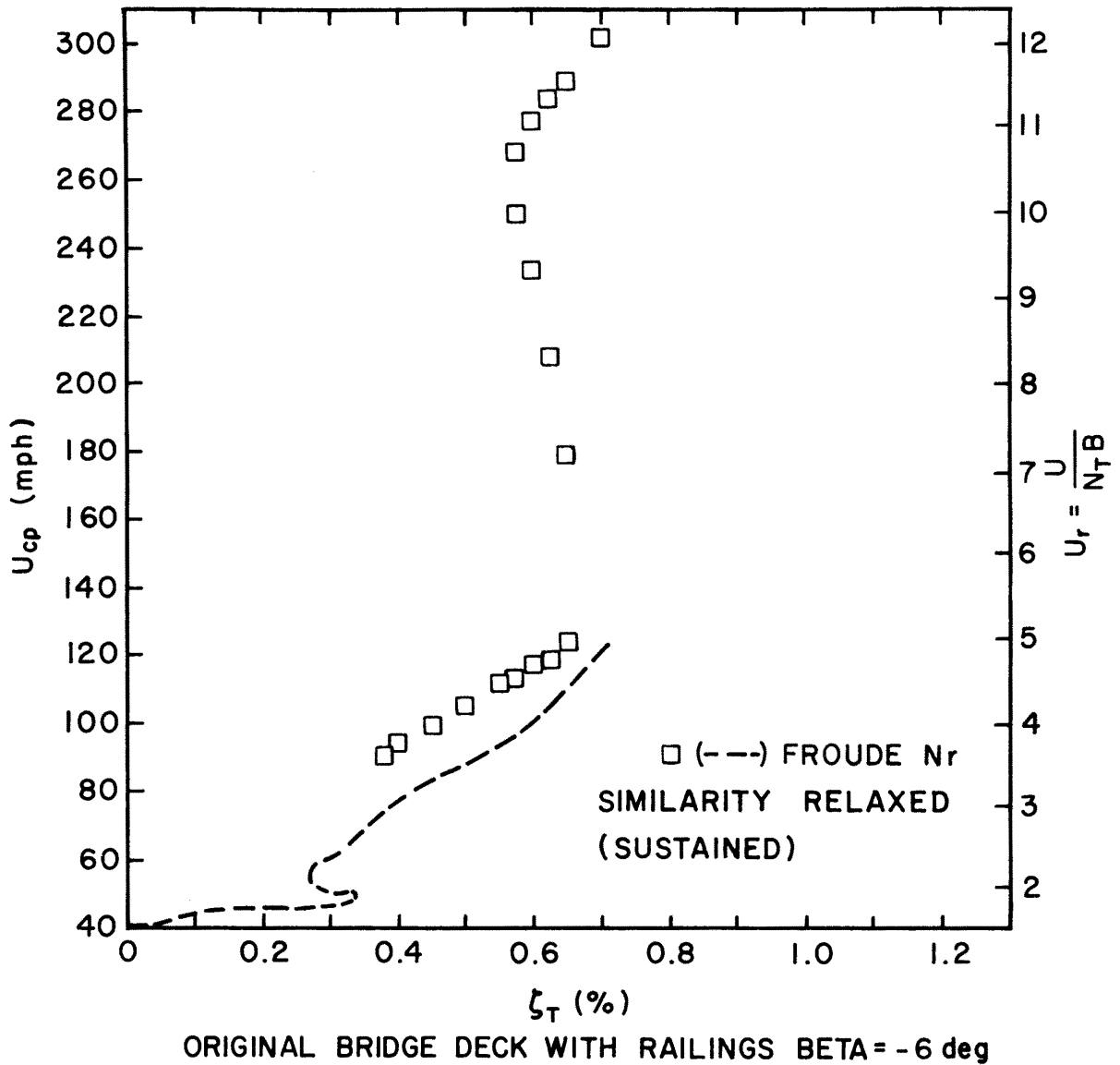


Figure 53. Prototype Critical Wind Speed, Froude Number Similarity Sustained and Relaxed, $\beta = -6^\circ$

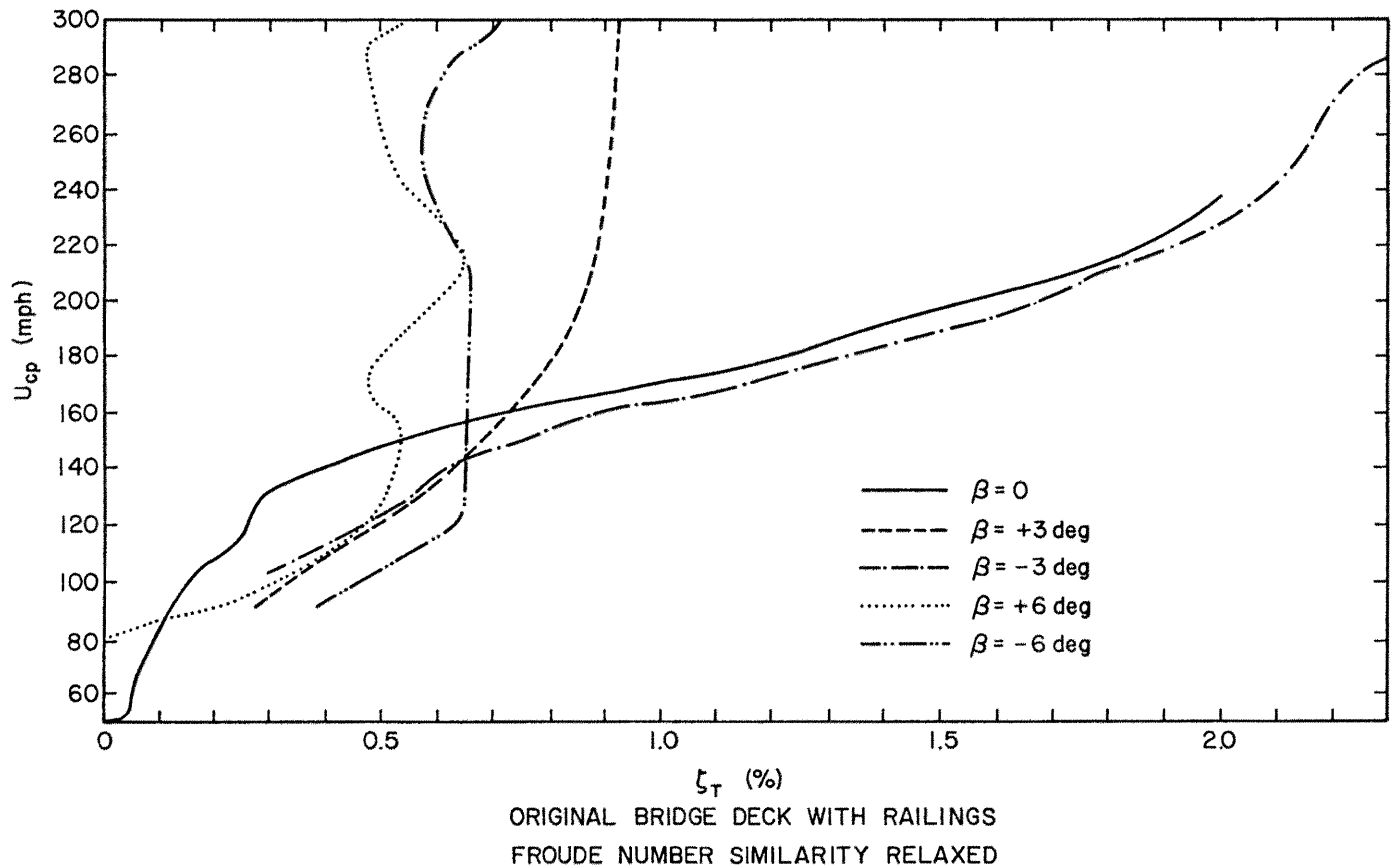


Figure 54. Prototype Critical Wind Speed for Different Angles of Attack, Froude Number Similarity Relaxed

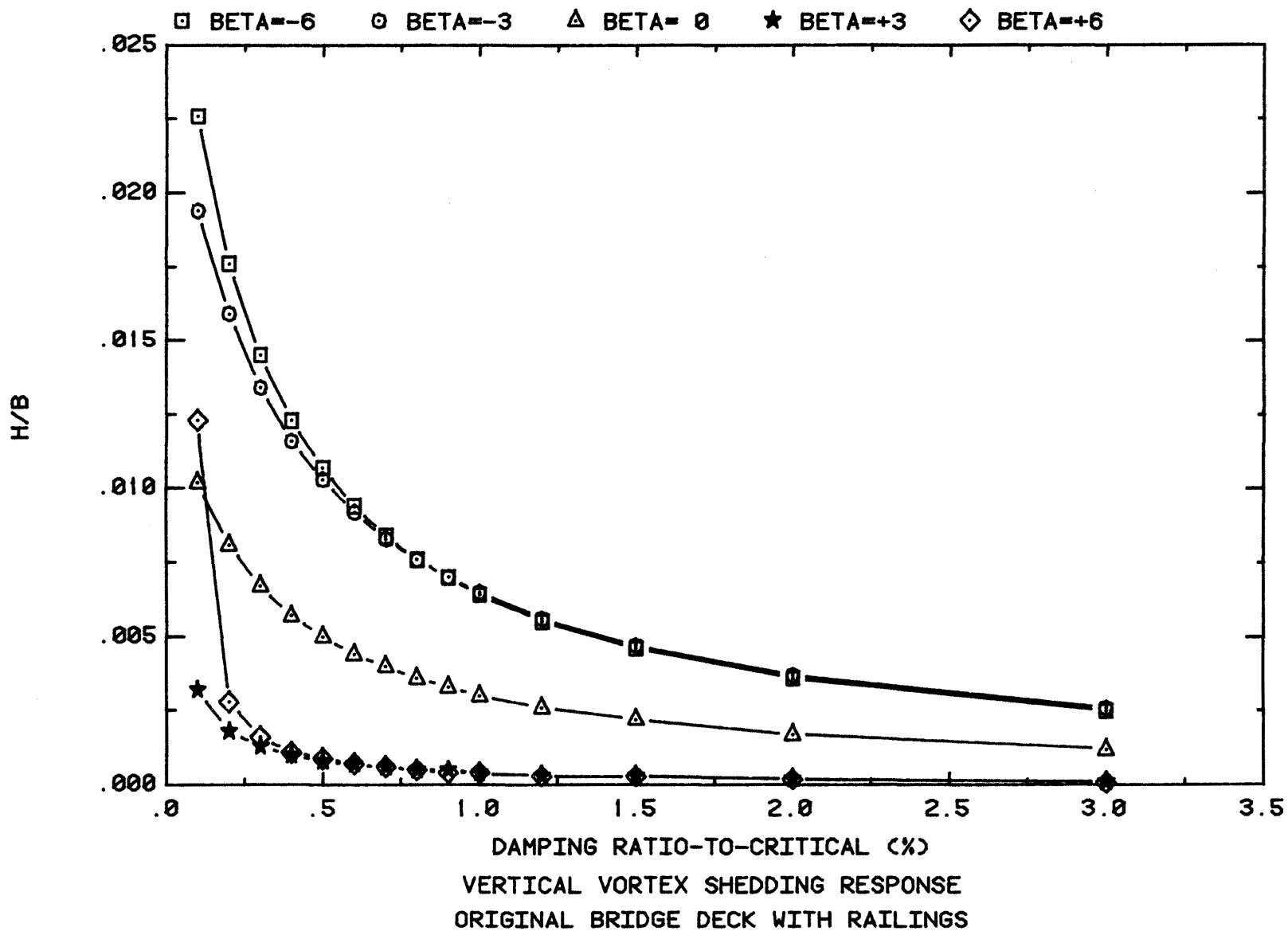
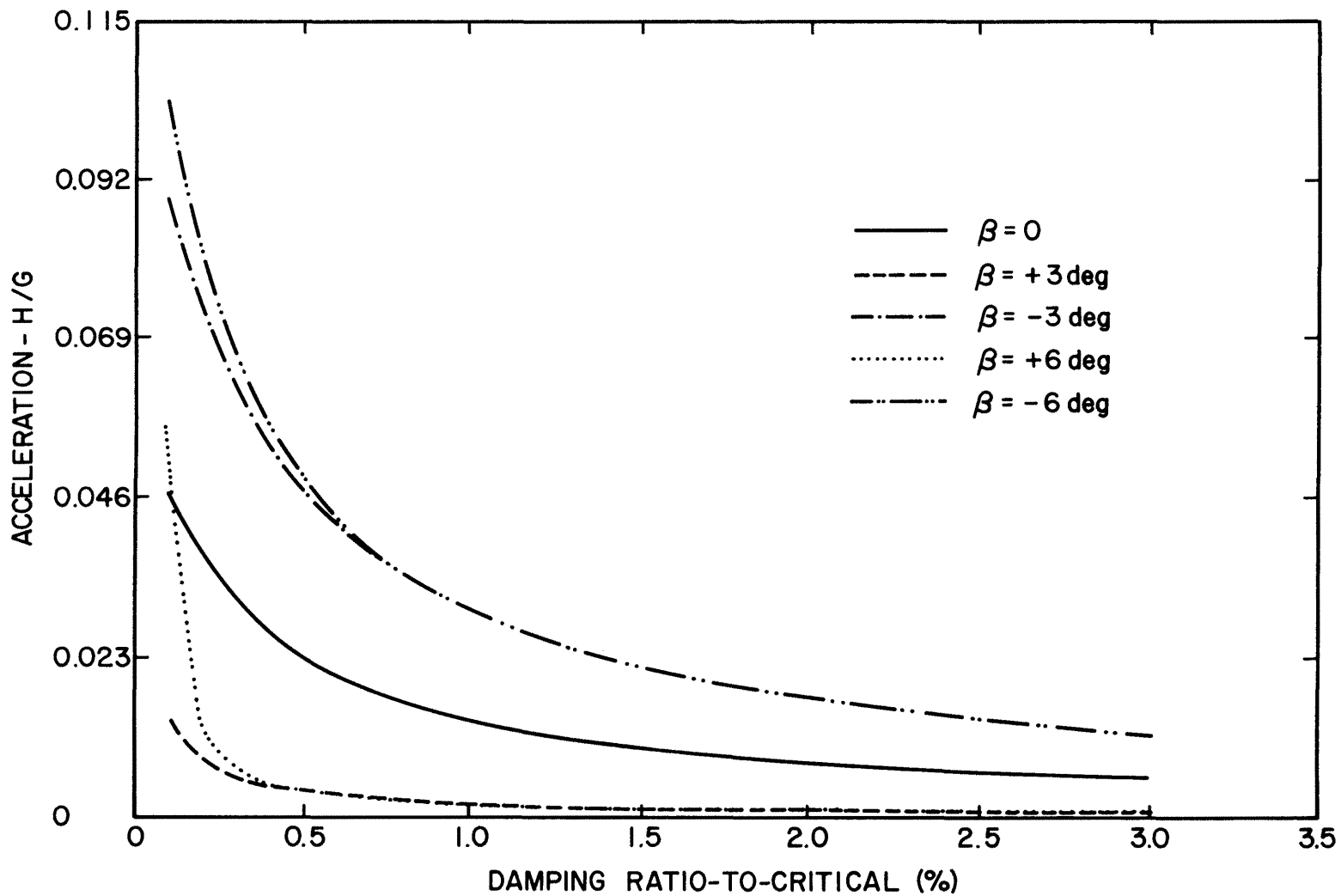


Figure 55. Prototype Vertical Vortex-Induced Response for Different Angles of Attack



VERTICAL VORTEX SHEDDING-ACCELERATIONS
ORIGINAL BRIDGE DECK WITH RAILINGS

Figure 56. Prototype Vertical Accelerations Associated with Vortex-Induced Response for Different Angles of Attack

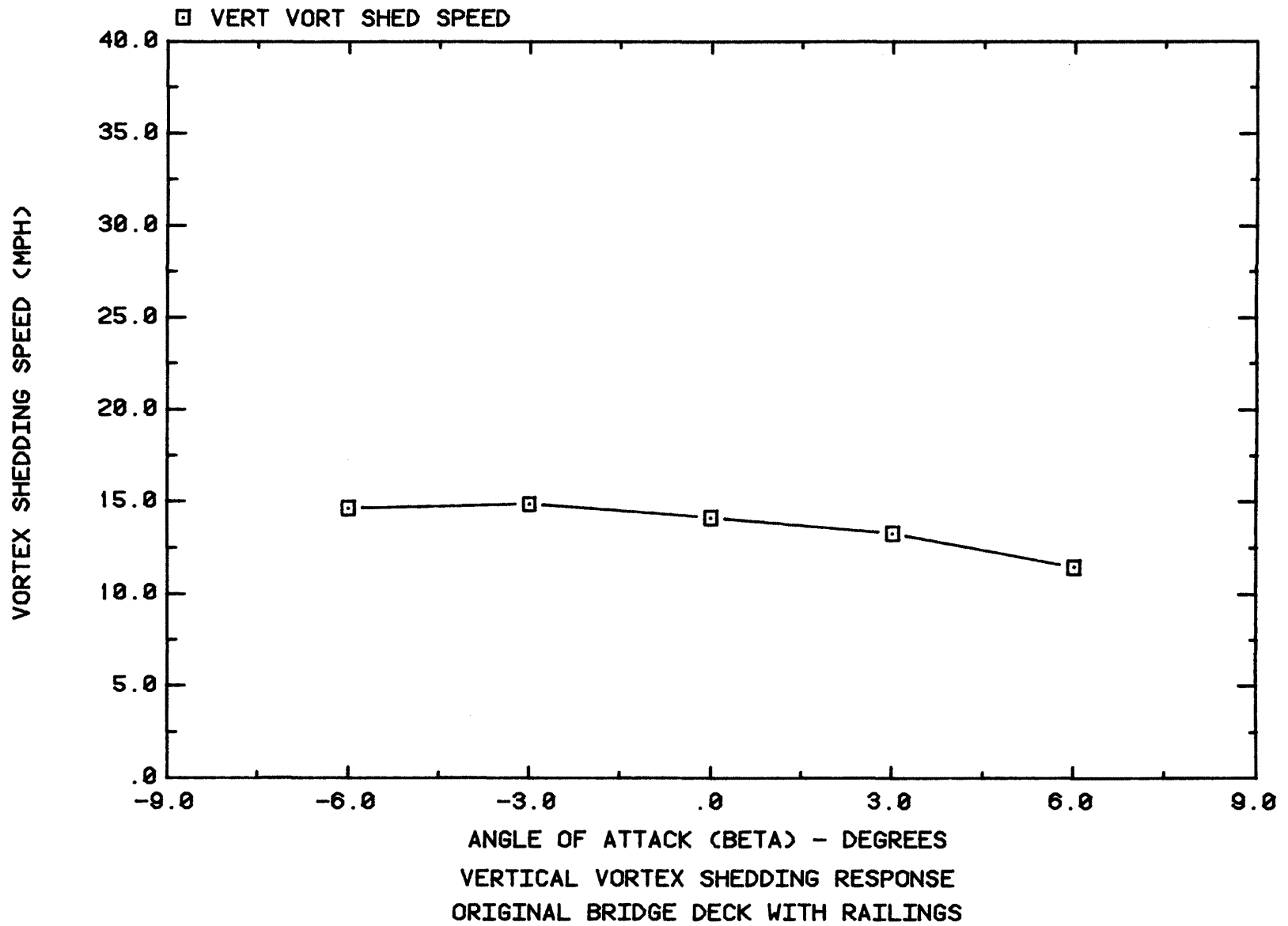


Figure 57. Prototype Speed Associated with Maximum Vortex-Induced Vertical Response

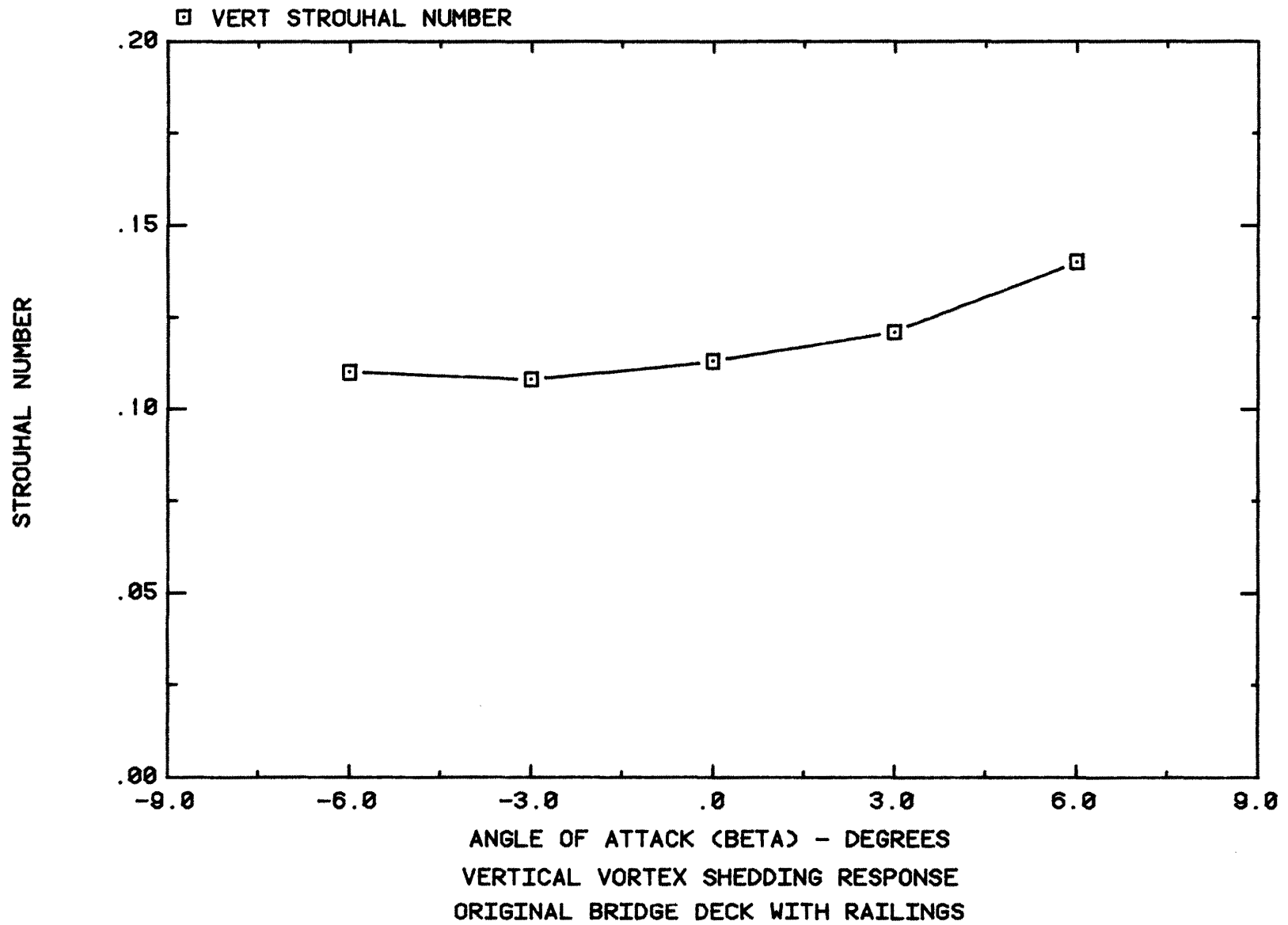


Figure 58. Strouhal Number Based on Vertical Vortex-Induced Response

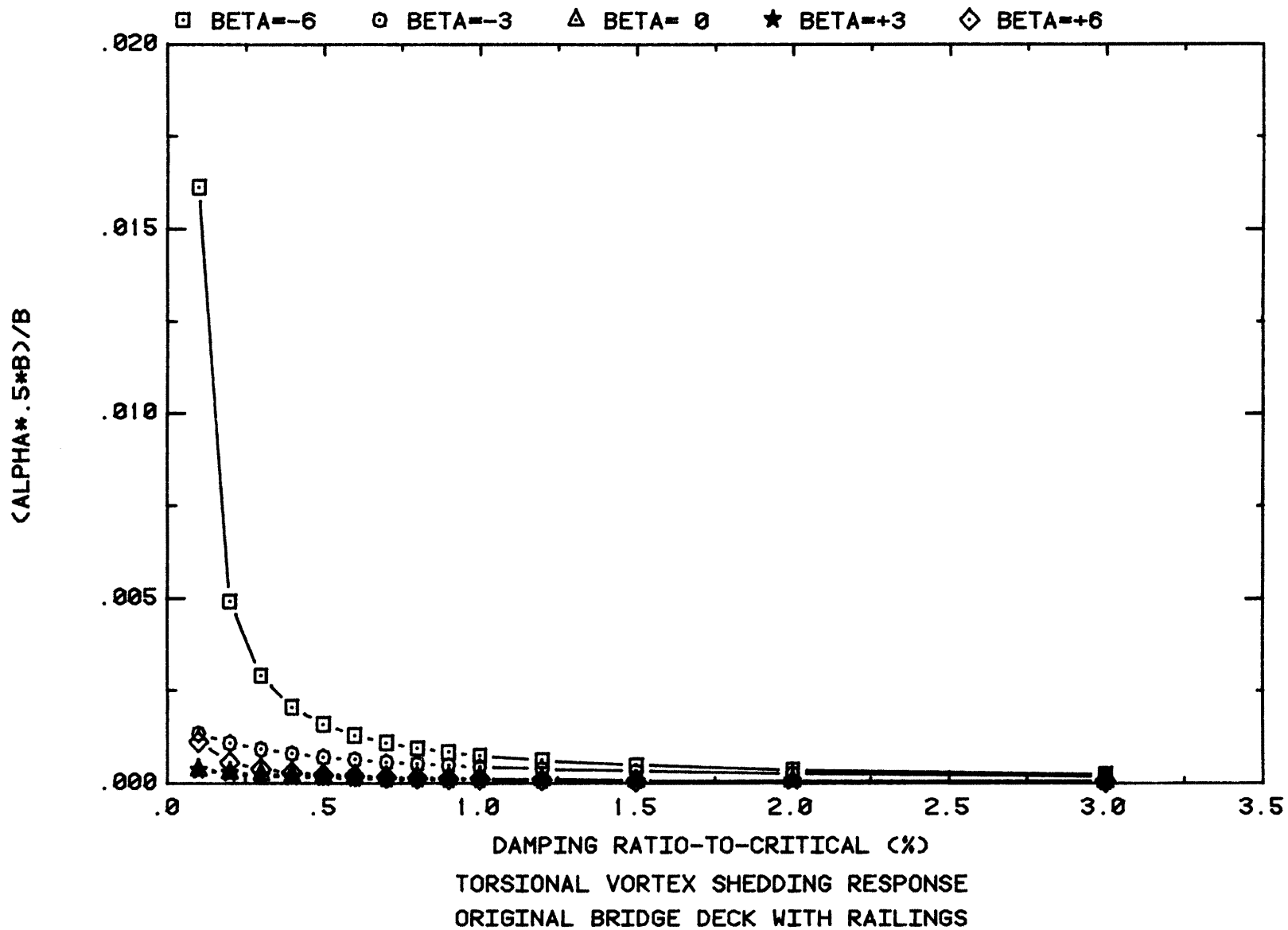
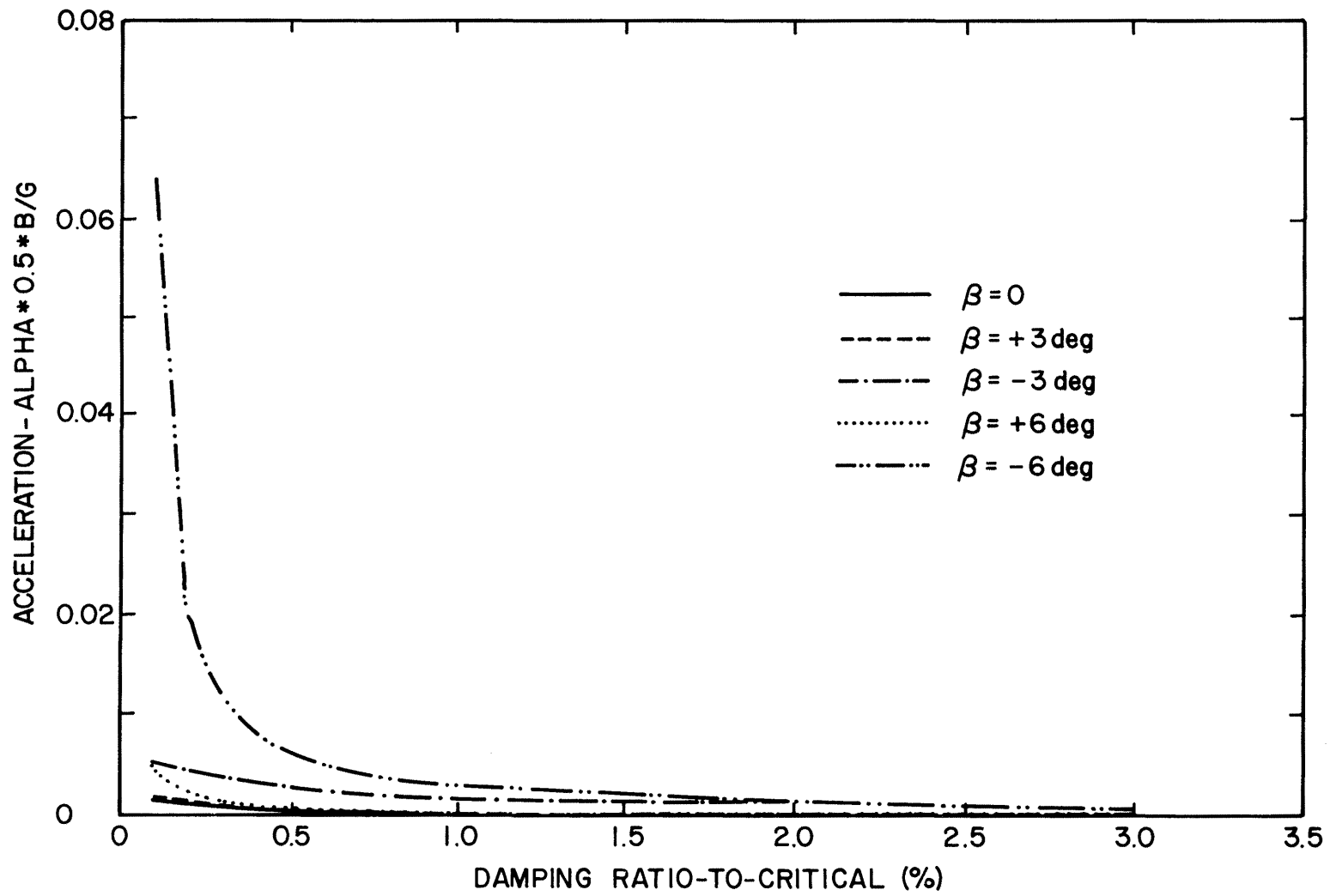


Figure 59. Prototype Maximum Vertical Deflections Associated with Torsional Vortex-Induced Response



TORSIONAL VORTEX SHEDDING-ACCELERATIONS
ORIGINAL BRIDGE DECK WITH RAILINGS

Figure 60. Prototype Maximum Vertical Accelerations Associated with Torsional Vortex-Induced Response

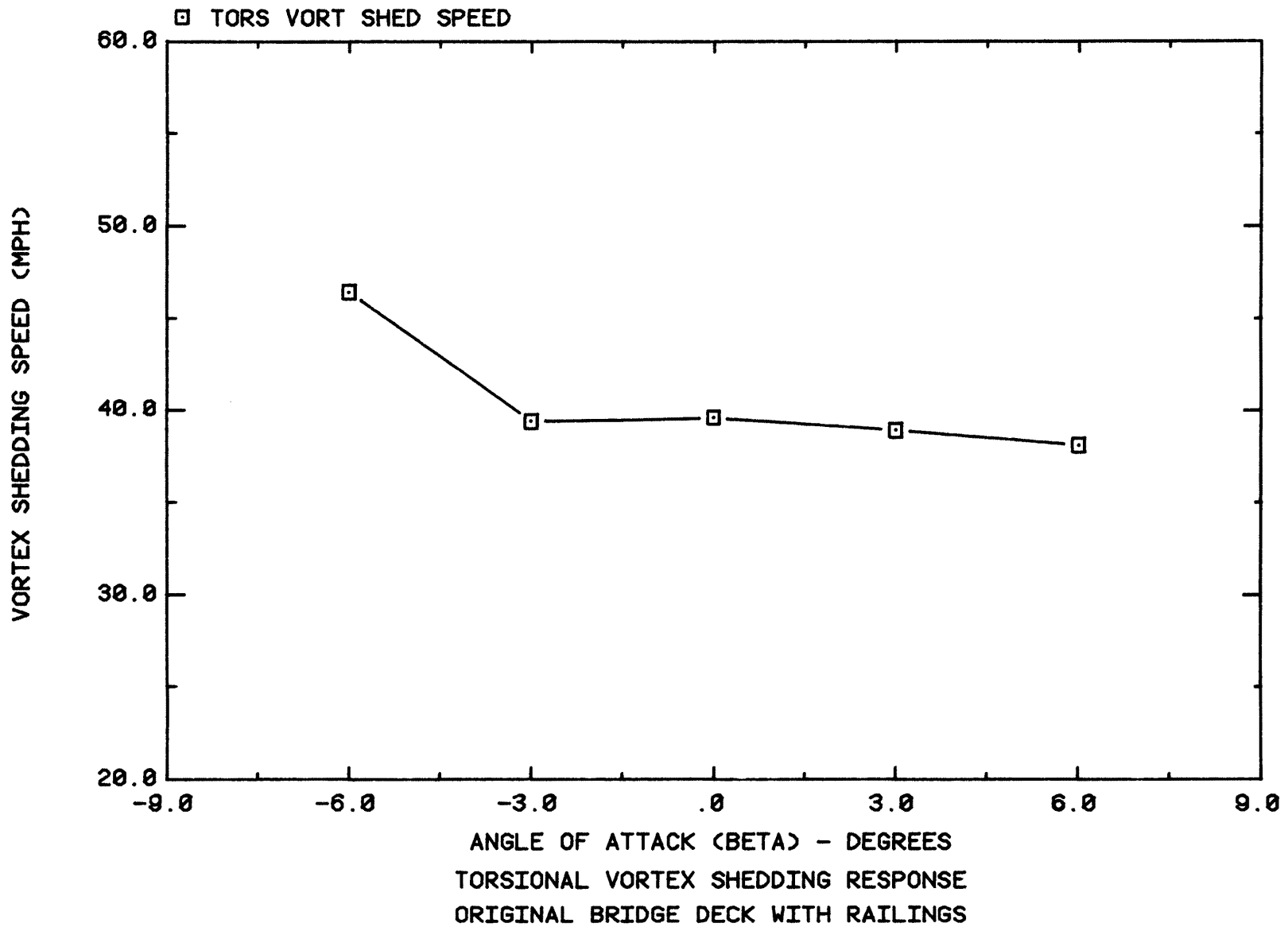


Figure 61. Prototype Speed Associated with Maximum Vortex-Induced Torsional Response

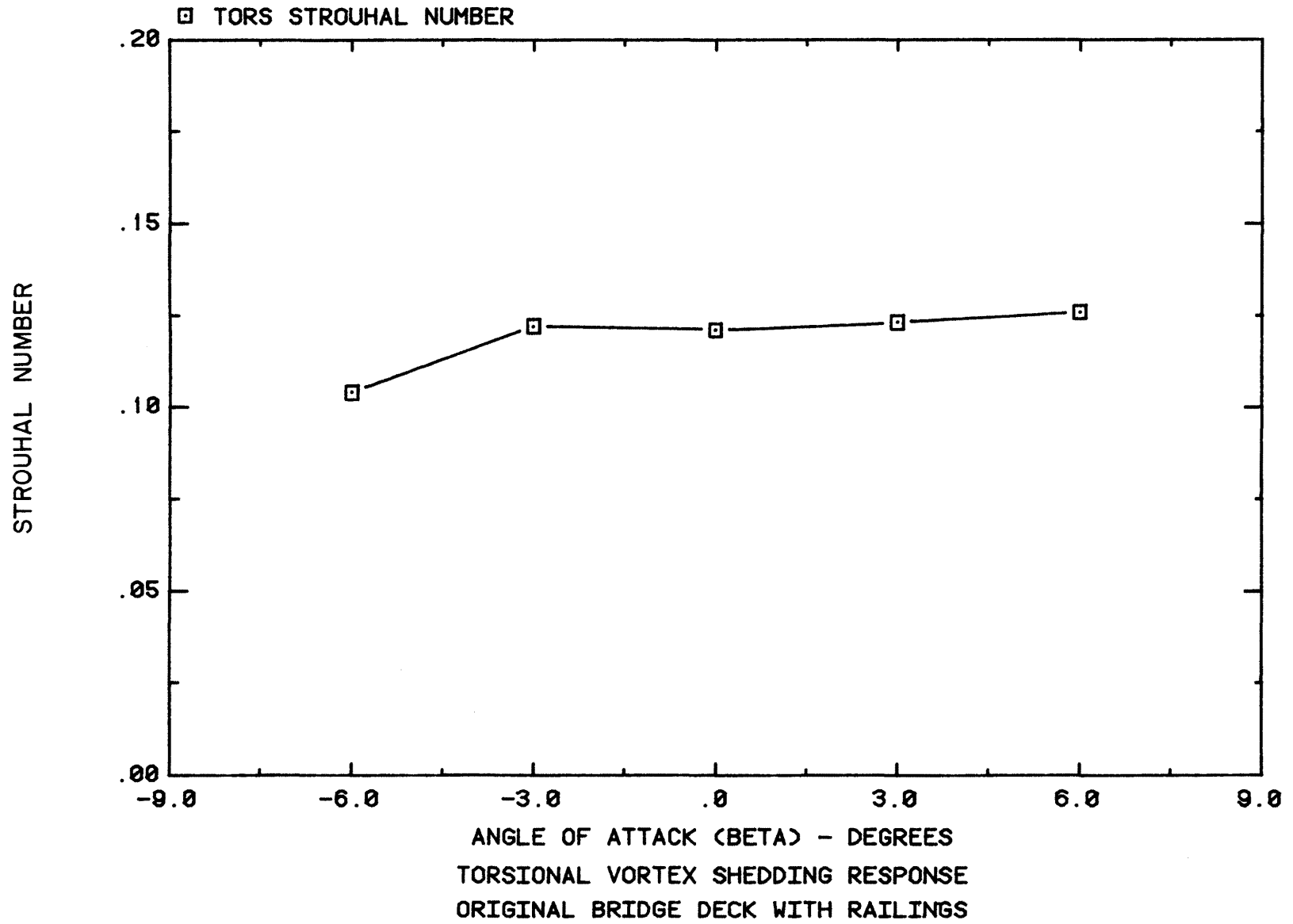
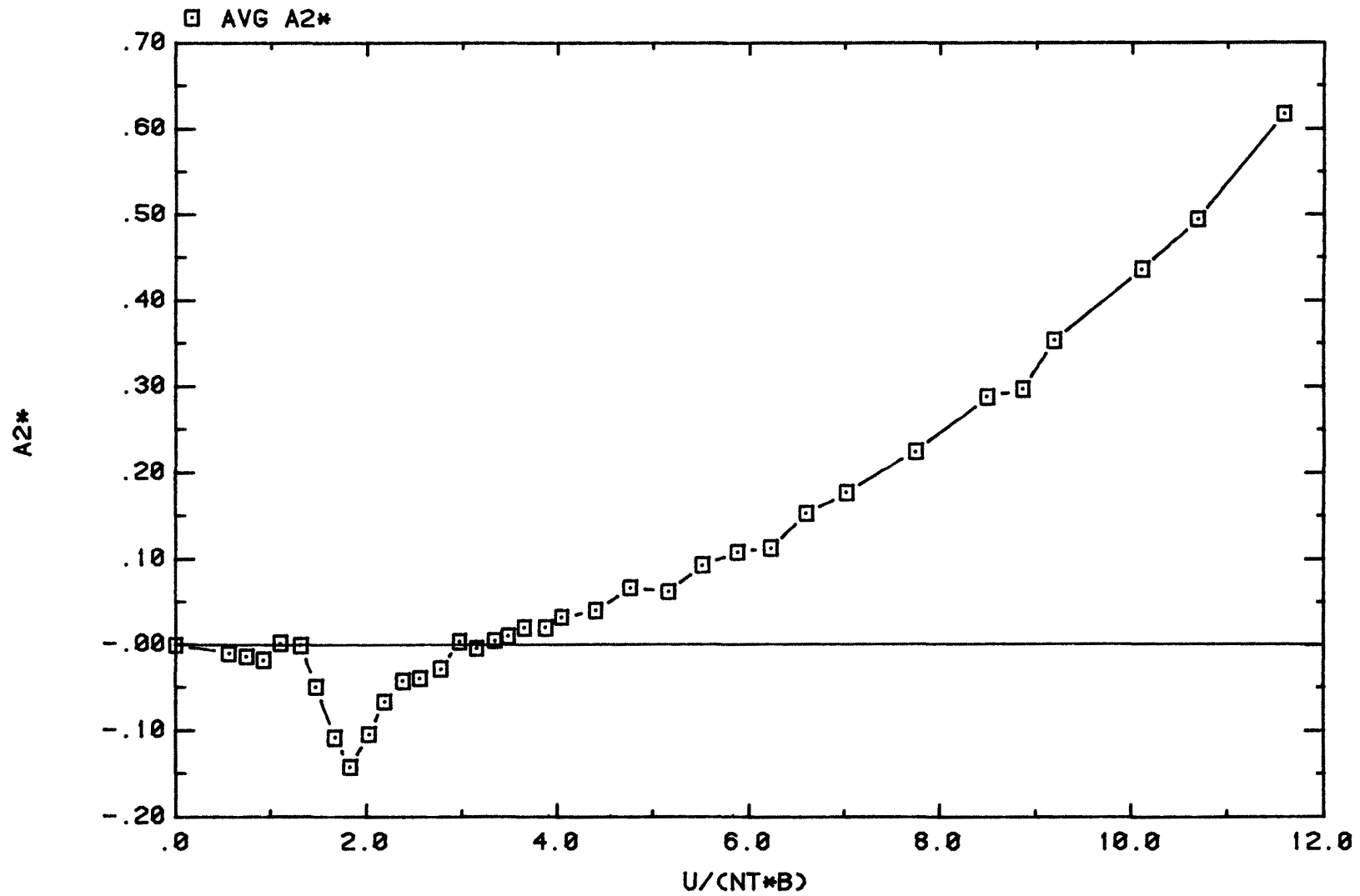


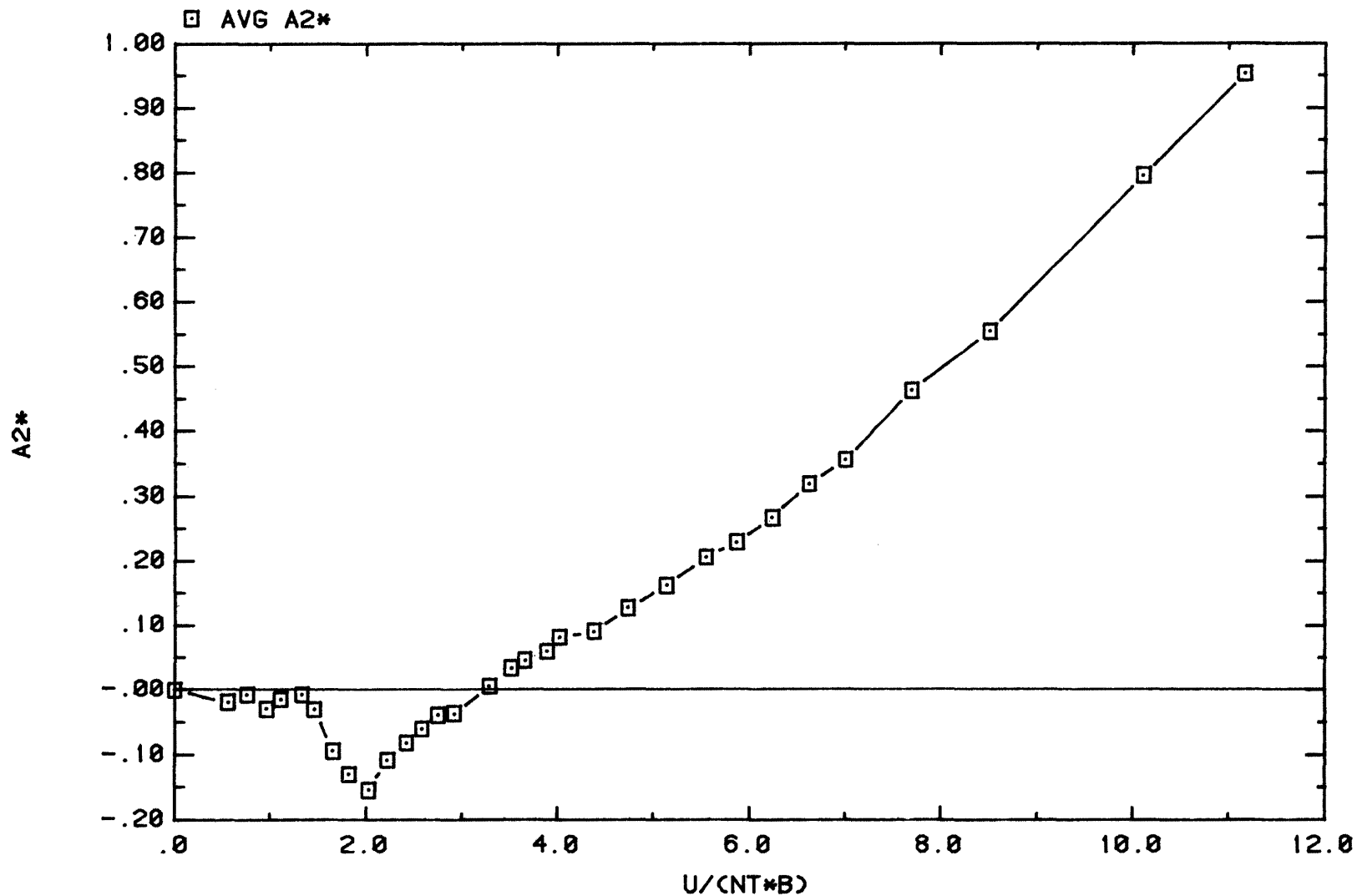
Figure 62. Strouhal Number Based on Torsional Vortex-Induced Response



CONFIGURATION BI-T-2

ORIGINAL BRIDGE DECK WITHOUT RAILINGS BETA= 0 DEG

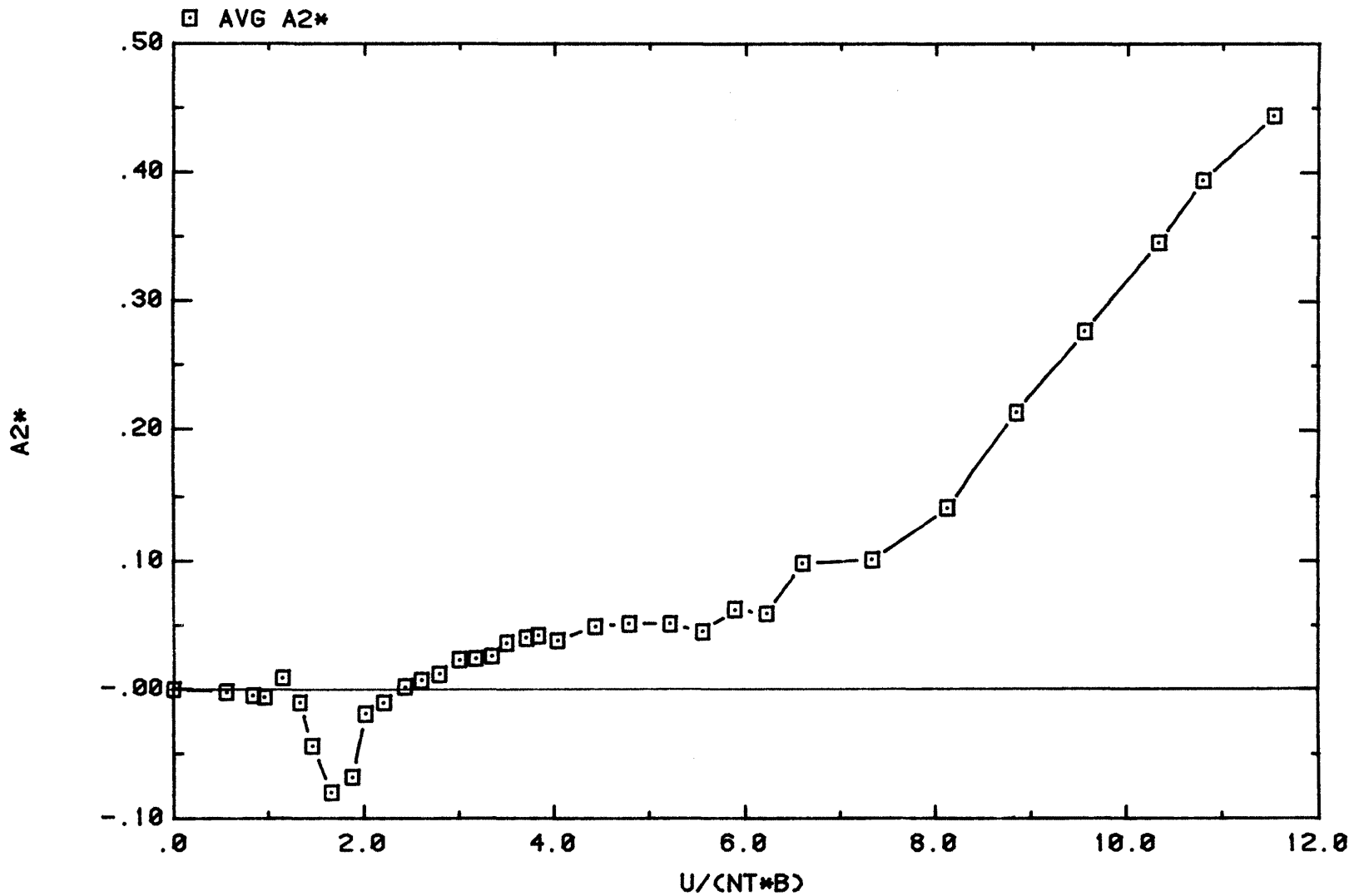
Figure 63. Aerodynamic Derivative A_2^* , Froude Number Similarity Relaxed, $\beta = 0^\circ$



CONFIGURATION BII -T-2

ORIGINAL BRIDGE DECK WITHOUT RAILINGS BETA=+3 DEG

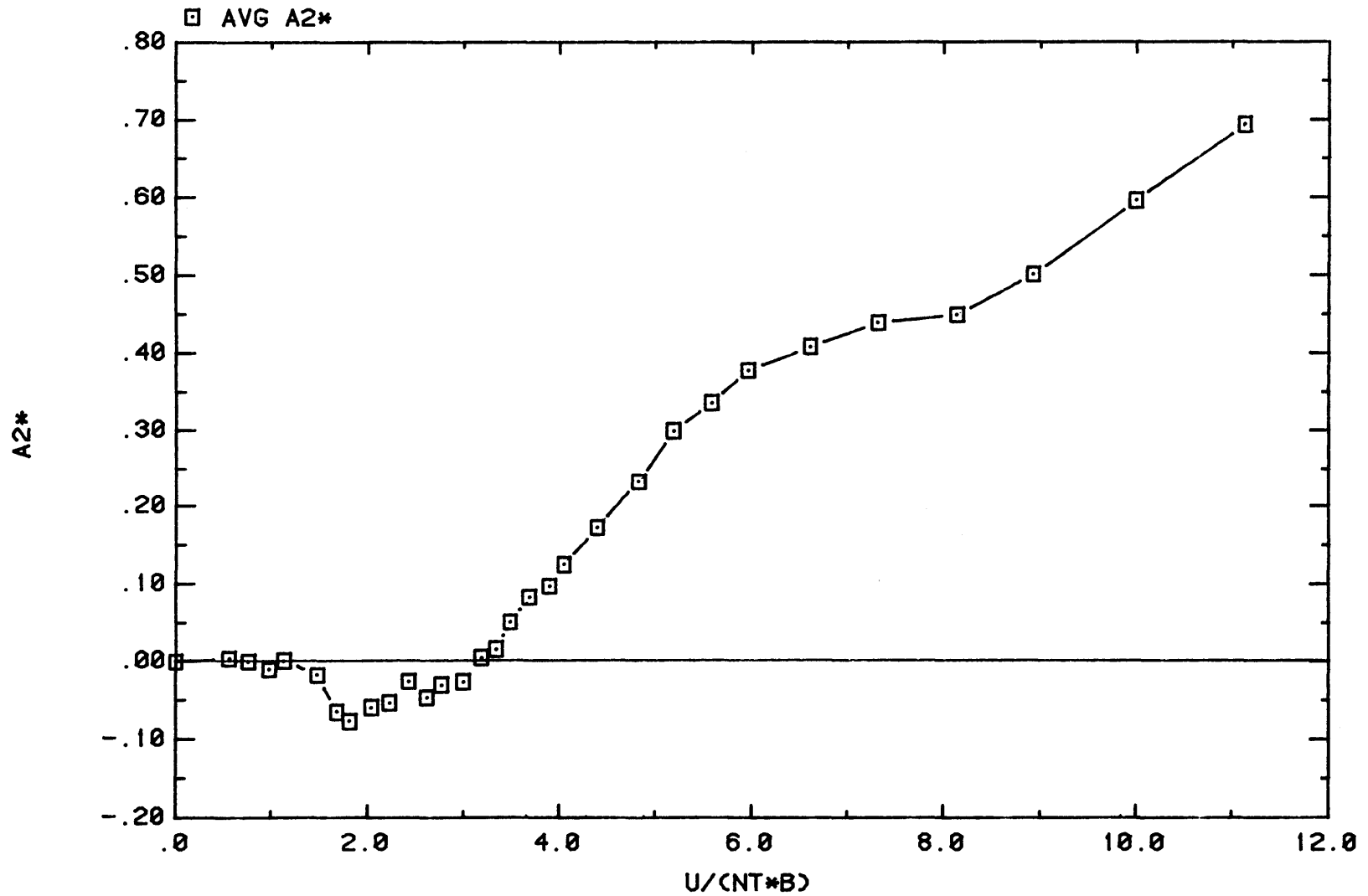
Figure 64. Aerodynamic Derivative A_2^* , Froude Number Similarity Relaxed, $\beta = +3^\circ$



CONFIGURATION BIII -T-2

ORIGINAL BRIDGE DECK WITHOUT RAILINGS BETA=-3 DEG

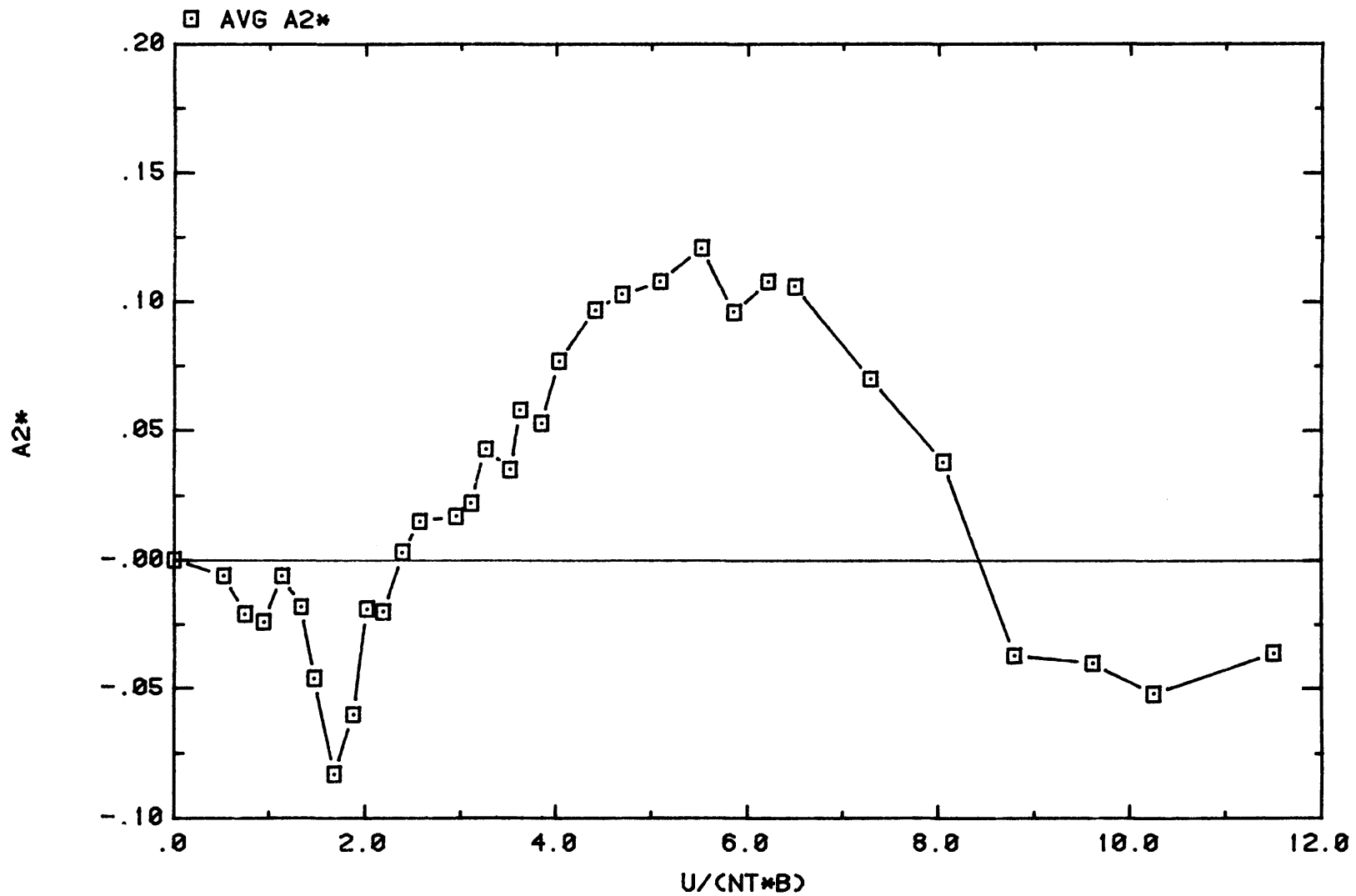
Figure 65. Aerodynamic Derivative A_2^* , Froude Number Similarity Relaxed, $\beta = -3^\circ$



CONFIGURATION BII6-T-2

ORIGINAL BRIDGE DECK WITHOUT RAILINGS BETA=+6 DEG

Figure 66. Aerodynamic qderivative A_2^* , Froude Number Similarity Relaxed, $\beta = +6^\circ$



CONFIGURATION BIII6-T-2

ORIGINAL BRIDGE DECK WITHOUT RAILINGS $\beta = -6^\circ$

Figure 67. Aerodynamic Derivative A_2^* , Froude Number Similarity Relaxed, $\beta = -6^\circ$

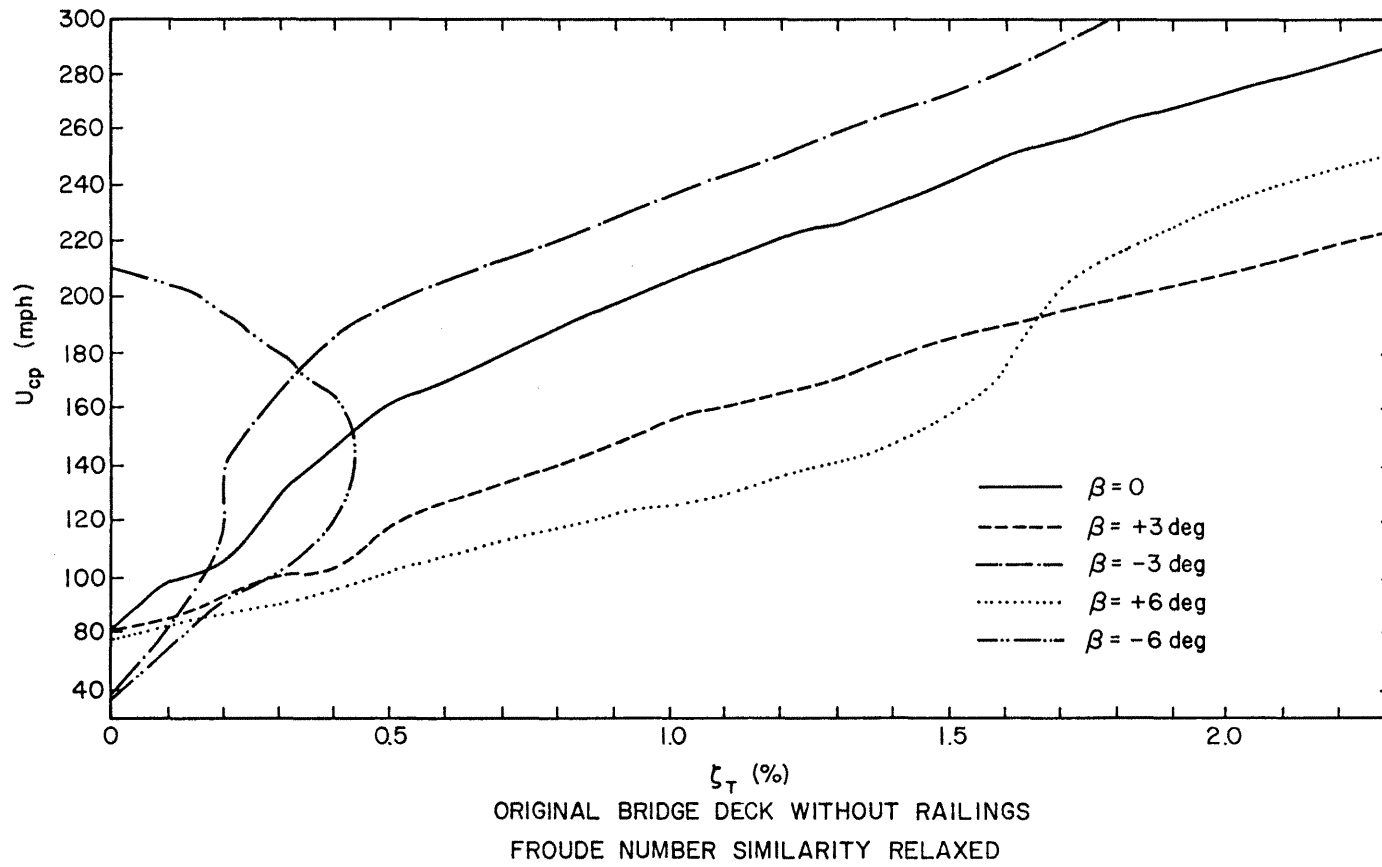


Figure 68. Prototype Critical Wind Speed

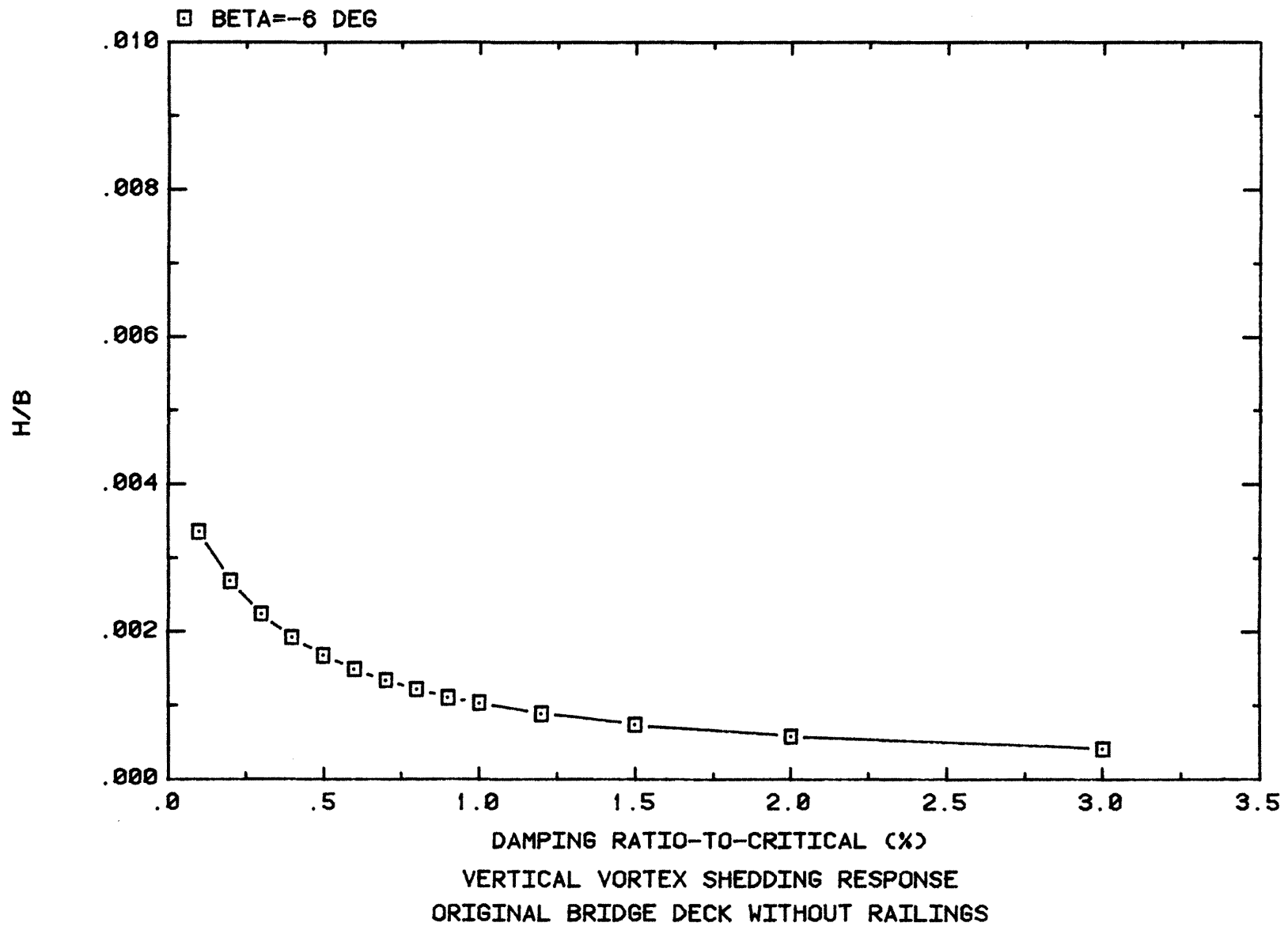


Figure 69. Maximum Vortex-Induced Response

11. TABLES

Table 1. Parameters for Prototype and "Exact" Model
(original bridge deck with railings)

Property		Units	Prototype*	"Exact" Model 1:80
Deck Width	(B)	ft	41.0	0.5125
Deck Depth	(D)	ft	5.0	0.0625
Mass per Unit Span	(m)	slug-ft ⁻¹	373.0	0.058281
Polar Mass Moment of Inertia per Unit Span (I)		slug-ft ² -ft ⁻¹	86000.0	0.002100
Inertia Ratio	(I/mB ²)	--	0.14	0.14
Vertical Bending Frequency	(N _V)	Hz	0.3	2.68
Torsional Frequency	(N _T)	Hz	0.9	8.05
Torsional-to-Vertical Frequency Ratio	(N _T /N _V)	--	3.0	3.0
Assumed Damping Ratio for Vertical Motion (ζ _V)		%	2.5	2.5
Assumed Damping Ratio for Torsional Motion (ζ _T)		%	2.5	2.5

*Based on data attached to letter of 28 March 1980 from Conrad P. Bridges,
Arvid Grant and Associates, Inc., to J. E. Cermak, Colorado State University.

Table 2. Parameters of Actual Model (original bridge deck with railings)

Property	Units	Model (No Dampers)		Damping Level					
				1		2		3	
		Value	Er	Value	Er*	Value	Er*	Value	Er*
B	ft	0.5125	0	0.5125	0	0.5125	0	0.5125	0
D	ft	0.0625	0	0.0625	0	0.0625	0	0.0625	0
m	slug-ft ⁻¹	0.048222	-21	0.050686	-15	0.049431	-18	0.052661	-11
I	slug-ft ² -ft ⁻¹	0.002258	7	0.002352	11	0.002314	9	0.002435	14
I/mB ²	--	0.18	22	0.18	22	0.178	21	0.176	20
N _v	Hz	3.25	18	3.17	15	3.21	7	3.11	4
N _T	Hz	8.88	10	8.70	7	8.77	8	8.55	6
N _T /N _v	--	2.73	-9	2.74	-9	2.73	-10	2.74	-9
ζ _v	%	0.10		0.12		0.71		2.3	
ζ _T	%	0.15		0.17		0.75		2.1	

$$* \text{Er} = \frac{(\quad)_{\text{actual}} - (\quad)_{\text{exact}}}{(\quad)_{\text{actual}}} [\%]$$

12. APPENDICES

APPENDIX A

Full-Span Torsional Flutter of the Prototype Bridge

The equation for torsional motion of a typical section of the bridge deck considered in Section 2.3 is given by Equations (13) and (14)

$$I[\ddot{\alpha} + 2\zeta_{\alpha}\omega_{\alpha}\dot{\alpha} + \omega_{\alpha}^2\alpha] = \rho B^4\omega_{\alpha}A_2^*\dot{\alpha} \quad (A1)$$

It is necessary to consider the spanwise modes of torsion that are expected to take part in full-span torsional flutter. It is usually sufficient to consider the mode of the lowest frequency (the fundamental mode) since the lowest flutter speed is sought. Therefore, the torsional displacement $\alpha(x,t)$ where x is a spanwise coordinate and t is time can be expressed in terms of the torsion fundamental spanwise mode $\phi_1(x)$ and the generalized coordinate $\alpha_1(t)$ as follows:

$$\alpha(x,t) = \phi_1(x) \cdot \alpha_1(t) \quad (A2)$$

Substituting (A2) in Equation (A1), multiplying by $\phi_1(x)$, and integrating over the span gives the following equation:

$$I_1\ddot{\alpha}_1 + (I_12\zeta_{\alpha}\omega_{\alpha} - C_1\rho B^4\omega_{\alpha}A_2^*)\dot{\alpha}_1 + I_1\omega_{\alpha}^2\alpha_1 = 0 \quad (A3)$$

where

$$I_1 = \int_0^L I(x)\phi_1^2(x)dx$$

and

$$C_1 = \int_0^L \phi_1^2(x)dx \quad .$$

From this equation the flutter condition has the following form:

$$A_2^* = \frac{2I_1}{\rho B^4 C_1} \zeta_{\alpha} \quad (A4)$$

If the bridge deck is uniform along the span and

$$I(x) = I = \text{const}$$

then

$$I_1 = I * C_1 .$$

The flutter condition (A4) for the full span of the prototype bridge becomes identical with the same requirement for the bridge section model (16)--

$$A_2 * \left(\frac{U_c}{NB} \right) = \frac{2I}{\rho B^4} \zeta_\alpha . \quad (A5)$$

APPENDIX B

Full-Span Vortex-Induced Response in Torsion

The equation of motion for the torsional degree-of-freedom of the bridge section model is similar to the equation of vertical motion (17) presented in Chapter 2.3.

$$I[\ddot{\alpha} + 2\zeta_{\alpha}\omega_{\alpha}\dot{\alpha} + \omega_{\alpha}^2\alpha] = \frac{1}{2}\omega U^2(2B^2)[KA_0^* \frac{B\dot{\alpha}}{U} + C_M \sin\omega t] \quad (B1)$$

where

A_0^* plays a role similar to H_0^*

C_M = pitching moment coefficient, and

ω = vortex-shedding frequency ($\omega \approx \omega_{\alpha}$).

The equation can be rewritten in a slightly different form

$$I[\ddot{\alpha} + 2\gamma_{\alpha}\omega_{\alpha}\dot{\alpha} + \omega_{\alpha}^2\alpha] = M_0 \sin\omega t \quad (B2)$$

where

$$\gamma_{\alpha} = \zeta_{\alpha} - \frac{\rho B^4}{2I} A_0^*$$

and

$$M_0 = \rho U^2 B^2 C_M.$$

The amplitude of the steady-state response of the oscillator (B2) can be approximated for $\omega \approx \omega_{\alpha}$

$$\alpha_0 \approx \frac{M_0}{2I\gamma_{\alpha}\omega_{\alpha}^2} = \frac{\rho U^2 B^2 C_M}{2I\gamma_{\alpha}\omega_{\alpha}^2}. \quad (B3)$$

If the amplitude α_0 and the damping ratio-to-critical γ_{α} are measured, then the pitching moment coefficient C_M can be estimated

$$C_M = \frac{2\alpha_0 \gamma_\alpha I \omega_\alpha^2}{\rho U^2 B^2} \quad (B4)$$

and the current value of the aerodynamic derivative A_0^* can be computed as follows:

$$A_0^* = (\zeta_\alpha - \gamma_\alpha) \frac{2I}{\rho B^4} \quad (B5)$$

The full-span vortex-shedding response in torsion can be estimated in the same manner as it has been done for the vertical motion. The torsional displacement $\alpha(x,t)$, where x is a spanwise coordinate and t is time, can be expressed in terms of the torsional fundamental spanwise mode $\phi_1(x)$ and the generalized coordinate $\alpha_1(t)$ --

$$\alpha(x,t) = \phi_1(x) \alpha_1(t) \quad (B6)$$

The equation of motion for the whole span can be written as follows:

$$I(x) [\ddot{\alpha}(x,t) + 2\gamma_\alpha \omega_\alpha \dot{\alpha}(x,t) + \omega_\alpha^2 \alpha(x,t)] = M_0 \sin \omega t \quad (B7)$$

and modified by introducing the expression (B6), multiplying by $\phi_1(x)$, and integrating along the span to give

$$I_1 [\ddot{\alpha}_1 + 2\gamma_\alpha \omega_\alpha \dot{\alpha}_1 + \omega_\alpha^2 \alpha_1] = M_{01} \sin \omega t \quad (B8)$$

where

$$I_1 = \int_0^L I(x) \phi_1^2(x) dx$$

and

$$M_{01} = M_0 \int_0^L \phi_1(x) dx.$$

The amplitude of the steady-state response of the oscillator (B8) is similar to the expression (B3)--

$$\alpha_{01} \approx \frac{M_{01}}{2I_1 \gamma_\alpha \omega_\alpha^2} = \frac{\rho U^2 B^2 C_M \int_0^L \phi_1(x) dx}{2I_1 \omega_\alpha^2 \gamma_\alpha} \quad (B9)$$

The maximum amplitude of the vortex-induced full-span response can be computed from (B6) and (B9)--

$$\alpha_0(x) \Big|_{\max} = \frac{\rho U^2 B^2 C_M \int_0^L \phi_1(x) dx}{2I_1 \omega_\alpha^2 \gamma_\alpha} \phi_1(x) \Big|_{\max} \quad (B10)$$

When the bridge deck is uniform along the span then this formula can be simplified to

$$\alpha_0(x) \Big|_{\max} = \frac{\rho U^2 B^2 C_M}{2I \omega_\alpha^2 \gamma_\alpha} F_M \quad (B11)$$

where

$$F_M = \frac{\int_0^L \phi_1(x) dx}{\int_0^L \phi_1^2 dx} \phi_1(x) \Big|_{\max}$$